

Introduction

“Dusty”, or “complex” plasmas are composed of a weakly ionized gas and charged microparticles. Dust and dusty plasmas are ubiquitous in space – they are present in planetary rings, cometary tails, interplanetary and interstellar clouds, the mesosphere, thunderclouds, they are found in the vicinity of artificial satellites and space stations, etc. Furthermore, the presence of dust particles plays a critical role in many important industrial processes (e.g., plasma vapor deposition, microchip production, etching, where growth of dust occurs as a matter of course during the production process) as well as in plasma fusion (where the possibility of producing radioactive and toxic dust in the plasma-wall interactions is an important design issue). Apart from that, plasmas containing microparticles individually visible under optical microscopy are actively investigated in many laboratories (and the term “complex plasmas” is used to distinguish systems specially designed for such investigations from naturally occurring dusty plasmas). After almost a century of study – the first observations of dust in discharges have been reported by Langmuir in 1924 – the current interest in complex plasmas began in the mid 1990’s, triggered by the laboratory discovery of plasma crystals.

The presence of charged microparticles in complex plasmas is essential for collective processes. Ensembles of microparticles give rise to new very-low-frequency wave modes which represent the oscillations of particles against the quasi-equilibrium background of electrons and ions. Characteristic frequencies associated with the dust component are in the range of 10-100 Hz. However, microparticles embedded in a plasma do not only change the charge composition, they also introduce new physical processes into the system, e.g., effects associated with dissipation and plasma recombination on the particle surface, variation of the particle charges, etc. These processes imply new mechanisms of the energy influx into the system. Therefore, properties of complex plasmas can be completely different from those of usual multicomponent plasmas.

Due to large charges carried by microparticles (typically, of the order of thousand elementary charges for a micron-size particle), the electrostatic energy of the mutual interaction is remarkably high. Therefore, in complex plasmas one can observe transitions from a disordered gaseous-like phase to a liquid-like phase and the formation of ordered structures of microparticles – plasma crystals. In addition, the shape of the interparticle interaction strongly depends on experimental conditions. These unique features distinguish complex plasmas from many other laboratory plasmas, where the ion charges are low, the interaction potentials are fixed, and the coupling strength is relatively weak.

In this introductory lecture course we discuss basic properties of complex (dusty) plasmas. The focus is made on the analysis of the most fundamental universal processes occurring in very different conditions, ranging from astrophysical and fusion plasmas to laboratory and technological gas discharges. This course is supposed to provide the necessary basis for further in-depth studies of the physics of complex plasmas, in particular for the follow-up course “Interdisciplinary plasma research”.

Recommended literature

V. E. Fortov and G. E. Morfill, *Complex and dusty plasmas: From Laboratory to Space*, (CRC Press 2010).

V. E. Fortov, A. V. Ivlev, S. A. Khrapak, A. G. Khrapak, and G. E. Morfill, *Complex (dusty) plasmas: Current status, open issues, perspectives*, Phys. Rep. **421**, 1 (2005).

V. E. Fortov, A. G. Khrapak, S. A. Khrapak, V. I. Molotkov, and O. F. Petrov, Phys. Usp. **47**, 447 (2004).

E. M. Lifshitz and L. P. Pitaevskii, *Physical Kinetics* (Pergamon, Oxford, 1981).

I. Charging of dust particles

The particle charge is one of the most important parameters of complex plasmas. It determines the particle interactions with plasma electrons and ions, with electromagnetic fields, between the particles themselves, etc. Hence, all studies of complex plasmas necessarily begin with a model for the particle charge. In this Chapter we first give brief overview of the charging mechanisms operating in different types of complex plasmas. Then, we primarily focus on complex plasmas in gas-discharges, where particle charging is due to the collection of electrons and ions from the surrounding plasma. We introduce the orbital motion limited (OML) theory and discuss important limitations of this approach. One of the most important issues – effect of collisions in plasmas – is described in detail. The Chapter ends with the description of charge fluctuations.

1 Main charging mechanisms

Charging is a result of interaction between the dust particle (grain) and surrounding plasma. Plasma electrons and ions can be collected or emitted by the dust grain, which obviously affects its charge state. In general, the evolution of the particle charge Q can be described as

$$\frac{dQ}{dt} = \sum_j q_j J_j, \quad (1)$$

where q_j is the charge of the j -th species and J_j is the corresponding flux to/from the surface of the dust grain (taken with proper sign). In equilibrium, $dQ/dt = 0$, the balance between all the currents associated with plasma collection/emission takes place.

We do not go into details of particle charging by electron emission processes, but only summarize the most important mechanisms operating in different types of complex (dusty) plasmas. These are:

- Thermionic emission (for sufficiently high temperatures);
- Photoelectric emission (photons with sufficiently high energy);
- Secondary electron emission (electrons with sufficiently high energy).

Emission of electrons tends to charge particles positively. The simplest (two-

component) complex plasma system would consist of positively charged dust particles and the electrons emitted by them. In this case, the flux of emitted electrons should be balanced by the flux of electrons collected from the surrounding electron background.

In typical gas discharges, which will be of main interest for us, emission processes are not important. The main charging mechanism is the collection of electrons and ions from the surrounding plasma. The equilibrium particle charge is determined by the balance of collected electrons and ions and is *negative*. This is because the electrons have much higher thermal velocities, so that the electron thermal flux directed to an initially uncharged particle exceeds considerably that of the ions. The grain collects more electrons than ions, and the emerging negative charge on the particle leads to the repulsion of the electrons and the attraction of the ions. The absolute magnitude of the charge grows until the electron and ion fluxes on the particle surface become equal (on average). On longer timescales, the charge is practically constant and experiences only small fluctuations around its equilibrium value, as discussed in Section I.5.

To a good accuracy, the charge of a small particle is given by the product of its radius a and surface potential φ_s , i.e., $Q \simeq a\varphi_s$. In turn, the *equilibrium* surface potential φ_s is mainly determined by the electron temperature T_e ,

$$\varphi_s \sim -zT_e/e, \quad (2)$$

where $z(> 0)$ is a numerical coefficient, T_e is measured in energy units, and e is the elementary charge. Physically, this is because in equilibrium most of the electrons have to be reflected by the potential barrier between the particle surface and surrounding plasma, so that the electron and ion fluxes can balance each other. The coefficient z depends on the particular regime which is realized for the electron and ion fluxes to the particle surface. Various effects can be important in different conditions and, as a result, the coefficient z can vary in a relatively wide range: The values between ~ 0.3 and ~ 3 are not unrealistic for normal discharge conditions, and can be even higher for high-pressure plasmas.

Exercise. Calculate the charge number of a $1 \mu\text{m}$ radius particle in a plasma with $T_e = 1 \text{ eV}$ assuming $z \simeq 1$.

In what follows, we will discuss several models that can be used to calculate/estimate the coefficient z in various practical situations related to complex plasmas in gas discharges. We start with the best known model of particle charging in dusty plasmas – the orbital motion limited theory.

2 Orbit motion limited (OML) approximation

This is historically (Mott-Smith and Langmuir, 1926) the most frequently used approach to describe the electron and ion fluxes collected by the dust grain in plasmas (note that OML is also extensively used in the context of electrical probes in plasmas). Although it does not take into account some important physical processes, it is natural to start with this idealized model, and then to discuss its limitations and possible improvements.

In the OML approach three major assumptions are employed: (i) The dust grain is isolated in the sense that other dust grains do not affect the motion of electrons and ions in its vicinity; (ii) Electrons and ions do not experience collisions during their approach to the grain; (iii) The barriers in the *effective* ion-grain potential are absent (this condition is discussed in Section I.2.3). Then, the conservation of energy and angular momentum is used to describe ion and electron collection.

Consider the motion of a light particle (electron or ion) of mass m in the vicinity of a massive dust particle placed at the origin of the coordinate system. If ρ is the impact parameter, r_0 is the distance of closest approach, v_∞ is the ion/electron velocity far from the center, and v_0 is the corresponding velocity at $r = r_0$, the angular momentum conservation yields

$$\rho m v_\infty = r_0 m v_0. \quad (3)$$

The energy conservation yields

$$\frac{1}{2} m v_\infty^2 = \frac{1}{2} m v_0^2 + U(r_0), \quad (4)$$

where $U(r)$ is the potential of interaction between electron/ion and the dust grain. From the second equation we get $v_0/v_\infty = \sqrt{1 - 2U(r_0)/m v_\infty^2}$, which yields the following relation between the impact parameter and the distance of the closest approach

$$\rho = r_0(v_0/v_\infty) = r_0 \sqrt{1 - 2U(r_0)/m v_\infty^2}. \quad (5)$$

Ion or electron hits the particle if the distance of the closest approach is smaller than the particle radius $r_0 \leq a$. Taking into account that $U(a) = e\varphi_s$ for ion-particle (attractive) interaction and $U(a) = -e\varphi_s$ for electron-particle (repulsive) interaction (φ_s is negative!) we get maximum impact parameters corresponding to collection. For the ions we have $\rho_c = a\sqrt{1 - 2e\varphi_s/m_i v^2}$ (starting from this point we omit the subscript in v_∞). For the electrons we have $\rho_c = a\sqrt{1 + 2e\varphi_s/m_e v^2}$ if they are sufficiently fast, so that $2e\varphi_s/m_e v^2 > -1$, and $\rho_c = 0$ otherwise (slow electrons cannot approach sufficiently close to the

particle due to repulsion). Here m_e and m_i denote the mass of electron and ion, respectively.

The velocity dependent collection cross sections are simply $\pi\rho_c^2$. We have therefore

$$\sigma_e(v) = \begin{cases} \pi a^2 \left(1 + \frac{2e\varphi_s}{m_e v^2}\right), & \frac{2e\varphi_s}{m_e v^2} > -1, \\ 0, & \frac{2e\varphi_s}{m_e v^2} \leq -1, \end{cases} \quad (6)$$

and

$$\sigma_i(v) = \pi a^2 \left(1 - \frac{2e\varphi_s}{m_i v^2}\right). \quad (7)$$

An obvious advantage of the OML approximation is that the cross sections are independent of the plasma potential distribution around the grain (they depend only on the surface potential).

2.1 Isotropic conditions

Electron and ion fluxes to the particle surface are determined by the integral of the corresponding cross sections with the velocity distribution functions $f_{e(i)}(v)$:

$$J_{e(i)} = n_{e(i)} \int v \sigma_{e(i)}(v) f_{e(i)}(v) d^3v, \quad (8)$$

where $n_{e(i)}$ is the electron (ion) density. Using the isotropic Maxwellian velocity distribution of the plasma species

$$f_{e(i)}(v) = (2\pi v_{T_{e(i)}}^2)^{-3/2} \exp(-v^2/2v_{T_{e(i)}}^2), \quad (9)$$

where $v_{T_{e(i)}} = \sqrt{T_{e(i)}/m_{e(i)}}$ is the electron (ion) thermal velocity, we get after the integration

$$J_e = \sqrt{8\pi} a^2 n_e v_{T_e} \exp\left(\frac{e\varphi_s}{T_e}\right), \quad (10)$$

$$J_i = \sqrt{8\pi} a^2 n_i v_{T_i} \left(1 - \frac{e\varphi_s}{T_i}\right). \quad (11)$$

The flux balance condition is simply $J_i = J_e$. Using the dimensionless (positive) coefficient z defined above in Eq. (2) and the electron-to-ion temperature and mass ratios, $\tau = T_e/T_i$ and $\mu = m_e/m_i$, respectively, the flux balance condition can be written as

$$\sqrt{\tau} \exp(-z) = \sqrt{\mu}(1 + z\tau), \quad (12)$$

where quasineutrality condition $n_i \simeq n_e$ has been used.

Exercise. Using the OML approximation calculate the reduced potential z for (a) H plasma with $\tau = 1$ and (b) Ar plasma with $\tau = 100$.

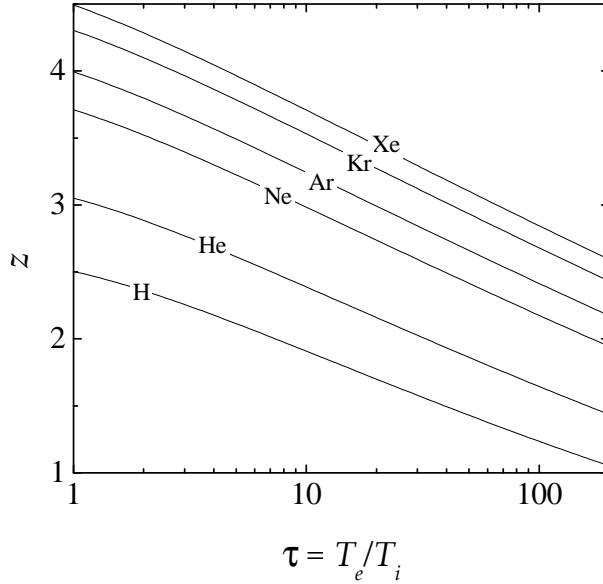


Fig. 1. *Reduced surface potential $z = e|\varphi_s|/aT_e$ of an individual spherical particle as a function of the electron-to-ion temperature ratio $\tau = T_e/T_i$ for isotropic Maxwellian plasmas of different gases.*

Thus in the framework of the OML approximation, the dimensionless surface potential z depends on two parameters, τ and μ (the latter is determined by the gas type). In Fig. 1, values of z are presented for different gases (H, He, Ne, Ar, Kr, Xe) as functions of τ . The reduced particle potential decreases with τ and increases with the gas atomic mass. For typical values of $\tau \sim 10-100$ in conventional gas discharges, the dimensionless charge calculated using the OML approach is in the range $z \simeq 2-4$.

2.2 Anisotropic conditions

Complex (dusty) plasmas are usually subject to electric fields. For example, in ground-based experiments with rf discharges the particles can levitate in the (pre) sheath above the lower electrode, while in dc discharges the particles are often trapped in striations (i.e. in the regions where electric field is sufficiently strong to balance for particle gravity). Both these regions are characterized by high degree of plasma anisotropy and strong electric fields. The presence of the electric fields causes plasma drifts relative to the dust component. This in turn can affect particle charging by changing the collection cross sections and velocity distribution functions of ions and electrons. The problem of charging becomes much more complicated than in the case of an isotropic plasma, and at present no self-consistent analytical solution exists.

To get an idea how the plasma drifts can affect particle charging the following

simplification can be used. The OML collection cross sections are assumed, but instead of isotropic Maxwellian distribution function one uses the *shifted Maxwellian distribution*, viz.

$$f_{i(e)}(\mathbf{v}) = \left(2\pi v_{T_{i(e)}}^2\right)^{-3/2} \exp\left[-\frac{(\mathbf{v} - \mathbf{u}_{i(e)})^2}{2v_{T_{i(e)}}^2}\right], \quad (13)$$

where $\mathbf{u}_{i(e)}$ is the average drift velocity of ions (electrons). Integration of the cross section (7) with the shifted Maxwellian function (13) yields the following expression for the ion flux

$$J_i = \sqrt{\pi} \frac{a^2 n_i v_{T_i}^2}{u_i} \left[\sqrt{\pi} (1 + 2\xi^2 + 2z\tau) \operatorname{erf}(\xi) + 2\xi \exp(-\xi^2) \right], \quad (14)$$

where $\xi = u_i/\sqrt{2}v_{T_i}$ and $\operatorname{erf}(x) = \frac{2}{\sqrt{\pi}} \int_0^x \exp(-t^2) dt$ is the error function. Similarly, the electron flux can be calculated, but the algebra is more tedious and we don't derive it here. In the limit $u_i \ll v_{T_i}$ expressions (14) reduces to (11). In the opposite limit we have

$$J_i = \pi a^2 n_i u_i \left[1 + (1 + 2z\tau)(v_{T_i}/u_i)^2 \right]. \quad (15)$$

In the regime of very high drift velocity, the ion and electron fluxes tend to the respective geometrical asymptotes, $J_{i,e} \simeq \pi a^2 n_{i,e} u_{i,e}$.

In most cases, the drift of electrons is negligible while the ion drift is large (this is another reason why we have not provided derivation of J_e for the case of arbitrary electron drift velocity). For example, this occurs in the regime of ambipolar plasma, in the (pre)sheath regions, i.e., where the electron distribution is close to Boltzmann, implying that the electric force acting on the electrons is compensated by the electron pressure. In this case the electron flux to the particle surface is given by Eq. (10) while for the ions one should use Eq. (14). The resulting surface potential is shown in Fig. 2 as a function of the ion drift velocity (for three values of n_e/n_i). The charge is practically constant for $u_i \lesssim v_{T_i}$, then it increases with u_i , attains a maximum at $u_i \simeq (2 - 3)C_{\text{IA}}$ (where $C_{\text{IA}} = \sqrt{T_e/m_i}$ is the ion sound speed), and starts decreasing. Comparison of results calculated with exact flux (14) and with asymptotic expressions (11) and (15) (the latter are indicated by dotted lines) shows almost no discrepancy, except for a narrow region near $u_i \sim v_{T_i}$.

Exercise. Estimate the ion Mach number at which the charge of a small particle immersed in a quasineutral Ar plasma with ion drift will reverse its sign (becomes positive).

The accuracy of neglecting the potential anisotropy caused by the ion flow (i.e., the assumption of the OML collection cross sections) was checked in

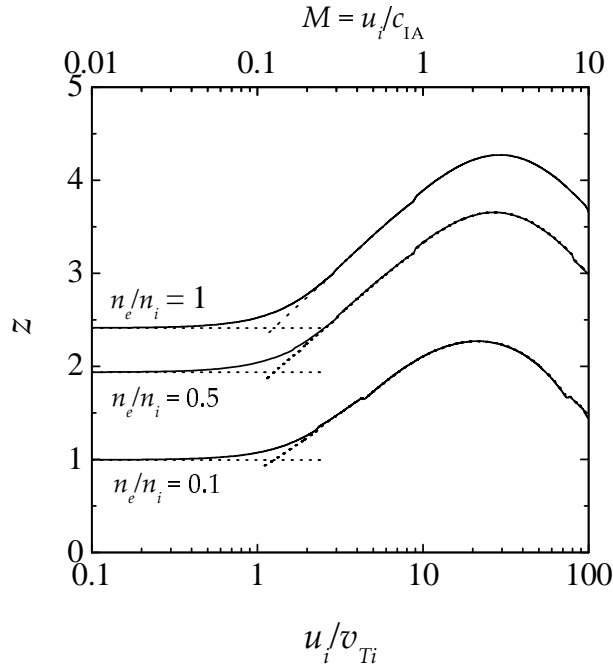


Fig. 2. Reduced surface potential $z = e|\varphi_s|/aT_e$ of an individual spherical particle as a function of the ion drift to ion thermal velocity ratio, u_i/v_{Ti} (or Mach number $M = u_i/c_{IA}$), for a plasma with the ion drift. The calculations are for three different electron-to-ion density ratios and correspond to an argon plasma with $\tau = 100$.

several numerical simulations. It was shown that the anisotropy is virtually negligible (with respect to the total ion flux) in the case of conducting particles. However, the agreement between simulation and OML theory becomes worse for a dielectric particle. This is because the latter acquires a significant dipole moment of the magnitude d , parallel to the flow direction, so that the potential near the particle can be approximated by

$$U(\mathbf{r}) = \frac{eQ}{r} + \frac{d}{r^2} \cos \theta, \quad (16)$$

where θ is the angle between \mathbf{r} and the flow axis. This anisotropy should be taken into account when calculating the ion flux (Ivlev, 1999). As shown in Fig. 3, the absolute magnitude of the charge of a dielectric particle turns out to be significantly larger than that of a conductive particle (when $d = 0$ and the OML approach is applicable, see Fig. 2).

Exercise. Using Lagrange's equations in spherical coordinates, show that motion in the field (16) can be integrated exactly.

Another circumstance which can affect the accuracy of expression (14) is the deviation of the ion velocity distribution function from the shifted Maxwellian. This topic is presently under active investigation.

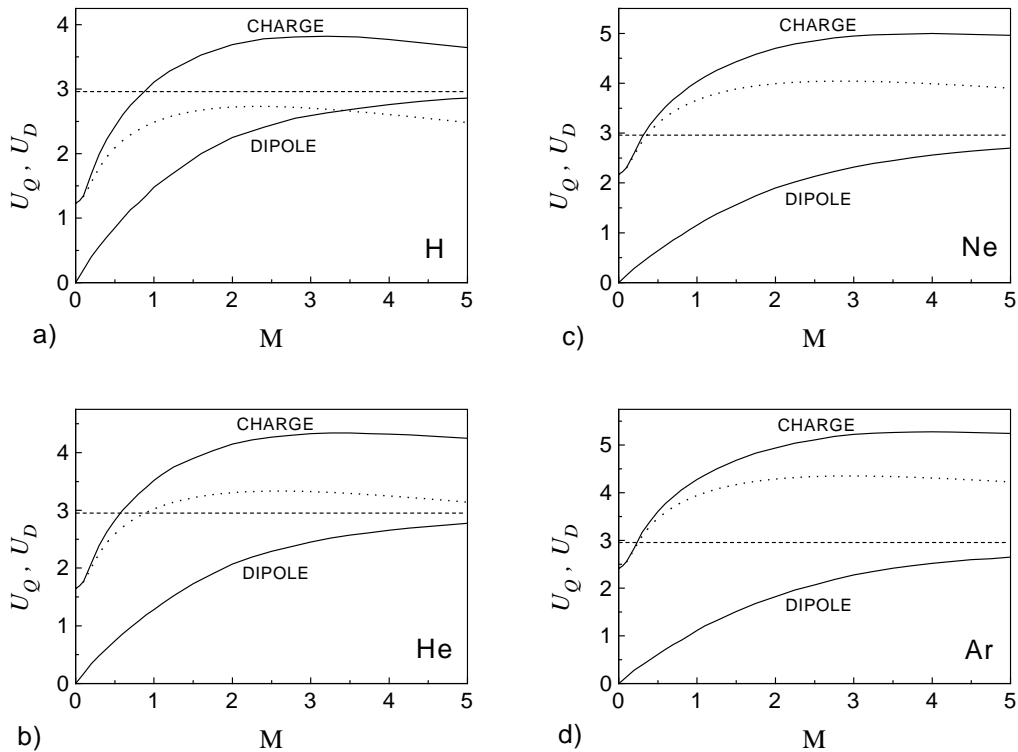


Fig. 3. The dimensionless charge, $U_Q = e|Q|/aT_e$ (in the text z is adopted), and the dimensionless dipole moment, $U_D = ed/a^2T_e$, of the dielectric particle (solid lines) versus Mach number of the plasma flow, $M = u_i/C_{1A}$ (Ivlev, 1999). The dotted line corresponds to a metal particle. The dashed line is the asymptote for the dipole curve. The figures correspond to (a) H, (b) He, (c) Ne, and (d) Ar.

2.3 Limitations of the OML approach

The assumptions underlying OML approach are not necessary met in reality. Below we discuss three major reasons, which can make the OML approach inapplicable.

The first reason is associated with the finite dust density in experiments and is known as the effect of “closely packed” grains (or “charge cannibalism”). This effect is two-fold. The grain component contributes to the quasineutrality condition: For an individual grain we assumed $n_i \simeq n_e$, whilst for a finite particle density n_d we should rewrite this as $n_e = n_i + (Q/e)n_d$. For negatively charged grains the ion density becomes larger than the electron density. This increases the ratio of the ion-to-electron flux and hence reduces the absolute value of the charge, compared to the case of an individual grain. The magnitude of the effect can be conveniently characterized by the “Havnes parameter” P , which is the ratio of the charge residing on the dust component to that on the

electron component,

$$P = |Z| \frac{n_d}{n_e} \equiv z \frac{aT_e n_d}{e^2 n_e}, \quad (17)$$

where $Z = Q/e$ is the charge number and n_d is the grain density. If we simply use expressions (10) and (11) for the electron and ion fluxes together with the quasineutrality condition, we get

$$\sqrt{\tau} \exp(-z) = \sqrt{\mu}(1 + z\tau)(1 + P). \quad (18)$$

The reduced potential tends to that of an individual particle when $P \ll 1$, while it is reduced considerably for $P \gg 1$. In addition, when the interparticle separation Δ is smaller than the characteristic length of interaction between ions (electrons) and the grain, then the ion (electron) trajectories are affected by the presence of neighboring grains, thus influencing charging. Several experiments demonstrated that the effect of ‘‘closely packed’’ grains can lead to substantial charge reduction under normal experimental conditions.

The second reason is associated with the fact that OML theory presumes the absence of barriers in the effective potential energy. The barriers are absent for repulsive interactions (i.e., for the electrons), but can emerge when the interaction is attractive (i.e. for the ions). As will be shown in Chapter II, the electrostatic potential $U(r)$ around a small absorbing object (dust grain) in plasmas scales as $\propto 1/r$ close to the object, $\propto 1/r^2$ far from it (in the collisionless regime), and at intermediate distances the potential decreases faster. These properties allow for the existence of barriers in the effective potential of ion-particle interaction, $U(r) + \frac{1}{2}mv_\infty^2(\rho/r)^2$. Some ions (with sufficiently low energy) will be reflected from the barriers. This effect leads to a decrease in the ion flux as compared to the OML theory and, hence, to an increase in $|Q|$ and z . For the Maxwellian ion velocity distribution there are always sufficiently slow ions, which are reflected from the barrier. However, if the fraction of such ions is small, then the corrections to OML are also small. Fortunately, this is usually the case under normal experimental conditions with sufficiently small particles (radius should be smaller than ~ 0.1 of the screening length). Therefore, corrections to the OML due to the presence of potential barriers can normally be neglected, provided the grains are small.

The third reason is due to collisions. In the OML approach collisions of electrons and ions when they travel to the grain are completely neglected. This can be a reasonable assumption when the electron and ion mean free paths $\ell_{e(i)}$ are very long compared to the particle size and the plasma screening length. In the opposite limit, OML obviously breaks down. The collection of ions and electrons becomes collision dominated, and it would be more appropriate to employ hydrodynamic equations to describe their fluxes towards the particle surface. From the practical point of view, the most interesting situation is when the electron mean free path is much longer than the plasma screening length, but the ion mean free path is of the order of the screening length (this

normally happens in gas discharges operating at pressures between several and several hundreds Pa). In this regime, ion-neutral collisions can enhance the ion flux (as compared to the OML model) dramatically. Collisions become the most important factor affecting and regulating the particle charge. Therefore, it is important to understand the related physics in detail.

3 Charging in strongly collisional regime

The focus of this Section is on charging of a small spherical grain immersed in a highly collisional plasma. Approximate expressions for charging fluxes and grain surface potentials in isotropic and anisotropic conditions are derived.

3.1 Isotropic conditions

The idealized model of charging considered below is based on the following main assumptions: (i) grain charging is determined by continuous absorption of electrons and ions from surrounding plasma; (ii) continuum equations apply to collision dominated species; (iii) all properties are spherically symmetric; (iv) no ion and electron sources or sinks exist except at the grain surface, which is fully absorbing; (v) temperatures of ions and electrons are uniform, but not necessarily equal to each other; (vi) ion (electron) mobility is constant, and the Einstein relation between mobility and diffusivity holds.

Conservation of ion and electron fluxes can be written as differential equations for ion and electron densities

$$4\pi r^2 D_j [\nabla n_j \pm (n_j e / T_j) \nabla \varphi] = J_j, \quad (19)$$

where $D_j \sim \ell_j v_{T_j}$ are the diffusion coefficients of ions ($j = i$) and electrons ($j = e$). In the left hand side of Eq. (19) the positive (negative) sign corresponds to ions (electrons). The electrostatic potential $\varphi(r)$ around the grain satisfies the Poisson equation $\Delta \varphi = -4\pi e(n_i - n_e)$. The boundary conditions for an absorbing grain surface are $\varphi(a) = \varphi_s$ and $n_{i(e)}(a) = 0$. Far from the individual grain (no other grains are present) $\varphi(\infty) = 0$ and $n_i(\infty) = n_e(\infty) = n_0$, where n_0 is the unperturbed plasma density.

In the limit $a/\lambda_{De} \rightarrow 0$ we get the following asymptotic expressions for the ion and electron fluxes to the grain:

$$J_i = 4\pi a n_0 D_i \frac{z\tau}{1 - \exp(-z\tau)}, \quad J_e = 4\pi a n_0 D_e \frac{z \exp(-z)}{1 - \exp(-z)}, \quad (20)$$

Note, that in the limit of an uncharged grain ($z \rightarrow 0$) the currents (20) reduce to the correct continuum limit results $J_{i(e)} = 4\pi an_0 D_{i(e)}$.

In practice, one can usually neglect the exponentially small terms appearing in the denominators of Eq. (20) and simplify these expressions as

$$J_i \simeq 4\pi an_0 D_i z \tau \quad (21)$$

$$J_e \simeq 4\pi an_0 D_e z \exp(-z). \quad (22)$$

The equilibrium surface potential (floating potential) is determined from the flux balance condition $J_e = J_i$. The result is particularly simple in a one-temperature plasma, $z \simeq \ln(D_e/D_i)$. Very good agreement between this expression and floating potentials obtained from the exact numerical solution in the limit $a/\lambda_{De} \rightarrow 0$ has been documented in the literature. In a two-temperature plasma the floating potential is $z \simeq \ln[(D_e/D_i)\tau]$.

The regime considered above corresponds to the situation where both electrons and ions are collision dominated. In this respect, this regime is sometimes referred to as “*fully collisional*” plasma (FCP). The regime where only one component – the ion component – is collision dominated, while electrons are not, can also be of interest. This situation will be considered below.

In noble gases the characteristic cross section for ion-neutral collisions σ_{in} is typically between one and two orders of magnitude larger than that for electron-neutral collisions σ_{en} . In addition, in argon, krypton, and xenon σ_{en} has a pronounced minimum for electron energies of about 1 eV, which is called the Ramsauer-Townsend effect. Consequently, there is a wide pressure range where the electron transport to the grain is collisionless while the ion transport is still collision dominated. This situation is sometimes described as “*partially collisional*” plasma (PCP).

The flux of collisionless electrons can be calculated using the OML theory, which yields Eq. (10) (see Section I.2). Similarly to the FCP case, electron distribution around a negatively charged grain is to a good accuracy given by the Boltzmann relation. The deviations are noticeable only in the region close to the grain surface, where the electron density approaches half of the Boltzmann value due to absorption. This leads us to conclusion that the ion transport to the grain is governed by essentially the same equations with identical boundary conditions as in the FCP case. Consequently, we can use Eq. (21) to estimate the ion flux to the grain. From the flux balance condition we then get for the reduced floating potential

$$z\tau \exp(z) \simeq \frac{1}{\sqrt{2\pi}} (a/\ell_i) (v_{Te}/v_{Ti}). \quad (23)$$

The floating potential depends on the plasma (ion) collisionality – z increases with decreasing ion mean free path ℓ_i , (i.e., with increasing collisionality).

3.2 Anisotropic conditions

To understand how ion flows can affect particle charging in the highly collisional regime we consider the following idealized situation: Absorbing particle is in the origin of the coordinate system, ions are flowing with velocity \mathbf{u} parallel to the x -axis, electrons provide immobile neutralizing background. The interaction between the ions and the particle is described by the pure Coulomb potential, $U(r) = Qe/r$. In this simple formulation the problem can be solved analytically (Hutchinson, 2007) and we sketch this solution.

If we neglect ion inertia, the equation to be solved is

$$\frac{Qe\mathbf{r}}{r^3} - m\nu \left(\frac{d\mathbf{r}}{dt} - \mathbf{u} \right) = 0, \quad (24)$$

where ν is the effective frequency of ion momentum loss (in collisions with neutrals). Measuring the distances in units of $\xi = \sqrt{|Q|e/m\nu u}$ and time in units of ξ/u the equations of ion motion in Cartesian coordinates become $\dot{x} = -x/r^3 + 1$ and $\dot{y} = -y/r^3$, which yields $dx/dy = (x - r^3)/y$. If we now introduce the angle θ that the vector \mathbf{r} makes with the x -axis and express the trajectory in terms of y and θ we get $ydy = \sin\theta d\theta$. This implies that along the trajectory we have

$$y^2 = \rho^2 - 2 - 2\cos\theta, \quad (25)$$

where ρ is the conventional impact parameter. There are two types of trajectories. First are finite and they end at the origin ($y = 0$). For these trajectories the angle θ varies in the range from 0 to π . The maximum impact parameter for this type of trajectories is therefore $\rho_c = 2$. If $a_0 = a/\xi$ is the reduced particle radius, then for $a_0 \leq 1$ all (and only) ions having finite trajectories are collected. The ion flux in dimensional form is

$$J_i = \pi\rho_c^2\xi^2n_iu = 4\pi an_iD_iz\tau, \quad (26)$$

where $D_i \sim v_{Ti}^2/\nu$ is the ion diffusion coefficient. This equation is equivalent to Eq. (21) derived above for the isotropic plasma regime.

For $a_0 > 1$ the particle collects all ions having finite trajectories and some ions having infinite trajectories. The tangent trajectory is characterized by $y = a_0 \sin\theta$ and $\cos\theta = a_0^{-2}$. We have therefore $\rho_c = \sqrt{a_0^2 + 2 + 1/a_0^2}$. The ion flux in dimensional form is

$$J_i = \pi\rho_c^2\xi^2n_iu = \pi an_iD_iz\tau \left(2 + \frac{z\tau D_i}{ua} + \frac{ua}{z\tau D_i} \right). \quad (27)$$

For very high drift velocity, the flux tends to its geometrical asymptote, $J_i \simeq \pi a^2 n_i u$.

Exercise. Find the ratio of the flux collected by the upstream and downstream sides of the sphere (simplified version of a Mach probe) in highly collisional plasma with the ion drift.

4 Charging in weakly collisional regime and interpolation for arbitrary collisionality

As we have seen, in the partially collisional plasma regime (when only ions are collisional), collisions suppress the ion flux, but do not affect the electron flux. In this regime, $|Q|$ increases, since the ion flux decreases. On the contrary, in the intermediate weakly collisional regime, the ion flux can increase considerably as a result of ion collisions with neutrals (Zobnin *et al.*, 2000). This results in a non-monotonous dependence of particle charge on ion collisionality. It is important to discuss this weakly collisional regime in detail, because it corresponds to the most common situation encountered in gas discharges. We will also discuss a possible approximation that can be used to describe the ion flux to the grain in the regime of arbitrary collisionality.

4.1 Role of ion-neutral collisions in weakly collisional regime

The following qualitative arguments for the role of ion-neutral collisions in the perturbed plasma region around a particle in the weakly collisional regime apply. It is instructive to think of a sphere of a radius R_0 such that inside this sphere the (attractive) interaction between an ion and the grain is sufficiently strong. The distance R_0 can be roughly determined from the condition that the energy of ion-grain interaction for $r \leq R_0$ is higher than the average ion kinetic energy after a collision with a neutral. If an ion undergoes a collision (especially of resonant charge exchange type) with a neutral within $r < R_0$, then a fast ion is removed and a slow ion is created. This new low-energy ion has very low probability to overcome the attraction of the grain and escape back into the plasma bulk. It will eventually reach the grain surface, either directly (low angular momentum) or through subsequent collisions (high angular momentum). Thus, essentially every (charge exchange) collision of an ion within $r < R_0$ results in ion collection by the grain. The collisional contribution to the collected ion flux can be estimated as the influx of ions through the spherical surface of radius R_0 ($\simeq \sqrt{8\pi} R_0^2 n_i v_{T_i}$) multiplied by the probability to experience a collision within this sphere ($\sim R_0/\ell_i \ll 1$ in the weakly collisional regime), where $n_i \simeq n_0$ is the ion density in the unperturbed region

far from the grain. We get therefore

$$\Delta J_{\text{coll}} \simeq \sqrt{8\pi} n_0 v_{T_i} (R_0^3 / \ell_i). \quad (28)$$

If we add this to the collisionless orbital motion limited (OML) ion flux (see Section I.2), we obtain an approximate expression derived by Lampe *et al.* (2003)

$$J_i \simeq \sqrt{8\pi} a^2 n_0 v_{T_i} \left[1 + z\tau + (R_0^3 / a^2 \ell_i) \right]. \quad (29)$$

Note that introducing the effective ion-neutral collision frequency, $\nu_{\text{in}} = v_{T_i} / \ell_i$, the collisional contribution can be written as $\Delta J_{\text{coll}} \simeq \sqrt{8\pi} R_0^3 n_0 \nu_{\text{in}}$. This is by about 20% larger than a simplified, but physically transparent estimate

$$\Delta J_{\text{coll}} \simeq (4\pi/3) R_0^3 n_0 \nu_{\text{in}}, \quad (30)$$

implying that the collisional correction to the ion flux is roughly the number of ion-neutral collisions per unit time inside the sphere of radius R_0 . In general, $n_i(r)$ can experience significant perturbations in the vicinity of the grain, but from the derivation above it is clear that the unperturbed value n_0 should be used in Eq. (30).

An important issue is related to an adequate definition of the interaction radius R_0 . A rough estimate can be obtained from the semi-obvious condition $|U(R_0)| \simeq T_i$, where $U(r)$ denotes the energy of interaction between the particle and the ions. The problem of the potential distribution about a charged particle in plasmas will be considered in detail in Chapter II. Now we consider two simple special situations. When ion-particle interaction is weak, which can be quantified as a smallness of the ion Coulomb radius $R_C \equiv |Q|e/T_i$ in comparison with the plasma screening length λ , screening is virtually unimportant with respect to the determination of R_0 . In this case one can simply assume $R_0 \sim R_C$. This situation can occur for sufficiently small grains. In the opposite case, screening becomes important. In the first approximation one can assume the Debye-Hückel (Yukawa) potential around the grain. Then, the ratio R_0/λ is given by the root of the transcendental equation $z\tau \exp(-x) = x(\lambda/a)$. In this case expression (29) can be further simplified (Khrapak *et al.*, 2005). The last term in the parentheses in Eq. (29) can be roughly estimated as $0.1z^2\tau^2(\lambda/\ell_i)$ in a wide range of plasma parameters relevant from the practical point of view. This results in

$$J_i \simeq \sqrt{8\pi} a^2 n_i v_{T_i} \left[1 + z\tau + 0.1z^2\tau^2(\lambda/\ell_i) \right]. \quad (31)$$

This expression is sometimes referred to as the collision enhanced collection (CEC) approximation. Note, that in this approximation z depends on τ and λ/ℓ_i , but is independent of the ratio a/λ .

Exercise. Using CEC find the condition indicating that the effect of ion-neutral collisions provides considerable contribution to the ion flux.

4.2 Electron impact ionization

The arguments applied above to evaluate the effect of ion-neutral charge exchange collisions are equally relevant to the electron impact ionization events (Khrapak and Morfill, 2012). When neutral atom is ionized within $r < R_0$ from the grain, a new slow ion is created, which has almost no chances to escape from the potential well. It will, therefore, very likely reach the grain surface. From the point of view of contribution to the collected ion flux, resonant charge exchange collisions and ionization events are essentially equivalent. The ionization-driven contribution to the ion flux is thus simply given by the ionization rate inside the sphere of radius R_0 surrounding the grain. In full analogy with Eq. (30) we write

$$\Delta J_I \simeq (4\pi/3)R_0^3\alpha n_0\nu_I, \quad (32)$$

where ν_I is the ionization frequency and the coefficient $\alpha (< 1)$ accounts for electron depletion near the grain. Normally, $\alpha \simeq 1$, because perturbations in $n_e(r)$ are essentially localized to a close proximity of the grain. Since R_0 is determined by the ion energy scale, for $\tau \gg 1$ the main contribution to the ionization comes from the region where the difference between $n_e(r)$ and n_0 is vanishingly small. The relative magnitude of ionization and collisional effects is therefore roughly given by the ratio of the corresponding frequencies:

$$\Delta J_I/\Delta J_{\text{coll}} \equiv \mathcal{K} \simeq \nu_I/\nu_{\text{in}}. \quad (33)$$

This implies that in the first approximation the effect of ion-neutral collisions and electron impact ionization can be added in a simple superposition, i.e. we can write

$$J_i \simeq J_{\text{OML}} + (1 + \mathcal{K}) \Delta J_{\text{coll}}. \quad (34)$$

As a final remark, we point out that although electron impact ionization often represents the dominant mechanism of plasma production in gas discharges, any other ionization mechanism would be equally important for charging.

Example 6: *Estimate the conditions when $\mathcal{K} \simeq 1$ for a typical gas discharge in Argon.*

4.3 Interpolation formula

We have derived approximate expressions for the ion flux, which are applicable in the weakly collisional (WC) regime and in the strongly collisional (SC) regimes. The questions arise, whether these can be combined to yield an approximation for arbitrary ion collisionality. Hutchinson and Patacchini (2007)

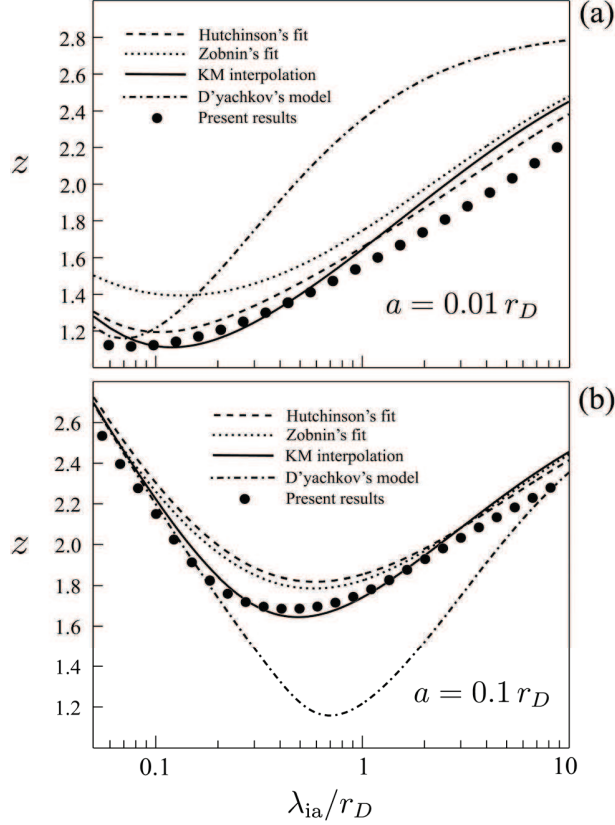


Fig. 4. The reduced grain potential z as a function of ion collisionality index λ_{ia}/r_D ($\equiv \ell_i/\lambda_D$ in our notation). The results are presented for two grain sizes: $a = 0.01\lambda_D$ (a) and $a = 0.1\lambda_D$ (b). Plasma parameters are: Ar discharge with $T_i = T_n = 0.03$ eV, $T_e = 30T_i$, and $n_e = n_i = 10^8$ cm $^{-3}$. Solid curves correspond to the KM interpolation formula, dashed curves to the fit by Hutchinson and Patacchini (2007), dotted curves to the fit by Zobnin et al. (2008), and dashed-dotted curves to the model by Dyachkovs et al. (2007). Symbols correspond to the numerical results obtained by Semenov et al. (2012). From Semenov et al. (2012).

proposed the following simple combination

$$J_{\text{eff}} = \left(J_{\text{WC}}^{-\gamma} + J_{\text{SC}}^{-\gamma} \right)^{-1/\gamma}, \quad (35)$$

which accurately describes the ion fluxes in the corresponding limits of weak and strong ion collisionality and provides a reasonable interpolation between these limits. Here γ is the adjustable parameter controlling the maximum value of the effective ion flux. The particle charge and reduced potential can be then calculated from the usual flux balance condition $J_{\text{eff}} = J_e$.

Khrapak and Morfill (2008) proposed to use CEC approximation [Eq. (31)] for J_{WC} and strongly collisional expression [Eq. (21)] for J_{SC} and also to set $\gamma = 1$. This KM interpolation demonstrates reasonable agreement with various numerical simulations reported in the literature, especially in the regime of

small particles ($a \ll \lambda$) and high electron temperatures $\tau \gg 1$. An example of calculating the reduced particle surface potential using different methods is shown in Fig. 4.

5 Charging kinetics and charge fluctuations

An important characteristic of particle charging is the *charging frequency* Ω_{ch} . This is defined as the relaxation frequency for small deviations of the charge from its equilibrium value Q_{eq} . In the situation when the charging occurs by collecting electrons and ions and the charge is negative we readily obtain from Eq. (1)

$$\Omega_{\text{ch}} = -d(J_i - J_e)/dZ|_{Z_{\text{eq}}}, \quad (36)$$

where $Z_{\text{eq}} = Q_{\text{eq}}/e$ and $J_i(Z_{\text{eq}}) = J_e(Z_{\text{eq}}) = J_{\text{eq}}$. For small deviations of the particle charge from equilibrium, $Z_1(t) = Z(t) - Z_{\text{eq}}$ we have

$$\frac{dZ_1}{dt} + \Omega_{\text{ch}}Z_1 = 0. \quad (37)$$

Up to this point the particle charge has been treated as a continuous *regular* variable. However, the charging currents represent in reality sequences of events bound to electron and ion absorption or emission by the dust particle surface. These sequences and time intervals between the successive acts of absorption and emission are random. As a result, the particle charge can fluctuate around its average value.

Charge fluctuations due to discrete nature of charging can be described as a stationary, Gaussian and Markovian (or the Ornstein-Uhlenbeck) process. This process was originally adopted to describe the stochastic behavior of the velocity of a Brownian particle. In the above case, it describes the behavior of the deviation of a particle charge number from its average value.

Let us derive the main properties of charge fluctuations. For simplicity, we limit consideration to the particle charging by electron and ion collection (generalization to other charging mechanisms is trivial). The charge distribution function $W(Z)$ is generally governed by the following master equation:

$$\left. \frac{\partial W}{\partial t} \right|_Z = J_i W|_{Z-1} + J_e W|_{Z+1} - (J_i W + J_e W)|_Z, \quad (38)$$

where $f|_Z \equiv f(Z)$. Taking into account that $|Z| \gg 1$ for practically all experimental conditions, we can expand the right-hand side of Eq. (38) around the equilibrium charge Z_{eq} , using $Z - Z_{\text{eq}}$ as the smallness parameter. To the

lowest order Eq. (38) is reduced to the Fokker-Planck equation,

$$\frac{\partial W}{\partial t} = \frac{\partial}{\partial Z} \left[\Omega_{\text{ch}}(Z - Z_{\text{eq}})W + J_{\text{eq}} \frac{\partial W}{\partial Z} \right]. \quad (39)$$

The steady-state solution yields the Gaussian charge distribution, $W(Z) \propto e^{-(Z-Z_{\text{eq}})^2/2\langle Z_1^2 \rangle}$, with the charge dispersion

$$\langle Z_1^2 \rangle = J_{\text{eq}}/\Omega_{\text{ch}} \equiv \sigma_Z^2 Z_{\text{eq}}^2, \quad (40)$$

where σ_Z^2 is the relative dispersion (a convenient parameter which we will use below).

Exercise. Calculate Ω_{ch} and σ_Z^2 in the OML approximation (see Section I.2) Make a numerical estimate for typical plasma conditions.

The derived Fokker-Planck equation is equivalent to the Langevin equation,

$$\frac{dZ_1}{dt} + \Omega_{\text{ch}}Z_1 = f(t). \quad (41)$$

The stochastic function $f(t)$ mimics random acts of the individual electron/ion collection and satisfies the following properties: $\langle f(t) \rangle = 0$ and $\langle f(t)f(t') \rangle = 2J_{\text{eq}}\delta(t-t')$. From the solution of Eq. (41),

$$Z_1(t) = Z_1(0)e^{-\Omega_{\text{ch}}t} + e^{-\Omega_{\text{ch}}t} \int_0^t f(t')e^{\Omega_{\text{ch}}t'} dt',$$

one can deduce the principal stochastic properties of $Z_1(t)$:

(1) The charge fluctuation amplitude has zero average,

$$\langle Z_1 \rangle = 0. \quad (42)$$

(2) The charge autocorrelation function decays exponentially,

$$\langle Z_1(t)Z_1(t') \rangle = \langle Z_1^2 \rangle e^{-\Omega_{\text{ch}}|t-t'|}. \quad (43)$$

(3) The process $Y(t) = \int_0^t Z_1(t')dt'$ is Gaussian but neither stationary nor Markovian,

$$\langle Y(t)^2 \rangle = \frac{2\langle Z_1^2 \rangle}{\Omega_{\text{ch}}^2} (\Omega_{\text{ch}}t + e^{-\Omega_{\text{ch}}t} - 1). \quad (44)$$

Equivalently, the stochastic properties are obtained by taking charge moments of Eq. (39). Usually, it is enough to use these properties for investigating the influence of charge fluctuations on dynamic processes in dusty plasmas. In particular, the following investigations can be mentioned: dust stochastic

“heating” (in terms of the kinetic energy) in an external electric field; instabilities of particle oscillations due to charge fluctuations, dust diffusion across a magnetic field with main application to astrophysical plasma. Some of these effects are considered in Section VI.

We note that the discreteness of the charging process is not the only reason for particle charge fluctuation. Spatial and temporal variations in plasma parameters, collective effects in dusty plasmas constitute other sources of charge fluctuations. These issues, however, have been much less investigated.

II. Electric potential around a dust particle

Interactions between charged particles in complex (dusty) plasmas are responsible for a rich variety of phenomena, including self-organization, formation of ordered structures, phase transitions, etc. As in all interacting particle systems, the pair interaction potential is one of the most important factors determining the physics of these phenomena. Let us, therefore, discuss interaction mechanisms which can operate in complex plasmas. First of all, it is clear that the charged particles interact electrically and this interaction is determined by the structure of the electric potential around the particles. We therefore first focus on the electrical potential distribution around a small charged object (dust grain) immersed in a plasma.

1 Debye-Hückel theory

It is often assumed that the electric potential around a small particle in isotropic plasmas can be described by the Debye-Hückel (Yukawa) form,

$$\varphi(r) = (Q/r) \exp(-r/\lambda), \quad (45)$$

where Q is the particle charge. This result can be obtained by assuming Boltzmann distributions for ions and electrons and solving the linearized Poisson equation. In the linear regime λ is equal to the linearized Debye radius $\lambda_D^{-2} = \lambda_{Di}^{-2} + \lambda_{De}^{-2}$.

Exercise. *Derive Eq. (45) using the linear plasma response formalism.*

Should we take into account the finite particle size, Eq. (45) becomes

$$\varphi(r) = \varphi_s(a/r) \exp\left(\frac{r-a}{\lambda}\right).$$

The relation between the charge and the surface potential is $Q = a\varphi_s(1+a/\lambda)$, which reduces to the vacuum result ($Q \simeq a\varphi_s$) used previously in typical for complex (dusty) plasmas situations with $a \ll \lambda$.

Linearization is often invalid in complex plasmas since the particle floating potential is $\varphi_s \sim -T_e/e$ and, therefore, ion-particle coupling is very strong close to the particle, provided $T_e \gg T_i$. Nevertheless, numerical solution of the non-linear Poisson-Boltzmann equation shows that the functional form of Eq. (45)

still persists, but the actual value of the particle charge should be replaced by an effective charge which is somewhat smaller in absolute magnitude.

2 Effect of plasma absorption on particles

An important characteristic property of complex (dusty) plasmas is the absorption of electrons and ions on the particle surface. The continuous ion and electron fluxes from the bulk plasma to the particle make their distributions non-Boltzmann. Although the deviations are only marginal for repelled electrons, for attracted ions they are quite substantial. In the absence of plasma production and loss in the vicinity of the particle, conservation of plasma flux completely determines the far asymptote of the potential. As a result, at large distances the potential is not screened exponentially but exhibits a power law decay. In collisionless plasmas the far asymptote scales as $\varphi(r) \propto r^{-2}$, while in collisional plasma $\varphi(r) \propto r^{-1}$.

To understand why the potential is not screened exponentially and has different asymptotes in collisionless and collisional limits the following approximate consideration can be useful. The deviation of ion and electron densities from the equilibrium (Boltzmann) values is due to continuous plasma absorption on the particle surface, which generates electron and ion fluxes in the surrounding plasma. Thus we roughly have $\delta n_{i,e}(r)/n_{i,e}(r) \simeq -J_{\text{eq}}/J_{i,e}(r)$, where $J_{i,e}(r)$ are the fluxes of ions and electrons entering the spherical surface of radius r *from the outside*, and J_{eq} denotes the equilibrium flux of electrons/ions, which is collected on the particle surface. Far from the particle, the electron density distribution is close to the equilibrium one, $n_e(r) \simeq n_0 \exp[e\varphi(r)/T_e]$, where n_0 is the unperturbed plasma density. In this region the plasma is quasineutral, which implies $n_i(r) \simeq n_0 \exp[-e\varphi(r)/T_i] + \delta n_i(r) \simeq n_e(r)$. Since at large distances the potential becomes sufficiently small we can expand exponential terms in power series. Keeping only the first two terms we immediately get

$$\varphi(r) \simeq -(T_i/e)[J_{\text{eq}}/J_i(r)]. \quad (46)$$

where we have assumed $T_e \gg T_i$. The last step in this consideration is to recognize that the influx $J_i(r)$ depends on the ion collisionality rate. For weakly perturbed collisionless Maxwellian ions the flux into the spherical surface of radius r is just $J_i \simeq \sqrt{8\pi}r^2n_0v_{T_i}$. In the highly collisional limit the ion flux is given by the Smoluchowski expression, $J_i(r) \simeq 4\pi rn_0D_i$, where $D_i \simeq \ell_i v_{T_i}$ is the ion diffusion coefficient. Substituting these expressions into Eq. (46) we immediately get asymptotic long-range behavior of the potential discussed above.

Closer to the particle (up to a distance of a few Debye radii from its surface),

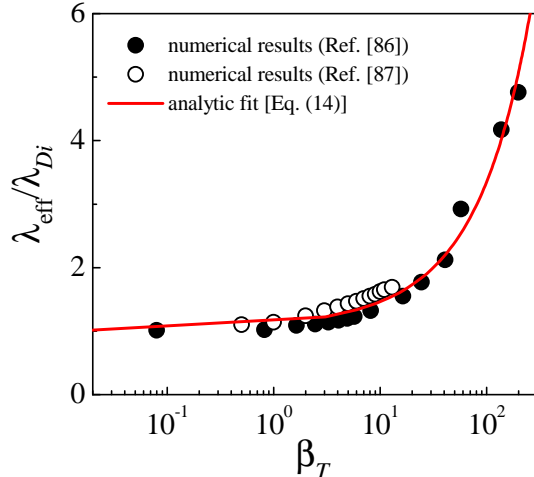


Fig. 5. Ratio of the effective screening length to the ion Debye radius, $\lambda_{\text{eff}}/\lambda_{D_i}$ as a function of the nonlinearity parameter $\beta_T = z\tau(a/\lambda_{D_i})$ of ion-particle interaction. Solid circles correspond to numerical calculations by Daugherty *et al.* (1992). Open circles correspond to numerical calculations by Klumov (2006). In both cases λ_{eff} is obtained from the best fit of the numerically calculated potential with the Debye-Hückel (Yukawa) expression. The solid curve corresponds to the fit of Eq. (47).

the Debye-Hückel (DH) form works reasonably well, but with $\lambda = \lambda_{\text{eff}}$, where the effective screening length λ_{eff} can deviate considerably from λ_D . For a particle much smaller than the ion Debye radius $\lambda_{\text{eff}} \simeq \lambda_D \simeq \lambda_{D_i}$. As the particle radius increases, λ_{eff} also increases and can reach values comparable to λ_{D_e} when $a \sim \lambda_{D_i}$. It has been suggested that the structure of the normalized electric potential computed numerically is rather insensitive to the separate values of the dimensionless parameters a/λ_{D_i} and $z\tau$, but depends universally on their product, the nonlinearity parameter for ion-particle interaction, $\beta_T = z\tau(a/\lambda_{D_i})$. Comparison between the available numerical results and the fit of the form

$$\lambda_{\text{eff}}/\lambda_{D_i} \simeq 1 + 0.013\beta_T + 0.105\beta_T^{1/2}, \quad (47)$$

shown in Fig. 5 demonstrates reasonable agreement.

3 Simple kinetic model

A simple linear kinetic model which accounts for the combined effect of ion absorption on the particle and ion-neutral collisions has been proposed independently by Filippov *et al.* (2007) and Khrapak *et al.* (2008). In this model a small (point-like) individual grain of negative charge Q immersed in a stationary isotropic weakly ionized plasma is considered. Plasma production and loss in the vicinity of the particle are neglected, except plasma absorption on the particle surface. This implies that the characteristic ionization/recombination length is considerably larger than the length scale under consideration. Elec-

tron density can be approximated with high accuracy by the Boltzmann distribution. The kinetic equation for the ions is

$$\frac{\partial f}{\partial t} + \mathbf{v} \cdot \frac{\partial f}{\partial \mathbf{r}} + \frac{e\mathbf{E}}{m} \cdot \frac{\partial f}{\partial \mathbf{v}} = -\nu(f - n_i f_M) - \delta(\mathbf{r})v\sigma(v)f, \quad (48)$$

where f is the ion velocity distribution function, f_M is the Maxwellian distribution (normalized to unity) and $n_i = \int f d^3v$ is the ion density. The first term on the right-hand-side is the model collision integral in the Bhatnagar-Gross-Krook form with a *constant* effective ion-neutral collision frequency ν . The second term represents the ion loss on a small particle and is expressed through the effective (velocity dependent) collection cross section $\sigma(v)$.

The equations for the electrons and ions are supplemented by the Poisson equation

$$\Delta\varphi = -4\pi e(n_i - n_e) - 4\pi Q\delta(\mathbf{r}). \quad (49)$$

Standard linearization procedure then yields

$$\varphi(r) = \varphi_I(r) + \varphi_{II}(r), \quad (50)$$

where the first term $\varphi_I(r)$ in is the familiar Debye-Hückel(DH) potential (45), while the second one, $\varphi_{II}(r)$, appears due to ion absorption by the particle and accounts for ion-neutral collisions. It is proportional to a certain integral over $\sigma(v)$ and depends on the (inverse) linearized Debye radius, $k_D = \sqrt{\lambda_{De}^{-2} + \lambda_{Di}^{-2}}$, ion collision frequency ν , and ion thermal velocity v_{Ti} . For a non-absorbing particle [$\sigma(v) \equiv 0$] only the conventional DH form survives, as expected. In this case ion-neutral collisions do not affect the potential distribution.

In the collisionless (CL) limit, using the OML collection cross section [Eq. (7)] we get the following long-range asymptote:

$$\varphi_{II}(r) \simeq -\frac{T_e}{e} \left(\frac{a}{r}\right)^2 \frac{1 + 2z\tau}{4(1 + \tau)}, \quad (51)$$

i.e. the potential scales as $\varphi(r) \propto r^{-2}$, as discussed in Section II.2.

Exercise. *Estimate the distance at which the transition from DH form to the long-range asymptote (51) occurs.*

In the opposite strongly collisional (SC) regime the actual form of $\sigma(v)$ is not important since the integral with $\sigma(v)$ can be directly expressed through the ion flux J_i . The potential is

$$\varphi_{II}(r) \simeq -\frac{e}{r} \frac{J_i}{D_i k_D^2} \left(1 - e^{-k_D r}\right), \quad (52)$$

where $D_i = v_{Ti}^2/\nu$ is the diffusion coefficient of the ions. The potential scales as $\varphi(r) \propto r^{-2}$, as discussed in Section II.2.

Exercise. Derive Eq. (52) using hydrodynamic (fluid) approximation for the ion component. Discuss the different behavior of the potential for negatively and positively charged grains.

The most interesting regime, relevant to many complex plasma experiments in gas discharges, is the weakly collisional (WC) regime, $\ell_i \gtrsim \lambda_D$. To calculate the potential in this case, the functional form $\sigma(v)$ is required, which is not known a priori. One of the reasonable simplifications would be to simply assume $\sigma(v) = \text{const}$, and express this constant in terms of the observable quantity – ion flux. We note, however, that to a good accuracy the (additional to Yukawa) potential in this case is simply a linear combination of Eqs. (51) and (52). After appropriate rearrangements we have therefore

$$\varphi_{\text{II}}(r) \simeq -\frac{e}{r} \frac{J_i}{k_D v_{T_i}} \left(\sqrt{\frac{\pi}{2}} \frac{1}{k_D r} + \frac{1}{k_D \ell_i} \right), \quad (53)$$

where the condition that Eq. (53) should essentially converge to Eq. (51) in the collisionless limit with OML flux has been used. The two terms in the square brackets of Eq. (53) correspond to absorption induced “collisionless” and “collisional” contributions, respectively.

Exercise. Estimate the distance at which the collisional contribution to the potential starts to dominate over the collisionless one.

To determine the ion flux J_i in Eq. (53) one can use approximations discussed in Sections I.3 and I.4. For instance, the CEC approximation [Eq. 31] can be employed in the weakly collisional regime and the continuum limit expression [Eq. (21)] in the strongly collisional limit. An example of the electric potential distribution calculated in this way is shown in Fig. 6. The plasma parameters used are representative for complex plasma experiments in gas discharges: argon gas, $\tau = 100$, and $k_D a = 0.01$. The solid curves correspond to numerical integrations for three different ion collisionality indexes $k_D \ell_i$, the dashed curve corresponds to the SC (in fact, FCP) limit, and the dotted curve to the CL limit. For reference, the dash-dotted curve shows the DH potential. Note that the particle surface potentials are different for different curves. This reflects the fact that not only the functional form of the potential, but also its initial value (at the surface), depend on the ion collisionality, as discussed in Section I.4.

4 Role of ionization and recombination

Here we focus on the effects associated with plasma production and loss in the surrounding plasma. For simplicity plasma absorption on the test particle surface is completely neglected. We assume that electron impact ionization is responsible for plasma production while plasma losses are due to the combined

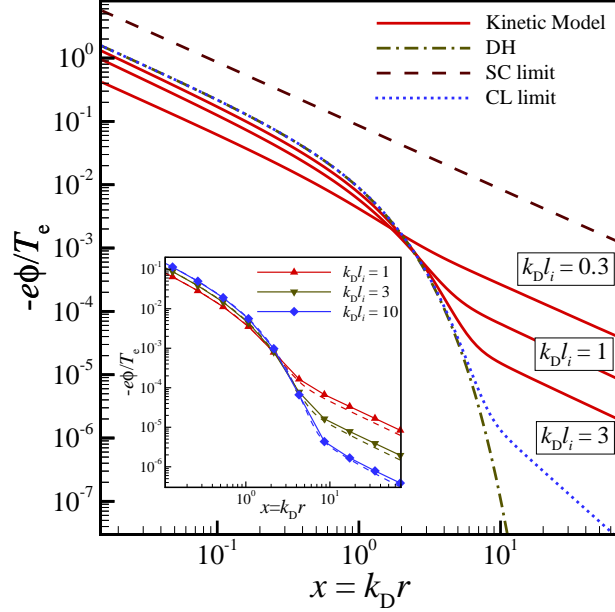


Fig. 6. Normalized electric potential around a small particle in an isotropic weakly ionized plasma versus normalized distance. The solid curves are obtained using numerical integrations. Dashed (dotted) curve corresponds to the analytic approximation in the strongly collisional (collisionless) limit. The dash-dotted curve shows the Debye-Hückel potential with the surface potential calculated from the (collisionless) OML model. The inset shows a comparison between direct numerical integrations (solid lines with symbols) and the approximate expression for the weakly collisional regime [Eqs. (50) and (53)]. From Khrapak *et al.* (2008).

effect of the three-body bulk recombination and ambipolar diffusion to plasma boundaries. Then using a simple linearized fluid approach we can show that in this case the electrical potential can be in general expressed as a sum of the unscreened Coulomb-like term (which is normally very small) and a pair of Debye-Hückel-like exponentially screened terms with quite different screening lengths (Khrapak *et al.*, 2010).

The continuity and momentum equations for ions are

$$\nabla(n_i \mathbf{v}_i) = \nu_I n_e - \nu_L n_i - \beta n_e n_i, \quad (54)$$

$$(\mathbf{v}_i \nabla) \mathbf{v}_i = -(e/m_i) \nabla \varphi - (v_{T_i}^2/n_i) \nabla n_i - \nu_i \mathbf{v}_i, \quad (55)$$

where \mathbf{v}_i is the velocity of the ions, ν_I is the ionization frequency, ν_L is the characteristic frequency of ambipolar losses, β is the recombination coefficient, and ν_i is the characteristic frequency of ion-neutral collisions. Similarly, the electron component is described by

$$\nabla(n_e \mathbf{v}_e) = \nu_I n_e - \nu_L n_e - \beta n_e n_i, \quad (56)$$

$$(\mathbf{v}_e \nabla) \mathbf{v}_e = (e/m_e) \nabla \varphi - (v_{T_e}^2/n_e) \nabla n_e - \nu_e \mathbf{v}_e, \quad (57)$$

where \mathbf{v}_e is the electron velocity and ν_e is the characteristic frequency of electron-neutral collisions. In the unperturbed state the plasma is charge neutral, $n_e = n_i = n_0$, and hence $\beta n_0 = \nu_I - \nu_L$. The system (54)-(57) is supplemented by the Poisson equation (49).

Standard linearization procedure applied to this system yields

$$\varphi(r) = \frac{Q}{r} \left(\delta + \epsilon_1 e^{-k_1 r} + \epsilon_2 e^{-k_2 r} \right), \quad (58)$$

where δ is normally quite small and can be neglected, $k_{1,2}$ can be expressed via k_D , ν_I/D_i , βn_0 , as well as ion and electron diffusion coefficients. The factors $\epsilon_{1,2}$ are, in turn, expressed via k_D , k_1 and k_2 .

This shows that in collisional plasmas, with the considered mechanisms of plasma production and loss, the electrical potential around a test charge consists of one unscreened Coulomb term and two exponentially screened Coulomb (Yukawa) terms with different screening lengths. This is quite different from the conventional Debye-Hückel picture of a test charge shielding in plasmas. The reason for this difference is obviously plasma production and loss processes. Normally, the unscreened term is quite small and can be neglected. The electrical potential can thus be well approximated by a double-Yukawa potential.

Exercise. Calculate the potential in the case of complete absence of plasma production and loss processes.

Exercise. Calculate the potential in the case when all losses are due to the three-body recombination.

5 Anisotropic conditions and plasma wakes

Electric fields are often present in laboratory conditions (e.g., in rf sheaths or dc striations). This induces an ion drift and, hence, creates a perturbed region of plasma density around the particle, caused by downstream focusing of ions – the so-called “plasma wake”. One can apply the linear dielectric response formalism to calculate the potential distribution in the wake. This approach is applicable provided ions are weakly coupled to the particle (i.e. the region of nonlinear ion-particle electric interaction is small compared to the plasma screening length). Note that higher ion drift velocities imply better applicability of the linear theory. The electrostatic potential created by a point-like charge at rest is defined in this approximation as

$$\varphi(\mathbf{r}) = \frac{Q}{2\pi^2} \int \frac{e^{i\mathbf{k}\mathbf{r}} d\mathbf{k}}{k^2 \epsilon(0, \mathbf{k})}, \quad (59)$$

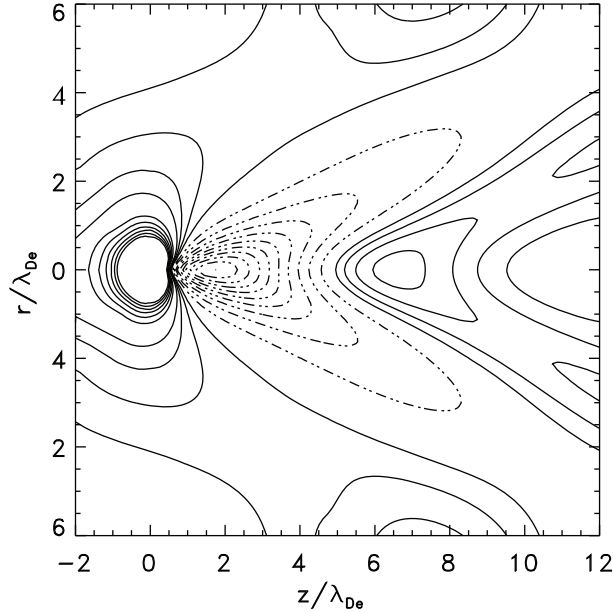


Fig. 7. *Example of plasma wake. The figure illustrates the complex structure of the wake potential $\varphi(\mathbf{r})$ (plasma flows to the right). Calculations are for collisionless ions with a shifted Maxwellian distribution ($M_T = 7.5$) and for Boltzmann electrons ($\tau = 25$). The (negatively charged) grain is at the center of the left-most node, solid and dashed curves indicate contour lines for negative and positive potentials, respectively, distance is in units of λ_{De} . From Lampe et al. (2000).*

where $\varepsilon(\omega, \mathbf{k})$ is the plasma permittivity and \mathbf{u} is the ion flow velocity. Using a certain model for the permittivity, one can in principle calculate the anisotropic potential distribution. The potential profile can also be obtained from numerical modeling.

Physically, the generation of plasma wakes in anisotropic dusty plasmas is similar to the generation of electromagnetic waves by a particle which is placed in a moving medium, and the analogy with the Vavilov-Cherenkov effect can be useful. The potential is no longer monotonic within a certain solid angle downstream from the particle, but has a well pronounced extremum (maximum for a negatively charged particle). Numerical modeling shows that the shape of the wake potential is sensitive to the ion-neutral collisions and the electron-to-ion temperature ratio which governs Landau damping. In typical situations, these mechanisms can effectively “smear out” the oscillatory wake structure, leaving a single maximum.

Let us illustrate how the wake potential depends on the plasma flow. The ion drift velocity is conveniently characterized by the value of the “thermal” Mach number, $M_T = u_i/v_{Ti}$. The pronounced anisotropic wake structure appears both in subthermal and superthermal regimes of the drift (both regimes are ubiquitous for typical experimental conditions). An example of potential distribution in the plasma wake is presented in Fig. 7.

First let us consider subthermal ion drift, $M_T \lesssim 1$. The potential profile in this case can be calculated from Eq. (59) analytically within the Bhatnagar-Gross-Krook (BGK) approach for the ion-neutral collision integral. The far-field potential has a well-known $\propto r^{-3}$ asymptote (Montgomery *et al.* 1968). By combining this with the near-field Yukawa core, in the case of small collisionality (viz., small ratio of the ion-neutral collision frequency to the ion plasma frequency) we can approximate the potential by the following expression (Kompaneets 2007):

$$\varphi(r, \theta) = Q \left[\frac{e^{-r/\lambda_D}}{r} - 2\sqrt{\frac{2}{\pi}} \frac{M_T \lambda_D^2}{r^3} \cos \theta - \left(2 - \frac{\pi}{2}\right) \frac{M_T^2 \lambda_D^2}{r^3} (3 \cos^2 \theta - 1) \right]. \quad (60)$$

Equation (60) is written in spherical coordinates, where θ is the angle between \mathbf{r} and \mathbf{u}_i , and is accurate to $o(M_T^2/r^3)$. It shows that microparticles attract each other in a certain solid angle along the flow, and repel in the transverse direction. Such behavior is usually observed in ground-based experiments – particles levitating in, e.g., (pre) sheaths of rf discharges form stable vertical “chains” (see Fig. 17).

In some ground-based experiments particles levitate in the regions where the electric field is so strong that the thermal Mach number can be significantly larger than unity; also, the collisionality can be rather high. The BGK collision integral is no longer applicable in this case, because in highly suprathermal regimes the ion *mean free path* rather than the collision frequency should be considered constant. Solution of the kinetic equation with a constant mean free path yields the following asymptotic form of the ion velocity distribution $f(\mathbf{v})$ in the formal limit $M_T \rightarrow \infty$:

$$f(\mathbf{v}) = n_i \sqrt{\frac{2m}{\pi T_{\parallel}}} \exp\left(-\frac{mv_z^2}{2T_{\parallel}}\right) \delta(\mathbf{v}_{\perp}), \quad v_z > 0, \quad (61)$$

whereas for $v_z < 0$ we have $f = 0$ (electric field \mathbf{E} is directed along the z axis). Here $T_{\parallel} = eE\ell_i$ is the field-induced “temperature” characterizing such *half-Maxwellian* distribution. The distribution function given by Eq. (61) significantly deviates from the velocity distribution obtained in the framework of the conventional BGK approach.

In such highly suprathermal collisional regime, $M_T \gg 1$, the wake potential given by Eq. (60) is no longer applicable as well. The calculations based on the constant-mean-free-path model provide the potential distribution for this case Kompaneets *et al.* (2007). We give (without derivation) the final result for the asymptotic behavior of the potential at large distances

$$\varphi(r, \theta) = -\frac{Q\lambda^2 \cos \theta}{\ell_i r^2} \left(\frac{2}{1 + \cos^2 \theta} \right)^{3/2} + O\left(\frac{1}{r^3}\right), \quad (62)$$

where $\lambda = [eE\ell_i/(4\pi n_i e^2)]^{1/2}$ is the “field-induced” Debye length. Equation (62) demonstrates that at large distances the test charge produces a dipole-like field, with the dipole moment $Q\lambda^2/\ell_i$. For a negatively charged grain ($Q < 0$), this dipole moment is directed along the ion drift. Note the difference from the pure dipole field, due to additional anisotropic factor $[2/(1 + \cos^2 \theta)]^{3/2}$.

III. Interactions between dust particles

Besides electrical effects, there exist other mechanisms that can contribute to interparticle interactions in complex plasmas. These are associated with the specific property of complex plasmas – their thermodynamic openness caused by the continuous exchange of matter and energy between the particles and surrounding plasma. We will consider two such mechanisms – ion and neutral shadowing interactions. We will also briefly discuss the emerging possibilities to tune and design interactions in complex plasmas.

1 Electrical interactions

Let us first consider the electric interaction between a pair of particles. Assuming for simplicity that the particles have equal charges which are independent of their separation r , the interaction energy is

$$U(r) = Q\varphi(r). \quad (63)$$

As discussed above, depending on plasma parameters and interparticle separation the interparticle electric interaction can exhibit properties of exponentially screened Coulomb (Yukawa) or inverse power-law ($\propto r^{-2}$ or $\propto r^{-1}$) potentials (as well as their combinations). Positively charged particles can attract each other electrically. In anisotropic plasmas, the interactions are greatly affected by the plasma wakes formed downstream from the particles.

2 Neutral shadowing

A specific mechanism of interaction can be associated with the neutral component, provided the particle surface temperature is different from the temperature of the surrounding neutral gas (Tsytovich *et al.* 1998). If the particle surface is hotter there is a net momentum flux from the particle into the plasma which results in the repulsion between a pair of particles placed close to each other. If the particle surface is colder, the momentum flux from neutral gas to the particle generates attraction between the particles. In the free molecular (kinetic) regime an expression for this “neutral shadowing” interaction

potential is

$$U_{\text{sh},n}(r) = \frac{3\pi}{8} \frac{\delta T}{T_n} \frac{a^4 p}{r}, \quad (64)$$

where p is the neutral gas pressure and $\delta T = T_s - T_n$ is the difference between the temperatures of the particle surface and surrounding neutral gas.

Some experiments and theoretical estimations demonstrate that in low pressure gas discharges the particle surface temperature is normally somewhat hotter (by about 10 – 20%) than the neutral gas temperature. This is, however, not sufficient to make this effect the dominant mechanism of interaction in complex plasmas.

3 Ion shadowing

Constant plasma absorption on the particle surfaces gives rise to a so-called “ion shadowing” interaction (Ignatov, 1996; Tsytovich *et al.* 1996). This interaction basically represents the ion drag force (see Section V.5) that one particle experiences as a consequence of the ion flux directed to another neighboring particle and vice versa. The ion shadowing force is always attractive. An approximate expression for the ion shadowing potential taking into account the effect of ion-neutral collisions in the weakly collisional regime is

$$U_{\text{sh},i}(r) \simeq -\frac{1}{3} \sqrt{\frac{2}{\pi}} \frac{Qe J_{\text{eq}} \Lambda Qe}{v_{T_i} T_i} \frac{1}{r}, \quad (65)$$

where J_{eq} is the equilibrium ion flux on the grain surface (see Section I.5) and Λ is the appropriate Coulomb logarithm (see Section IV.2) Although the ion shadowing interaction is not pairwise, because it depends on the mutual orientation of the particles (when more than two particles are involved), for sufficiently rarefied systems (when interaction occurs mostly through binary collisions) Eq. (65) is expected to be a good approximation.

Analysis of Eqs. (53) and (65) reveals that at large distances both interaction potentials are proportional to J_{eq} , which is not surprising since both interaction mechanisms stem from the conservation of the ion flux collected by the particle. Both interactions have r^{-1} long-range asymptote. Therefore, depending on their relative magnitudes either attraction or repulsion occurs.

Exercise. *Derive an approximate condition when ion shadowing dominates over the electrical repulsion.*

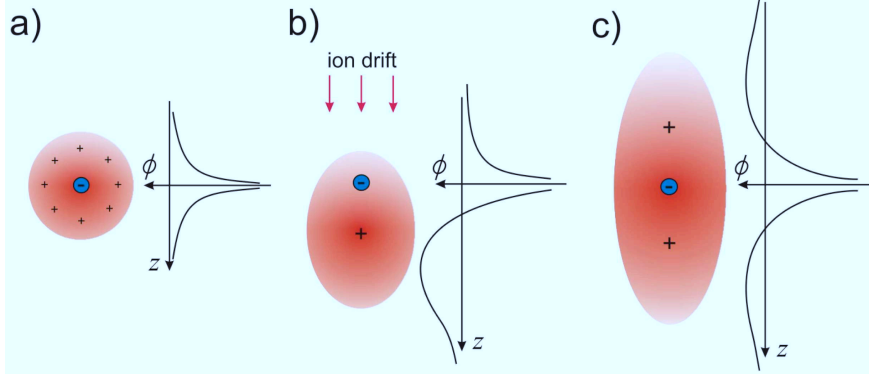


Fig. 8. *Field-induced potential of a dust particle. (a) The polarizable ion cloud around the particle and, hence, the particle potential $\varphi(\mathbf{r})$ are spherically symmetric in the absence of an external electric field. (b) When a dc field is present, the center of the ion cloud is shifted downwards from the particle (wake effect), generating a non-reciprocal potential $\varphi(\mathbf{r}) \neq \varphi(-\mathbf{r})$. (c) A reciprocal potential is created by employing an uniaxial ac electric field.*

4 Tunable interactions

The external electric field can play the role of a new degree of freedom that allows us to “tune” the interaction between particles, as illustrated in Fig. 8. Without an external field, the cloud of compensating plasma charges surrounding negatively charged microparticles is spherical (it is usually referred to as “Debye sphere”). When a dc field is applied, the cloud is shifted downstream from the particle, along the field-induced ion drift, and acquires a fairly complicated shape (then it is called “plasma wake”, see Section II.5). In this case the pair interaction between charged microparticles is generally nonreciprocal (i.e., non-Hamiltonian, see Section VII.2.1). The non-reciprocity of the interaction could only be eliminated if the wake potential were an even function of coordinates, i.e., $\varphi(\mathbf{r}) = \varphi(-\mathbf{r})$. A simple “recipe” to create such a potential is as follows (Ivlev, 2008): One has to apply an ac field of a frequency that is (i) much lower than the inverse timescale of the ion response (ion plasma frequency, typically $\sim 10^7 \text{ s}^{-1}$) and, at the same time, (ii) much higher than the inverse dust response time (dust plasma frequency, typically $\sim 10^2 \text{ s}^{-1}$ or less). Then the ions react instantaneously to the field whereas the microparticles do not react at all. The effective interparticle interaction in this case is determined by the *time-averaged* wake potential. The result-

ing interaction is rigorously reciprocal (Hamiltonian), so that one can directly apply the formalisms of statistical physics.

Quantitatively, the field-induced interaction can be determined from the linearized dielectric response formalism (see Section II.5). For subthermal ion drift the interaction potential is given by Eq. (60), which basically represents the far-field asymptotics for the potential expanded into a series over small ion Mach numbers M_T (with the angular dependence of the first three coefficients being proportional to that of the corresponding multipoles, i.e., charge, dipole, quadrupole). Furthermore, all “odd” terms ($\propto M_T^j$ with odd j) are proportional to linear combinations of the odd-order Legendre polynomials whereas “even” terms are combinations of the even-order polynomials. Thus, for an ac field $E(t)$ with $\langle E \rangle_t = 0$, all odd-order terms disappear in the time-averaged potential $\langle \varphi \rangle_t$, which becomes an even function of coordinates. Thus, the effective pair interaction $Q\langle \varphi \rangle_t$ is a sum of a spherically-symmetric core (represented, e.g., by the Debye-Hückel potential) and a field-induced contribution, with the leading term due to the quadrupole part of the wake. The latter is given by

$$U_{\text{field}}(\mathbf{r}) = - \left(2 - \frac{\pi}{2} \right) \frac{\langle M_T^2 \rangle_t Q^2 \lambda_D^2}{r^3} (3 \cos^2 \theta - 1). \quad (66)$$

The charge-quadrupole interaction is identical to the interaction between two equal and parallel dipoles of magnitude $\simeq 0.65 M_T Q \lambda_D$ (the time-averaging brackets are omitted). This implies that for small M_T the field-induced interactions are *equivalent* to dipolar interactions.

IV. Momentum exchange between plasma species

The momentum exchange between different species plays an exceptionally important role in complex plasmas. For example, the momentum transfer in collisions with the neutral gas “cool down” the system, in particular grains and ions, introducing some damping. The forces associated with the momentum transfer from electrons and ions to the charged grains – the electron and ion drag forces – often determine static and dynamical properties of the grain component, affect wave phenomena, etc. The momentum exchange in grain-grain collisions and its competition with the momentum transfer in grain-neutral gas collisions governs grain transport properties, scalings in fluid flows, etc.

In this Chapter, we assume the Debye-Hückel (Yukawa) potential around the dust particle and perform a detailed analysis of the binary collisions involving the dust particles. First, the momentum transfer cross section for different types of collisions is calculated and analytical approximations for some limiting cases are derived. These approximations are used to estimate the characteristic momentum exchange rates in complex plasmas. This provides us with a unified theory of momentum exchange in complex plasmas in the *binary collision approximation*.

1 Momentum transfer cross section

The momentum transfer (scattering) cross section in the binary collision approximation can be defined as the integral over the impact parameters

$$\sigma_s = 2\pi \int_0^\infty [1 - \cos \chi(\rho)] \rho d\rho, \quad (67)$$

where χ is the deflection (scattering) angle. The latter depends on the impact parameter in the following way, $\chi(\rho) = |\pi - 2\varphi(\rho)|$, where $\varphi(\rho) = \rho \int_{r_0}^\infty dr r^{-2} [1 - U_{\text{eff}}(r, \rho)]^{-1/2}$, $U_{\text{eff}}(r, \rho) = \rho^2/r^2 + 2U(r)/\mu v^2$ is the reduced effective potential energy, and μ is the reduced mass. The distance of closest approach, $r_0(\rho)$, in the integral above is the largest root of the equation $U_{\text{eff}}(r, \rho) = 1$.

Exercise. Calculate the momentum transfer cross section for collisions between small point-like particles and a stationary hard sphere of radius a as-

suming (a) absorption upon collision and (b) specular reflection upon collision.

In the context of complex plasmas we consider binary collision between two particles of masses m_1 and m_2 interacting via isotropic Yukawa potential

$$U(r) = -(U_0/r) \exp(-r/\lambda),$$

where λ is the *effective* screening length, $U_0 > 0$ for attraction and $U_0 < 0$ for repulsion. The particle trajectories during collision are ballistic, i.e., any types of multiple collisions are neglected. The problem is equivalent to the scattering of a single particle of reduced mass, $\mu = m_1 m_2 / (m_1 + m_2)$, in the central field $U(r)$ (located at the center of masses of colliding particles). First, we address the case of point-like particles and then briefly discuss the role of the finite grain size.

The *scattering parameter*, $\beta(v) = |U_0|/\mu v^2 \lambda$, is the ratio of the Coulomb radius, $R_C = |U_0|/\mu v^2$, to the effective screening length λ . It characterizes the “coupling” between colliding particles: The coupling is weak when the characteristic distance of interaction $R_0 \sim R_C$, introduced through $|U(R_0)| = \frac{1}{2}\mu v^2$, is shorter than λ , i.e., when $\beta(v) \ll 1$. In the opposite limit, $\beta(v) \gg 1$, when $R_0 \gg \lambda$, the coupling is strong. In addition, the normalized momentum transfer cross section, σ_s/λ^2 , depends only on β , which makes $\beta(v)$ a *unique parameter* which describes momentum exchange for Yukawa interactions.

Exercise. *Derive the momentum transfer cross section for Yukawa potential in the limit of weak coupling.*

The theory of Coulomb scattering, which assumes an unscreened (Coulomb) potential and a cutoff at $\rho_{\max} = \lambda$ in the integral (67), is widely used to describe momentum exchange in collisions between charged particles (e.g., electron-ion collisions in plasmas). It holds for $R_C \sim R_0 \ll \lambda$ or $\beta \ll 1$, i.e., in the limit of weak coupling. However, for $\beta \geq 1$ the theory of Coulomb scattering is not applicable: In this case the interaction range R_0 is larger than the screening length and a considerable fraction of the interaction occurs outside the Debye sphere providing substantial contribution to the momentum transfer. The use of a cutoff at $\rho_{\max} = \lambda$ considerably underestimates the momentum transfer in this case.

What are characteristic values of the scattering parameter for different types of collisions involving dust grains in complex plasmas? Taking into account that $|U_0| \sim |Z|e^2$ for grain-electron and grain-ion collisions, and $|U_0| \sim Z^2 e^2$ for grain-grain collisions we get the following hierarchy of characteristic scattering parameters: (i) *Grain-electron* collisions, $\beta_T^{de} \sim z(a/\lambda) \sim 0.01 - 0.3$; (ii) *Grain-ion* collisions, $\beta_T^{di} \sim z\tau(a/\lambda) \sim 1 - 30$; *Grain-grain* collisions, $\beta_T^{dd} \sim z_d(a/\lambda) \sim 10^3 - 3 \times 10^4$, where $z_d = Z^2 e^2 / a T_d \equiv z|Z|(T_e/T_d)$ is the normalized potential energy of two dust grains which are just touching. We also assumed $z \sim 1$,

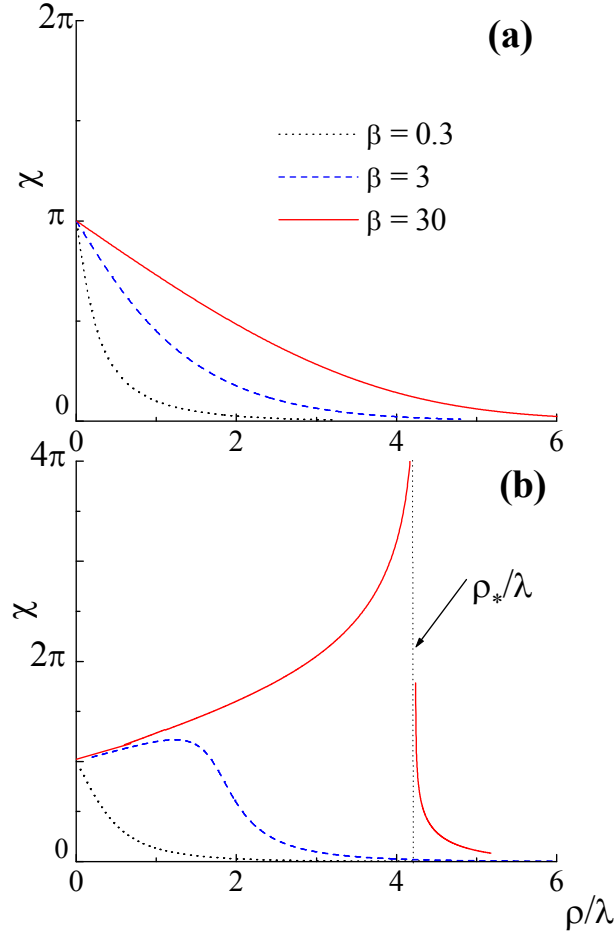


Fig. 9. Scattering angle χ versus the normalized impact parameter ρ/λ , where λ is the effective screening length. The numerical calculations for a repulsive (a) and attractive (b) Yukawa interaction potential are plotted for three different scattering parameters $\beta = 0.3, 3$ and 30 . The vertical dotted line at $\rho \simeq 4.2\lambda$ in (b) indicates the transitional impact parameter ρ_* at which χ diverges.

$\tau \sim 10^2$, $a/\lambda \sim 0.01-0.3$, $|Z| \sim 10^3$, and $z_d = z|Z|\tau = 10^5$ (for $T_d = T_i$), which is typical for complex plasmas. These estimates show that the coupling is weak only for grain-electron collisions. At the same time, coupling for grain-ion and grain-grain collisions is usually strong, and the theory of Coulomb scattering fails to describe such collisions.

The numerical calculation of the momentum transfer cross sections for a wide range of β ($0.1 < \beta < 10^3$) for both attractive and repulsive Yukawa potential has been reported (Khrapak *et al.* 2004). First, the dependence of the scattering angle on the impact parameter, $\chi(\rho)$, was obtained. Then, Eq. (67) was numerically integrated yielding the momentum transfer cross sections. The obtained results are presented in Figs. 9 and 10.

The scattering angle $\chi(\rho)$ decreases monotonically for repulsive interactions

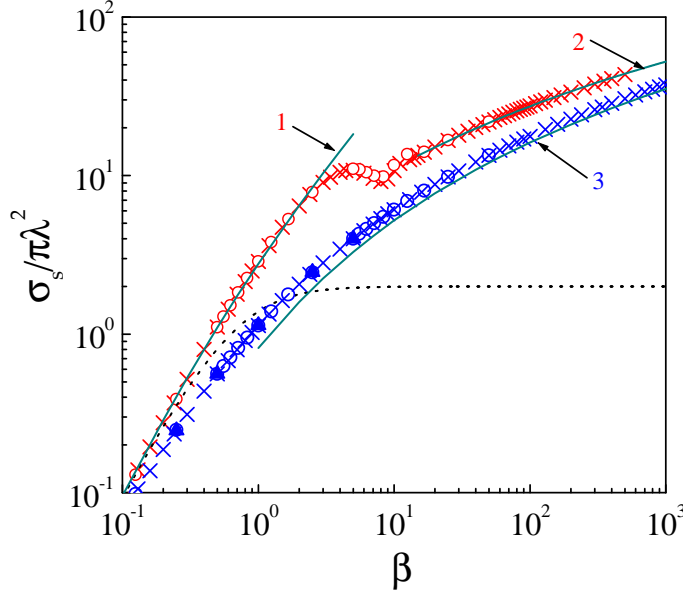


Fig. 10. Momentum transfer cross section, σ_s , normalized to $\pi\lambda^2$ (where λ is the effective screening length), versus the scattering parameter β . The upper data are for attractive and the bottom data are for repulsive Yukawa potentials. Crosses correspond to the numerical results by Khrapak et al. (2004), (blue) triangles are numerical results by Lane and Everhart (1960), and circles are numerical results by Hahn et al. (1971). Solid curves correspond to the following analytical expressions: 1 - Eq. (70); 2 - Eq. (71); 3 - Eq. (69). The dotted line corresponds to the Coulomb scattering theory [Eq. (68)]. All the results are for pointlike particles.

for all β . In contrast, for attractive interactions a monotone decrease of the scattering angle is observed only for $\beta \lesssim 1$, whilst for $1 \lesssim \beta \lesssim \beta_{\text{cr}}$ it becomes a non-monotone function of ρ , and at $\beta > \beta_{\text{cr}} \simeq 13.2$ the scattering angle diverges at the “transitional” impact parameter $\rho_* \simeq \lambda(\ln \beta + 1 - \frac{1}{2} \ln^{-1} \beta)$. The divergence of the scattering angle for attractive interactions arises from the barrier in the effective potential U_{eff} . Note also that when $\beta \ll 1$ the trajectories are mainly deflected within the plasma screening length (at $\rho/\lambda \lesssim 1$). In the opposite case $\beta \gg 1$ the scattering angle can be substantial even for $\rho \gg \lambda$, both for repulsive and attractive interaction. (This is another demonstration of the fact that the Coulomb scattering theory is inappropriate for $\beta \gtrsim 1$, as discussed above.)

The results obtained for the momentum transfer cross section (Fig. 10) show the following features: The cross section for the attractive potential is always larger than that for the repulsive potential (they converge in the limit of weak coupling $\beta \ll 1$). The cross section for the repulsive potential grows monotonically, while for the attractive potential a local maximum and minimum appear near $\beta = \beta_{\text{cr}}$. This non-monotonic behavior is a consequence of the bifurcation which the scattering angle $\chi(\rho)$ experiences in the range $1 \lesssim \beta \lesssim \beta_{\text{cr}}$. It is

also evident from Fig. 10 that the Coulomb scattering theory (shown by the dotted line) considerably underestimates the cross section for both repulsion and attraction when $\beta \gtrsim 1$.

Now let us consider different limiting cases when an analytical description for the momentum transfer cross section is possible.

Repulsive potential. In the limit of weak coupling the Coulomb scattering theory is applicable. The Coulomb scattering cross section is

$$\sigma_s^C/\pi\lambda^2 = 2\beta^2 \ln(1 + 1/\beta^2) \quad (68)$$

is shown by the dotted line in Fig. 10. For $\beta \gtrsim 1$ Eq. (68) is no longer applicable, however, an asymptotic analytical approximation for the case $\beta \gg 1$ can be obtained as follows. The relevant characteristic of the steepness of the potential is the parameter $\gamma_0 = |d \ln U(r)/d \ln r|_{r=R_0}$. The case $\gamma_0 \gg 1$ corresponds to a rapidly decreasing steep potential so that the momentum is mostly transferred in a spherical “shell” of radius R_0 , and thickness $\sim R_0/\gamma_0$. Hence, the scattering resembles that of a hard sphere potential and with increasing γ_0 the momentum transfer cross section tends to

$$\sigma_s^{\text{HS}}/\pi\lambda^2 \simeq (R_0/\lambda)^2. \quad (69)$$

For the Yukawa potential $\gamma_0 = 1 + R_0/\lambda \gg 1$, provided $\beta \gg 1$. A rapidly converging analytical solution for $R_0(\beta)$ is $R_0/\lambda \simeq \ln 2\beta - \ln \ln 2\beta$.

Attractive potential. For weak coupling ($\beta \ll 1$) the theory of Coulomb scattering and Eq. (68) are applicable. An extension of the standard Coulomb scattering theory into the regime of moderate β has been proposed by Khrapak *et al.* (2002). The idea is to take into account all the trajectories with a distance of closest approach shorter than λ . The definition of the maximum impact parameter (cutoff) then becomes $r_0(\rho_{\text{max}}) = \lambda$ instead of $\rho_{\text{max}} = \lambda$ and leads to a modification of the Coulomb logarithm. The *modified Coulomb* momentum transfer cross section is

$$\sigma_s^{\text{MC}}/\pi\lambda^2 \simeq 4\beta^2 \ln(1 + 1/\beta). \quad (70)$$

Although this approach is not rigorous, Eq. (70) shows very good agreement with numerical results up to $\beta \sim 5$ (see Fig. 10) and agrees exactly, of course, with Coulomb scattering theory for $\beta \ll 1$.

The case of long range scattering ($\beta \gg 1$) required a new physical approach, which was formulated by Khrapak *et al.* (2003). The existence of the potential barrier in U_{eff} at $\beta > \beta_{\text{cr}}$ and the discontinuity in $\chi(\rho)$ it causes, play a crucial role for the analysis of collisions. As shown in Fig. 9 the dependence of the scattering angle on the impact parameter in the limit of long range interactions ($\beta = 30$) has the following features: For “close” ($\rho < \rho_*$) collisions we have

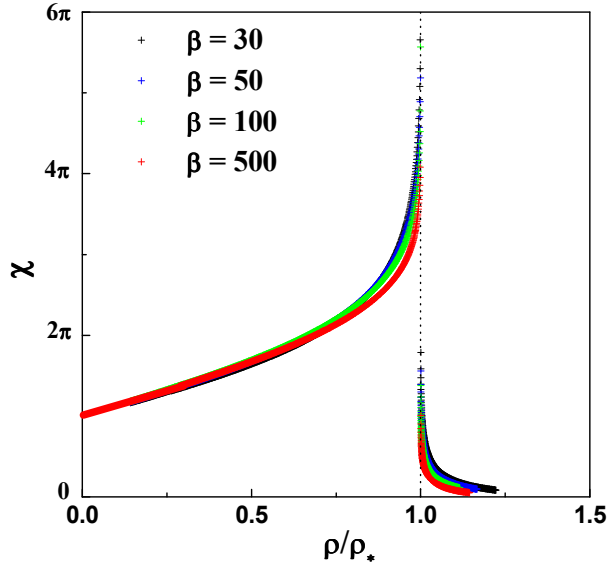


Fig. 11. Scattering angle χ versus the normalized impact parameter ρ/ρ_* for the attractive Yukawa potential (ρ_* is the transitional impact parameter). The numerical calculations are for four different scattering parameters β .

$\chi \rightarrow \pi$ at $\rho \rightarrow 0$, and $\chi(\rho)$ grows monotonically until $\rho = \rho_*$, where it diverges; for “distant” collisions ($\rho > \rho_*$) the scattering angle decreases rapidly, due to the exponential screening of the interaction potential.

It is convenient to consider the contributions from close and distant collisions into the momentum transfer separately. It turns out that the behavior of χ as a function of the normalized impact parameter ρ/ρ_* is *practically independent* of β for $\rho < \rho_*$, see Fig. 11. This self-similarity allows us to present this contribution to the cross section (normalized to $\pi\lambda^2$) as $\simeq \mathcal{A}(\rho_*/\lambda)^2$, where $\mathcal{A} = 2 \int_0^1 [1 - \cos \chi(\xi)] \xi d\xi$ and $\xi = \rho/\rho_*$. The numerical factor \mathcal{A} can be determined by direct numerical integration. The result is $\mathcal{A} = 0.81 \pm 0.01$ for all β in the wide range $\beta_{\text{cr}} \leq \beta \leq 500$. For distant collisions the scattering angle decreases rapidly in the vicinity of ρ_* . This makes it possible to apply the small angle approximation to estimate their contribution to the cross section (normalized to $\pi\lambda^2$) as $\simeq 2.0 + 4.0 \ln^{-1} \beta$. Combining these contributions and keeping terms up to $\mathcal{O}(1)$, we have

$$\sigma_s^{\text{SC}}/\pi\lambda^2 \simeq 0.81(\rho_*/\lambda)^2 + 2.0, \quad (71)$$

where $(\rho_*/\lambda)^2 \simeq \ln^2 \beta + 2 \ln \beta$. Expression (71) is valid for $\beta \geq \beta_{\text{cr}}$ and pointlike particles. Figure 10 shows the very good agreement between Eq. (71) and numerical calculations.

Let us briefly discuss the role of finite grain size. Due to relatively strong repulsion, finite size can usually be neglected for grain-electron and grain-grain collisions (it becomes important only when the grain is essentially uncharged).

The effect of finite size is more important for attractive (grain-ion) interactions. It can be easily shown that in the limit of very large β , the momentum transfer is mostly associated with ions having $\rho < \rho_*$. These ions are absorbed by the particle (OML approach is not working anymore) and the momentum transfer cross section simply tends to $\simeq \pi\rho_*^2$. Note that this estimate would work reasonably well also for point-like particles [see Eq. (71)]. Thus, the momentum transfer is usually relatively insensitive to the grain size.

2 Momentum exchange rates

Let us consider a *test* particle (dust grain) moving through a gas of *field* particles (electrons, ions, or dust grains) having an isotropic Maxwellian velocity distribution function. The test particle velocity u_d is assumed to be smaller than the field particle thermal velocity v_{T_α} . Introducing the momentum exchange rate $\nu_{d\alpha}$ through $du_d/dt = -\nu_{d\alpha}u_d$ we get

$$\nu_{d\alpha} = \frac{1}{3} \sqrt{\frac{2}{\pi}} \frac{n_\alpha \mu_{d\alpha}}{m_d v_{T_\alpha}^5} \int_0^\infty v^5 \sigma_\Sigma(v) \exp(-v^2/2v_{T_\alpha}^2) dv,$$

where $\sigma_\Sigma(v)$ is the corresponding total momentum transfer cross section (function of the relative velocity), $\mu_{d\alpha}$ is the reduced mass, and $\alpha = e, i, d$. Some results following from this expression are given below.

Exercise. Calculate the characteristic momentum transfer frequencies in electron-ion and ion-ion collisions in a conventional (electron + ion) two-temperature plasma.

2.1 Grain-electron collisions

For grain-electron interactions usually $\beta_T^{de} \ll 1$ and the standard Coulomb scattering approach is applicable. This yields

$$\nu_{de} \simeq (2\sqrt{2\pi}/3)(m_e/m_d)n_e v_{T_e} a^2 z^2 \Lambda_{de}. \quad (72)$$

In the typical case $(2/z)(\lambda/a) \gg 1$ we obtain $\Lambda_{de} \simeq 2 \ln[(2/z)(\lambda/a)]$ with logarithmic accuracy.

2.2 Grain-ion collisions

For grain-ion interaction β_T^{di} often exceeds unity and then the Coulomb scattering approach is not applicable. In the case $\beta_T^{di} \lesssim 5$, Eq. (70) can be used.

This yields

$$\nu_{di} \simeq (2\sqrt{2\pi}/3)(m_i/m_d)n_i v_{Ti} a^2 z^2 \tau^2 \Lambda_{di}, \quad (73)$$

where

$$\Lambda_{di} \simeq 2 \int_0^\infty e^{-x} \ln[1 + 2(\lambda/a)(x/z\tau)] dx \quad (74)$$

is the *modified* Coulomb logarithm for ion-grain scattering. In the opposite limit of very large scattering parameters, $\beta_T^{di} > \beta_{cr} \simeq 13.2$, the total momentum transfer cross section is to good accuracy $\sigma_\Sigma \simeq \pi\rho_*^2$, where $\rho_* \sim \lambda \ln \beta_T^{di}$. This yields

$$\nu_{di} \simeq (8\sqrt{2\pi}/3)(m_i/m_d)n_i v_{Ti} \rho_*^2. \quad (75)$$

2.3 Grain-grain collisions

For grain-grain interactions the standard Coulomb scattering approach can be employed only for extremely small grain charges and/or extremely high grain energies, so that $\beta_T^{dd} = z_d(a/\lambda) \ll 1$. This situation is of very little practical interest. In the regime $\beta_T^{dd} \gg 1$, which is much more typical for complex plasmas, the analogy with hard sphere collisions can be used. The result is

$$\nu_{dd} \simeq (4\sqrt{2\pi}/3)n_d v_{Td} R_0^2. \quad (76)$$

V. Forces on dust particles

Knowledge of the forces acting on microparticles in complex plasmas is essential for understanding dynamic phenomena and equilibrium configurations of complex plasmas observed in experiments. The purpose of this Chapter is to give an overview of the major forces exerted on dust under various plasma conditions.

1 Gravity

In ground-based conditions the *gravitational force*

$$F_g = m_d g \quad (77)$$

usually plays the crucial role. Here m_d is the particle mass and $g \simeq 980 \text{ cm/s}^2$ is the gravitational acceleration. In order to levitate the particles in laboratory, the gravitational force should be counterbalanced by other forces.

2 Electrical force

The *electrical force* due to electric field in the (pre)sheath or striation regions of discharges can balance the gravity. The magnitude of the electric force is

$$\mathbf{F}_{\text{el}} = Q\mathbf{E}, \quad (78)$$

where \mathbf{E} is the electric field strength. The particle charge in the electric field is implicitly dependent on the field magnitude through e.g., induced plasma and/or charging anisotropy, ion (electron) drift velocities, etc.

Exercise. Estimate the electric field required to balance the gravity of a $a = 1 \text{ } \mu\text{m}$ particle (mass density $\sim 1 \text{ g/cm}^3$), charged to $Q \sim -10^3 e$.

3 Neutral drag

The *neutral drag force* is the main mechanism responsible for friction when a particle is moving through a stationary plasma. This is because the ionization fraction is usually quite low, on the order of $10^{-7} - 10^{-6}$. Neutral drag can be also important when gas is flowing relative to the particles. When the Knudsen number $\text{Kn} = \ell_n/a$ is large the free-molecular regime is realized. We sketch the derivation of the neutral drag force (Epstein 1924) in this regime. The general expression for the force associated with the momentum transfer from a light species α to the massive grain at rest is

$$\mathbf{F}_\alpha = m_\alpha n_\alpha \int \mathbf{v} v \sigma_\alpha(v) f_\alpha(\mathbf{v}) d^3v, \quad (79)$$

where m_α , $f_\alpha(\mathbf{v})$ and $\sigma_\alpha(v)$ are the corresponding mass, velocity distribution function, and (velocity dependent) momentum transfer cross section ($\alpha = n$ in the considered situation). The force is the result of an asymmetry in the velocity distribution function. For subthermal ($u < v_{T_n}$) relative drift velocity, the small asymmetric component f_{n1} can be written as $f_{n1} \simeq f_{n0}(\mathbf{v} \cdot \mathbf{u}/v_{T_n}^2)$, where f_{n0} is the isotropic (Maxwellian) distribution function. The momentum transfer cross section for specular reflection is $\sigma_n(v) = \pi a^2$. The integration then yields

$$F_n = (8\sqrt{2\pi}/3)a^2 n_n T_n (u/v_{T_n}). \quad (80)$$

A coefficient of order unity can appear in front of Eq. (80), depending on details of interaction between neutrals and the grain surface. For instance, if full accommodation takes place, this coefficient is $1 + \pi/8 \simeq 1.39$. The force can also be written as

$$F_n = m_d \nu_{dn} u, \quad (81)$$

where ν_{dn} is the momentum exchange rate in grain-neutral collisions. This is important quantity, which characterizes the strength of frictional dissipation in complex plasmas.

Exercise. Estimate ν_{dn} for an $a = 1 \mu\text{m}$ particle (mass density $\sim 1 \text{ g/cm}^3$) in room-temperature Ar at a pressure of $p = 10 \text{ Pa}$.

For high (superthermal) relative velocities ($u \gg v_{T_n}$), the neutral drag force is proportional to the velocity squared, $F_n \simeq \pi a^2 n_n m_n u^2$. In the limit of small Knudsen numbers $\text{Kn} \ll 1$ the well known Stokes expression, $F_n = 6\pi\eta a u$, where η is the viscosity of neutral gas, applies. In most cases Eq. (80) is sufficient to calculate the neutral drag force (Epstein drag) in complex plasmas.

4 Ion drag

The *ion drag force* – the momentum transfer from the flowing ions to charged microparticles (grains) embedded into a plasma – is inevitable and exceptionally important factor in dusty (complex) plasmas. Ion flows are usually induced due to “global” large-scale electric fields that always exist in plasmas (e.g., ambipolar or sheath fields in plasma discharges). Knowledge of the ion drag force as a function of the plasma parameters (which may vary over a quite broad range) is necessary for understanding various phenomena occurring in laboratory and space environment.

The traditional way to derive the ion drag force on the test charged particle is based on the binary collision approach. The force is determined by the momentum exchange rate in the dust-ion collisions, averaged over given velocity distribution of ions (see Section IV.2). An alternative way to calculate the ion drag force is the kinetic approach based on the so-called linear dielectric response formalism. Instead of calculating single ion trajectories and then integrating the resulting momentum transfer, one can solve the Poisson equation coupled to the kinetic equation for ions and obtain the self-consistent electrostatic potential around the particle. The polarization electric field at the origin of the test charge gives us the force on the particle.

Below we present main results of both approaches and briefly discuss their complementarity.

4.1 Binary collision approach

In the framework of this approach, the ion drag force F_{id} is completely determined by the (velocity-dependent) total momentum transfer cross section for the dust-ion collisions, σ_{Σ} , which was introduced in Section IV.1. Note that σ_{Σ} includes the collection and scattering contributions, but the scattering usually dominates. The force is $F_{\text{id}} = m_d \nu_{di} u$, where u is the ion flow velocity and ν_{di} is the momentum exchange rate (the latter is given by averaging over the ion velocity distribution). The force depends on the magnitude of the thermal scattering parameter, $\beta_T = e^2 |Z| / \lambda T_i$, where λ is the effective screening length (which does not necessarily coincide with the Debye screening length, see Section II.2).

For subthermal flows ($M_T \equiv u_i / v_{T_i} \ll 1$), we directly employ results of Section IV.2.2: At moderate $\beta_T \lesssim 5$, Eq. (73) yields

$$F_{\text{id}} = \frac{1}{3\sqrt{2\pi}} \left(\frac{T_i}{e} \right)^2 \Lambda \beta_T^2 M_T, \quad (82)$$

where $\Lambda(\beta_T) \simeq 2 \int_0^\infty e^{-x} \ln(1 + 2x/\beta_T) dx$ is the modified Coulomb logarithm (integrated over the Maxwellian distribution function). Here we also assume $\lambda \simeq \lambda_{Di}$ for subthermal ion flows with moderate ion-grain coupling. Equation (82) yields the scaling $F_{id} \propto (Z/\lambda)^2$. In the linear regime $\beta_T \ll 1$ the logarithm is reduced to $\Lambda \simeq \ln \beta_T^{-1}$, which is identical to the results of the standard Coulomb scattering theory.

Exercise. Calculate the collection component of the ion drag force and compare it with the scattering component, Eq. (82).

In the opposite regime of strongly nonlinear scattering, $\beta_T \gg \beta_{cr} \simeq 13$, we obtain from Eq. (75)

$$F_{id} \simeq \frac{2}{3} \sqrt{\frac{2}{\pi}} \left(\frac{T_i}{e}\right)^2 \ln^2 \beta_T M_T. \quad (83)$$

In this case the force depends logarithmically on the scattering parameter and, hence, on Z and λ . Note that in this regime the effective screening length can exceed considerably the ion Debye radius, as discussed in Section II.2. Although the collection component can dominate in this extreme regime, the resulting cross section is practically equal to that for a point-like (non-absorbing) particle, as discussed in Section IV.1.

For superthermal ion flows with $M_T \gg 1$, the drift velocity rather than the thermal velocity should be used to evaluate the scattering parameter β . Also, the screening is determined by the electrons rather than by ions in this case, $\lambda \simeq \lambda_{De}$. Therefore, the scattering parameter decreases rapidly with the Mach number, and we can expect the linear scattering (weak coupling, $\beta \sim \beta_T/M_T^2 \leq 1$) to be typical for $M_T \gg 1$. Then the momentum transfer cross section is given by Eq. (68) and after the integration over the shifted Maxwellian distribution the force is

$$F_{id} \simeq \left(\frac{T_i}{e}\right)^2 \ln \left(\frac{\lambda_{De} M_T^2}{\lambda_{Di} \beta_T} \right) \frac{\beta_T^2}{M_T^2}. \quad (84)$$

(Application of the binary collision approach implies that the ion mean free path should nevertheless exceed the electron screening length λ_{De}). The ion drag decreases as $\propto M_T^{-2}$ at large Mach numbers (neglecting a weak logarithmic dependence). For very high flow velocities the momentum flux onto the grain (collection) dominates over the scattering part and then the force tends to the “geometrical asymptote”, $F_{id} \simeq \pi a^2 n_i T_i M_T^2$, which does not depend on the grain charge.

4.2 Kinetic approach

The binary collision approach is not intrinsically consistent. There are the following reasons for that: (i) While the ion interacts with the charged particle, the interactions with other species (in particular – the ion-neutral collisions) are *neglected*. (ii) The approach *presumes* certain potential distribution around the test charge, although the potential is a self-consistent function of the plasma environment (e.g., ion flow velocity). (iii) The approach *presumes* certain distribution function for ions (usually, the shifted Maxwellian distribution). All these issues can be successfully resolved by employing the *self-consistent* kinetic approach.

Calculation of the ion drag force is based on the linear dielectric response formalism: The self-consistent distribution of the electrostatic potential around a grain of charge Q is given by Eq. (59). Being embedded into a flowing plasma, the grain induces the plasma polarization. The magnitude of the polarization field at the charge origin $\mathbf{r} = 0$ determines the force acting on the grain due to flowing ions: $\mathbf{F}_{\text{id}} = -Q\nabla\varphi_{\text{p}}|_{\mathbf{r}=0}$. Of course, the ion drag acts on the grain together with the usual electrostatic force due to the global field, $\mathbf{F}_{\text{el}} = Q\mathbf{E}$. The ion drag force is obviously parallel to the flow and can be written as

$$F_{\text{id}} = \frac{Q^2}{\pi} \int_0^{k_{\text{max}}} \int_{-1}^1 k\mu \text{Im}[\varepsilon^{-1}(0, \mathbf{k})] dk d\mu, \quad (85)$$

where $\mu = \cos\theta$. The linear kinetic approach is not valid in the immediate vicinity of the charged particle, where the electrostatic perturbations are too strong. The size of this vicinity is equal by the order of magnitude to the ion Coulomb radius $R \sim R_C(1 + M_T^2)^{-1}$, which defines the upper limit of integration, $k_{\text{max}} \sim R^{-1}$. The criterium of applicability of Eq. (85) is the relative smallness of the *actual* contribution to the force from the “nonlinear” region $r \leq R$.

The plasma permittivity $\varepsilon(\omega, \mathbf{k}) = 1 + \chi_e + \chi_i$ is determined by the electron and ion responses. For electrons the Boltzmann form is typically assumed, $\chi_e \simeq (k\lambda_{\text{De}})^{-2}$. The ion contribution is obtained from the solution of the linearized kinetic (or, sometimes, fluid) equation coupled to the Poisson equation. In the simplest case of collisionless plasma with subthermal ion drift we have

$$\varepsilon(0, \mathbf{k}) \simeq 1 + \frac{1}{k^2\lambda_{\text{D}}^2} - i\sqrt{\frac{\pi}{2}} \frac{k u \mu}{k^3\lambda_{\text{Di}}^2 v_{T_i}}. \quad (86)$$

Then from Eq. (85) it follows

$$F_{\text{id}} \simeq \frac{Q^2 u}{\sqrt{2\pi} \lambda_{\text{D}i}^2 v_{T_i}} \int_0^{k_{\text{max}}} \int_{-1}^1 \frac{k^3 \mu^2}{(k^2 + k_{\text{D}}^2)^2} dk d\mu, \quad (87)$$

where $k_{\text{D}} = 1/\lambda_{\text{D}}$ is the inverse (linearized) Debye radius. Integration over μ yields $2/3$, while integration over k gives $\simeq \frac{1}{2} \ln(1 + k_{\text{max}}^2/k_{\text{D}}^2)$. Using the inverse Coulomb radius as k_{max} we finally get

$$F_{\text{id}} \simeq \frac{1}{3} \sqrt{\frac{2}{\pi}} \left(\frac{T_i}{e}\right)^2 \beta_T^2 M_T \ln\left(\frac{\lambda_{\text{D}}}{R_{\text{C}}}\right), \quad (88)$$

which coincides (in leading logarithmic term) with the result of the binary collision approach (82) in the limit of weak ion-grain coupling ($R_{\text{C}} \ll \lambda_{\text{D}}$), i.e. when the linear response formalism is applicable. Note that in terms of the ion kinetics, the origin of the derived force is the Landau damping.

In order to include the ion-neutral collisions, one can use the BGK approximation for the ion collision integral, $\text{St}f_i = \nu_{in}(n_i\Phi - f_i)$, where $\Phi(v) = (2\pi v_{T_n}^2)^{-3/2} \exp(-v^2/2v_{T_n}^2)$ is the (isotropic) Maxwellian velocity distribution of neutrals normalized to unity, $n_i = \int f_i d\mathbf{v}$ is the ion density, and ν_{in} is the ion-neutral collision frequency. The *functional form* of the BGK collision integral is particularly suitable for the description of the charge-exchange collisions. Generally, the ion-neutral collision cross section is a complicated (monotonically decreasing) function of the ion velocity which cannot be generally approximated by any simple scaling. It is reasonable, therefore, to choose the approximation $\nu_{in} = \text{const}$, which allows us to represent the model collision operator in the convenient algebraic form.

For subthermal ions one can use conventional plasma permittivity for collisional Maxwellian plasmas. The result is (Ivlev *et al.* 2004)

$$F_{\text{id}} \simeq \frac{1}{3} \sqrt{\frac{2}{\pi}} \left(\frac{T_i}{e}\right)^2 \left[\ln \beta_T^{-1} + \frac{1}{\sqrt{2\pi}} \mathcal{K}(\lambda_{\text{D}}/\ell_i) \right] \beta_T^2 M_T + O(M_T^3), \quad (89)$$

where $\mathcal{K}(x) = x \arctan x + (\sqrt{\frac{\pi}{2}} - 1) \frac{x^2}{1+x^2} - \sqrt{\frac{\pi}{2}} \ln(1+x^2)$ is the ‘‘collision function’’, and $\ell_i = v_{T_n}/\nu_{in}$ is the ion mean free path. For $\ell_i \geq \lambda_{\text{D}}$ the function \mathcal{K} is negligibly small compared to the Coulomb logarithm and Eq. (89) yields the standard collisionless expression for the ion drag force. In the opposite limit $\ell_i \ll \lambda_{\text{D}}$ the hydrodynamic effects become more important, and the expression in the brackets in Eq. (89) changes from $\ln \beta_T^{-1}$ to $\ln[(\ell_i/\lambda_{\text{D}})\beta_T^{-1}] + \sqrt{\frac{\pi}{8}}(\lambda_{\text{D}}/\ell_i)$. If collisions become ‘‘very frequent’’, $\ell_i \leq \beta_T \lambda_{\text{D}}$, the kinetic effects disappear completely and the force can be derived from the fluid dynamics approach, resulting to $F_{\text{id}} \simeq \frac{1}{6} (T_i/e)^2 (\lambda_{\text{D}}/\ell_i) \beta_T^2 M_T$. We see that frequent ion-neutral collisions ($\ell_i \ll \lambda_{\text{D}}$) enhance the force at small M_T (compared to collisionless

case). This is due to the ion focusing: Each collision “eliminates” the angular momentum the ion had (with respect to the particle) before the collision. Therefore, the motion of the flowing ions becomes more “radial” due to the attraction towards the negatively charged particle – the “focusing center” (wake) downstream moves closer to the particle. This additional focusing implies the local increase of the ion density and, hence, increase of the force. Note, however, that ion absorption on the particle can suppress this effect. In particular, in highly collisional situation ion absorption becomes very important, which reduces the ion drag force and even can change its direction.

The conventional susceptibility is no longer applicable for ions at large Mach numbers: shifted Maxwellian distribution is not a proper choice of the ion distribution function in this case. Analytical results are available for the regime $M_T \gg 1$. Ivlev *et al.* (2004) derived the following expression for the force

$$F_{\text{id}} \simeq \sqrt{\frac{2}{\pi}} \left(\frac{T_i}{e}\right)^2 \ln \left(4 \frac{\ell_i}{\lambda_D} \frac{M_T}{\beta_T}\right) \frac{\beta_T^2}{M_T} + O(M_T^{-2}). \quad (90)$$

Note that at large M_T the kinetic approach yields the force which scales as $F_{\text{id}} \propto M_T^{-1}$, in contrast to the scaling $\propto M_T^{-2}$ in the binary collision approach [see Eq. (84)]. This is because the ion distribution deviates significantly from the shifted Maxwellian form in the supersonic regime. The scaling $F_{\text{id}} \propto M_T^{-1}$ is not affected by a particular dependence of ν_{in} on the ion velocity and, hence, it is a generic feature of the self-consistent approach at large Mach numbers.

4.3 Complementarity of the two approaches

Comparing the results of the linear kinetic approach and the binary collision approach, the most important conclusion to be drawn is that these approaches are not really competitive but rather *complementary*: Binary collision approach is more suitable to describe highly nonlinear collisionless cases when both the ion Coulomb radius R_C and the mean free path exceed the screening length. This situation is typical for subthermal ion flows, when R_C is relatively large. Small Mach numbers also imply weak distortion of the potential around the charged particle and weak deviation of the ion distribution from the shifted Maxwellian function. Therefore, there is no need to employ the self-consistent kinetic approach in this case. On the other hand, for superthermal ions (when R_C decreases rapidly with the Mach number and, hence, the linear theory can be better applied!) both the particle potential and ion distribution function are highly anisotropic, and then the self-consistent kinetic approach is necessary. Also, in contrast to the binary collision approach, the kinetic approach allows us to take into account ion-neutral collisions.

5 Electron drag

Similar to the ion drag force, the *electron drag force* arises due to the momentum transfer from the electrons drifting relative to the charged particles. In the binary collision approximation the electron drag force is $F_{\text{ed}} = m_d \nu_{de} u_e$, where ν_{de} is given by Eq. (72). Compared to the ion drag force, the effect of the electron drag is usually ignored because the electron-to-ion mass ratio is small. This is reasonable when $u_e \sim u_i$, e.g., in rf discharges, where electrons and ions drift together due to the ambipolar diffusion. However, in the case of *independent* (mobility limited) drift (e.g., in the positive column of a dc discharge) the ratio of the ion-to-electron drag forces is *independent* of masses and can be approximately estimated as $F_{\text{id}}/F_{\text{ed}} \sim (T_e/T_i)^2 (\sigma_{en}/\sigma_{in})$, where $\sigma_{e(i)n}$ is the transport cross section for electron (ion) collisions with neutrals. It has been shown (Khrapak and Morfill, 2004) that the electron drag force can indeed dominate over the electric and ion drag force in most of noble gases with relatively small electron temperatures ($T_e \lesssim 1$ eV).

6 Thermophoretic force

If a temperature gradient is present in a neutral gas, then the particle experiences a *thermophoretic force*. The force is due to asymmetry in the momentum transfer from neutrals and is directed towards lower gas temperatures. The force can be derived from Eq. (79), taking into account that in the considered case, the asymmetric part of the velocity distribution function of the component can be approximated as

$$f_{n1}(\mathbf{v}) \simeq \frac{m_n \kappa_n f_{n0}}{n_n T_n^2} \left(1 - \frac{m_n v^2}{5 T_n} \right) \mathbf{v} \cdot \nabla T_n, \quad (91)$$

where κ_n is the thermal conductivity of the neutral component. This expression can be for instance derived by linearizing the kinetic equation with the BGK-like collision operator and expressing the effective collision frequency via the thermal conductivity. It is easy to check that this form ensures that there is no net flux: $\mathbf{j}_n = \int \mathbf{v} f_{n1} d^3v = 0$ (i.e., $\mathbf{u}_n = 0$). The Fourier's law for heat transfer is also satisfied: $\mathbf{q}_n = \int (m_n v^2/2) \mathbf{v} f_{n1} d^3v = -\kappa_n \nabla T_n$. For grain-neutral collisions $\sigma_n(x) = \pi a^2$, and the integration yields

$$F_{Tn} = -\frac{8\sqrt{2\pi}}{15} \frac{\kappa_n a^2}{v_{Tn}} \nabla T_n. \quad (92)$$

This expression was derived by Waldmann (1959). Since $\kappa_n \sim v_{Tn}/\sigma_{nn}$, we have $F_{Tn} \sim (a^2/\sigma_{nn}) \nabla T_n$, i.e. the thermophoretic force depends on the particle radius, gas type (through σ_{nn}), and temperature gradient, but does not depend

on the gas pressure and temperature. Thermophoretic force is widely used for particle levitation in ground-based conditions as well as for controlled manipulations of particle clouds.

Exercise. *Show that for a particles of about $1 \mu\text{m}$ radius and mass density $\sim 1 \text{ g cm}^{-3}$ in an argon plasma, the thermophoretic force is comparable to the force of gravity at temperature gradients $|\nabla T_n| \sim 10 \text{ K cm}^{-1}$.*

6.1 Ion and electron thermophoresis

If a temperature gradient is present in electron or ion components, then particle will experience the *electron* or *ion thermal forces*. In gas discharges, electron thermal force is more important since relatively high temperature gradients $\sim \mathcal{O}(1\text{eV/cm})$ can be established. These thermal forces have components associated with electron (ion) collection by the particles as well as with scattering in the particle electrical potential. The scattering component (which often dominates) is directed towards the region of *higher* temperatures. The physical reason is that the (Coulomb) scattering momentum transfer cross section quickly decreases with velocity ($\propto v^{-4}$), so that the cold electrons (ions) are more effective in transferring their momentum upon scattering. Thus, complex plasmas provide a natural example of systems, where “negative thermophoresis” can be realized.

Exercise. *Derive the expression for the electron thermal force in weakly ionized plasmas.*

7 Polarization force

This force arises due to plasma polarization around the grain. It can be derived from the linear Poisson equation of the form $\Delta\varphi = \lambda^{-2}\varphi + 4\pi Q\delta(\mathbf{r})$, where $\lambda^{-2} = \lambda_D^{-2} - 2\lambda_D^{-3}(\mathbf{r}\nabla\lambda_D)$ using the standard perturbation technique (Hamaguchi and Farouki, 1994). Here λ_D and $\nabla\lambda_D$ should be evaluated at the position of the grain at $\mathbf{r} = 0$. The result is

$$\mathbf{F}_{\text{pl}} = -\frac{Q^2}{2} \frac{\nabla\lambda_D}{\lambda_D^2}. \quad (93)$$

It does not depend on the sign of the particle charge and is directed towards the region with smaller Debye radius. Theory predicts that this force can be important when significant inhomogeneities are present (e.g. low frequency waves propagation in complex plasmas).

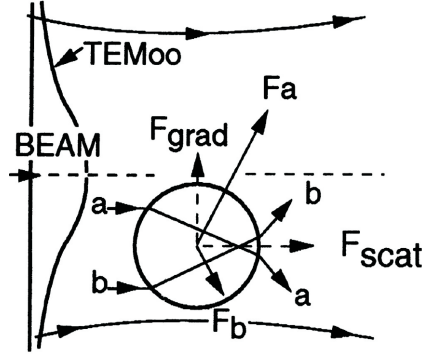


Fig. 12. Sketch showing principal components of the radiation force (courtesy of A. Ashkin). By considering two rays (“a” and “b”) of the laser beam (which is inhomogeneous in the transverse direction), one can decompose the resulting momentum-exchange forces (F_a and F_b) acting on a particle into the scattering component along the beam, F_{scat} , and the gradient component pointed transversely, F_{grad} .

8 Radiation forces

The radiation force exerted on a particle by a laser beam provides an exceptionally important mechanism of the particle manipulation. The force is determined by the radiation intensity I and consists of several components which originate from rather different physical mechanisms. The principal component is the scattering force $F_{\text{scat}} = C_{\text{scat}}(I/c)$, which is due to the refraction of the laser beam in the particle and which is pointed in the direction of the beam propagation. Here, the scattering cross section C_{scat} depends on the scattering regime, viz., on the ratio of the radiation wavelength λ (in this context, such notation cannot cause confusion with the screening length) to the particle radius a . In a general case, $C_{\text{scat}}(\lambda/a)$ is described by Mie theory: For the Rayleigh regime, when λ/a is large, $C_{\text{scat}} = \frac{128}{3}\pi^5(a^6/\lambda^4) \left(\frac{n_r^2-1}{n_r^2+2}\right)^2$, where $n_r > 1$ is the relative refractive index of the particle [determined by the dielectric function in the optical frequency range, $n_r^2 \simeq \text{Re } \varepsilon_r(\omega)$]. For the opposite, geometrical-optics regime, C_{scat} naturally tends to the geometrical refractive limit. The second contribution is the gradient force $\mathbf{F}_{\text{grad}} = -2\pi a^3 \left(\frac{n_r^2-1}{n_r^2+2}\right)^2 (\nabla I/c)$, which is due to the particle polarization in an inhomogeneous radiation field.

The effect of the two components of the radiation force is illustrated in Fig. 12. In experiments with complex plasmas F_{grad} (which pulls a particle towards the beam focus – the effect utilized in laser tweezers) is usually significantly smaller than F_{scat} and hence plays a minor role. The last (potentially important) contribution is the photophoretic force, which is basically the thermophoretic force driven due to inhomogeneous heating of a particle by laser radiation. For homogeneous radiation this force is parallel to the beam but its direction can reverse, depending on what part of the particle – front or rear – received

stronger heating (which depends, in particular, on details of the refraction regime). The relative importance of this force in complex plasmas still needs to be studied.

VI. Dynamics of dust particles

In most of the ground-based experiments, negatively charged dust particles can only levitate in the regions of sufficiently strong electric fields, where the electric force and other forces exerted in a plasma compensate for gravity. This occurs, for example, in the pre-sheath and sheath regions of an rf discharge or in striations of a dc discharge. As shown in Fig. 13, the electric field E in these regions rapidly increases downwards. The particle charge Q varies with height, both due to the ion acceleration in the electric field (see Fig. 2) and a decrease of the ratio n_e/n_i with E . Usually, the (negative) charge first somewhat decreases and attains a minimum, then it starts increasing and eventually can even reach positive values.

1 Nonlinear dynamics of individual particles

Let us first consider elementary dynamics of a single particle. If the vertical coordinate (height) $x = 0$ is assigned to the equilibrium position, then for small displacements around the equilibrium the net force acting on a particle (in addition to the neutral friction force $-\nu_{dn}\dot{x}$) can be expanded into series over x . This yields the following equation of motion:

$$\ddot{x} + \nu_{dn}\dot{x} + \Omega_v^2 x = \alpha_1 x^2 + \alpha_2 x^3 + \dots \quad (94)$$

Here Ω_v is the resonance frequency of vertical oscillations, coefficients α_i characterize nonlinearity, and ν_{dn} is the damping rate due to neutral friction. The major contribution to the net force is normally due to the electrostatic interaction, and then the resonance frequency is determined by $m_d \Omega_v^2 = -d(QE)/dx|_{x=0}$. Depending on the discharge parameters and the particle mass, the nonlinear coefficients are determined either by the sheath/striation field profile or by the charge variations with the height.

Due to relatively large mass of the dust particles, the magnitude of the resonance frequency Ω_v is rather low (typically in the range 1 – 30 Hz). The oscillation amplitude $A(\omega)$ reaches the maximum at $\omega = \sqrt{\Omega_v^2 - \frac{1}{2}\nu_{dn}^2}$, the width of the resonance peak is $\sim \nu_{dn}$. Hence, changing ω and measuring $A(\omega)$, one can determine Ω_v and ν_{dn} . As the excitation amplitude increases, the oscillations reveal all features peculiar to an anharmonic oscillator: hysteresis of the frequency response curve, shift of the resonance frequency, and secondary res-

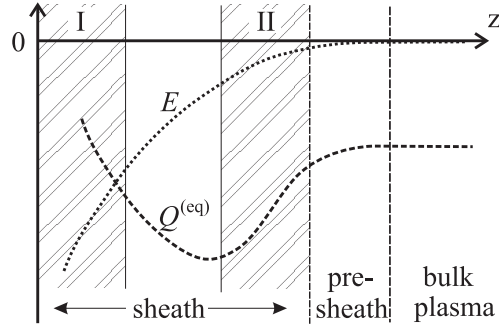


Fig. 13. Qualitative dependence of the equilibrium particle charge, Q_{eq} , and the vertical electric field, E , on the height (illustrated for a rf plasma). In the region I the particle equilibrium is unstable, in the region II the particle motion can be unstable due to “delayed charging” effect (see text).

onances, which is illustrated in Fig. 14. Knowledge of the resonance frequency and of the nonlinear coefficients, recovered from the fitting of the measured curves with the analytical formulas, allows us to obtain spatial distributions of the electric field and/or dust particle charge in a plasma.

Exercise. Express the characteristic length of the electric field inhomogeneity, $\ell_E = |E/(dE/dx)|_{x=0}$, via the resonance frequency Ω_v (assuming constant charge).

2 Nonconservative dynamics of individual particles

Complex plasmas are non-Hamiltonian systems, not only because of conventional friction of grains against the background neutral gas, but also due to specific plasma interactions that give rise to new classes of non-Hamiltonian dynamics. Under certain conditions these interactions result in spontaneous excitation of individual and collective particle motion. Below we consider a few interesting examples of such dynamics.

The simplest class of non-Hamiltonian dynamics is realized when the charge is a function of the coordinates (Zhakhovskii *et al.*, 1997), $Q = Q(\mathbf{r})$: The force $Q\mathbf{E}$ acting on a particle in a potential electric field $\mathbf{E}(\mathbf{r}) = -\nabla\varphi(\mathbf{r})$ cannot be expressed in terms of a gradient of a scalar function, because $\nabla \times (Q\nabla\varphi) \equiv \nabla Q \times \nabla\varphi$ is not equal to zero in the general case. The dynamics is Hamiltonian only when the charge gradient is collinear with the electric field (in this case, the force depends on a single longitudinal coordinate and therefore it can always be written as a derivative of some scalar function over the coordinate). Thus, particles with variable charges could gain energy from the ambient plasma.

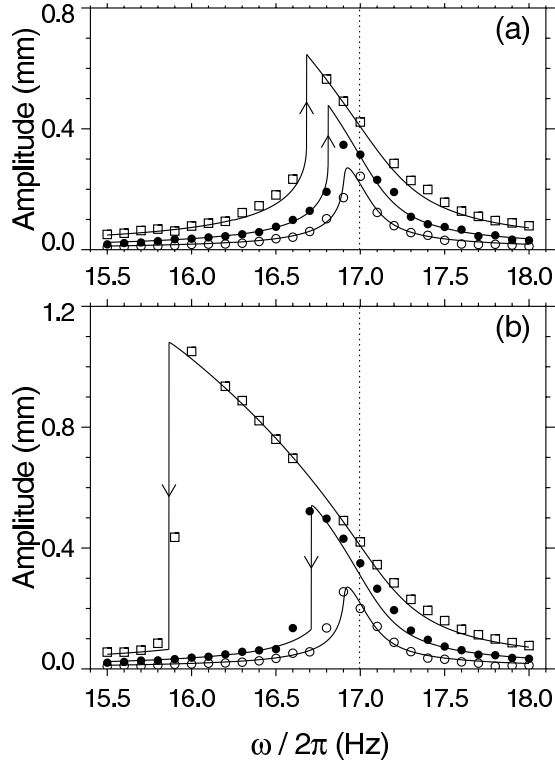


Fig. 14. Amplitude of the vertical particle oscillations in a rf sheath. The data for a $7.6 \mu\text{m}$ particle are shown near the primary resonance for increasing (a) and decreasing (b) frequency of excitation, ω , and for different amplitude of the sinusoidal excitation voltage: 50 mV (open circles), 100 mV (closed circles), and 200 mV (squares). Solid lines show the least-squares fit of the points to theory. The vertical dotted line indicates the position of the resonance frequency, Ω_v , obtained from the fit.

Another example of nonconservative dynamics is due to the so-called “delayed charging” effect (Ivlev *et al.*, 2000), which stems from the fact that the charging frequency Ω_{ch} [see Eq. (36)] of a particle is finite. The equation of vertical motion for a single particle is

$$\ddot{x} + \nu_{dn}\dot{x} = \frac{QE}{m_d} - g, \quad (95)$$

Now we neglect nonlinear effects and set $E(x) \simeq E_0 + E'_0 x$ (a prime denotes the derivative at $x = 0$). Substituting this expression together with $Q = Q_0 + \delta Q$ in Eq. (95) and using the condition $Q_0 E_0 = m_d g$, we obtain

$$\ddot{x} + \nu_{dn}\dot{x} - \frac{Q_0 E'_0}{m_d} x = g \frac{\delta Q}{Q_0}. \quad (96)$$

According to Eq. (37), the kinetic equation for the charge is

$$\dot{Q} = -\Omega_{\text{ch}} (Q - Q_{\text{eq}}),$$

where the equilibrium charge is $Q_{\text{eq}}(x) \simeq Q_0 + Q'_0 x$. Thus, we get the following kinetic equation for the charge variation:

$$\delta\dot{Q} = -\Omega_{\text{ch}} (\delta Q - Q'_0 x). \quad (97)$$

For a harmonic solution of Eqs (96) and (97), i.e., for $x, \delta Q \propto e^{i\omega t}$, we obtain

$$(i\omega + \Omega_{\text{ch}}) \left(-\omega^2 + i\nu_{dn}\omega - \frac{Q_0 E'_0}{m_d} \right) = \frac{Q'_0 E_0}{m_d} \Omega_{\text{ch}}. \quad (98)$$

The derived dispersion relation is easy to interpret. The left-hand side is the product of two factors: The first one describes the charge variation decay, the second one – vertical oscillations. The right-hand side represents the coupling between the two modes. We assume that the oscillations are weakly damped, $\text{Re } \omega \gg \nu_{dn}$, and that the dust charging mode is weakly coupled with the oscillation mode, i.e., $\Omega_{\text{ch}} \gg |\omega|$. Solving the obtained equation with these assumptions, we get approximate expressions for the frequency and damping rate,

$$\begin{aligned} \text{Re } \omega &\simeq \sqrt{-\frac{(QE)'_0}{m_d}} \equiv \Omega_v, \\ 2 \text{Im } \omega &\simeq \nu_{dn} + \frac{Q'_0 E_0}{m_d \Omega_{\text{ch}}}. \end{aligned} \quad (99)$$

As sketched in Fig. 13, the charge is practically independent of x in the bulk plasma, but as the electrode is approached it decreases rapidly ($|Q_{\text{eq}}|$ increases) in the pre-sheath and just below the sheath edge. At even smaller x , the charge attains a minimum and then starts increasing. Normally, particles are trapped near the sheath edge, where $(QE)'_0 < 0$. But, if the amplitude of oscillations is too large and a particle enters the region I, where $(QE)'_0 > 0$, the motion becomes unstable and the particle drops onto the electrode.

There is one more region of instability in Fig. 13, where $Q'_0 E_0$ is negative and its absolute value exceeds a certain threshold, so that the damping rate $\text{Im } \omega$ is negative as well (region II). Due to delayed charging, the particle dynamics is non-conservative (even in the absence of friction): On the way down, $|Q(x)|$ is always less than the equilibrium value $|Q_{\text{eq}}(x)|$, whereas on the way up the opposite inequality holds. Therefore, the particle gains energy during the whole circle of oscillation, and if this exceeds the energy dissipation due to friction, then oscillations become unstable.

Exercise. Estimate (order of magnitude) the threshold damping rate ν_{dn} and the corresponding gas pressure threshold for the delayed charging instability. Assume $a = 3 \mu\text{m}$, $\ell_Q/\ell_E = 3$, $\Omega_{\text{ch}} = 10^5 \text{ s}^{-1}$, and $\Omega_v = 10^2 \text{ s}^{-1}$.

Now, let us consider the role of random charge fluctuations for the vertical oscillations. For simplicity, we now assume $Q_{\text{eq}} = Q_0 = \text{const}$. By substitut-

ing in Eq. (95) the expansions of $E(x)$ and keeping only linear terms in the resulting equation, we get

$$\ddot{x} + \nu_{dn}\dot{x} + \Omega_v^2 \left(1 + \frac{Q_1(t)}{Q_0} \right) x = g \frac{Q_1(t)}{Q_0}, \quad (100)$$

where $Q_1(t)$ is the fluctuating part of the charge, with the stochastic properties governed by Eqs (42) and (43). Using the fluctuation-dissipation theorem, it can be easily shown that for typical conditions $\nu_{dn}, \Omega_v \ll \Omega_{ch}$ the mean kinetic energy of vertical oscillations associated with the random force at the right-hand side of Eq. (100) saturates at

$$\mathcal{E}_d \simeq \frac{\sigma_Z^2 m_d g^2}{2\nu_{dn}\Omega_{ch}},$$

In accordance with Eq. (40), the relative charge dispersion (due to charge discreteness) is $\sigma_Z^2 \sim |Z_{eq}|^{-1}$, where $Z_{eq} \equiv Q_{eq}/e$.

Exercise. *Estimate (order of magnitude) \mathcal{E}_d for typical experimental conditions (micron particles, gas pressure around 1 Pa).*

In addition to this “heating”, the charge variations can trigger the parametric instability of the oscillations. This occurs due to the random variations of the oscillation frequency in Eq. (100) which has a form of the Mathieu equation. The conditions for the parametric resonance are always satisfied, since rapid charge fluctuations can be considered as the white noise with respect to slow particle oscillations. Thus, if the frictional damping is low enough, the mean kinetic energy grows exponentially with time, $\mathcal{E}_d \propto e^{\Gamma_{\mathcal{E}} t}$, with the growth rate

$$\Gamma_{\mathcal{E}} \simeq \sigma_Z^2 \frac{\Omega_v^2}{\Omega_{ch}} - \nu_{dn}. \quad (101)$$

This process of the stochastic acceleration (specific for complex/dusty plasmas) represents yet another example of the Fermi acceleration. It will be further discussed in the next section.

To conclude this section we consider yet another interesting problem associated with charge fluctuations – particle diffusion across a magnetic field (Khrapak and Morfill, 2002). It was suggested that this transport mechanism can be very effective in astrophysical conditions (e.g., inner Jovian magnetosphere). In this simplest formulation, the equation of particle motion is

$$\dot{\mathbf{v}} = \frac{Q}{mc} \mathbf{v} \times \mathbf{B}, \quad (102)$$

where $\mathbf{v}(t)$ is the particle velocity, \mathbf{B} is the magnetic field strength, and c is the speed of light. We assume that the constant magnetic field is directed

along the z axis and introduce a new variable $u = v_x + iv_y$ for the transverse velocity components. The resulting equation for $u(t)$ is

$$\dot{u} = -i\Omega_0 \left(1 + \frac{Q_1(t)}{Q_{\text{eq}}} \right) u, \quad (103)$$

where $\Omega_0 = Q_{\text{eq}}B/mc$ is the constant part of the Larmor frequency.

Random charge fluctuations allow the guiding center of a particle to move in a random way, leading to particle displacement from the unperturbed orbit and, consequently, to diffusion across a magnetic field. Note, that this process is essentially different from the classical diffusion across a magnetic field due to collisions. We use conventional definition for the transverse diffusion constant

$$D_{\perp} = \lim_{t \rightarrow \infty} \frac{\langle \Delta \mathbf{r}_{\perp}^2(t) \rangle}{4t} \equiv \lim_{t \rightarrow \infty} \frac{1}{4t} \int_0^t \int_0^t dt_1 dt_2 \langle \mathbf{v}_{\perp}(t_1) \cdot \mathbf{v}_{\perp}(t_2) \rangle. \quad (104)$$

where \mathbf{r}_{\perp} and \mathbf{v}_{\perp} are particle position and velocity in a plane perpendicular to the magnetic field and $\langle \dots \rangle$ denotes averaging over the velocity distribution *and* charge fluctuations. Since $\mathbf{v}_{\perp}(t_1) \cdot \mathbf{v}_{\perp}(t_2) \equiv \text{Re}[u(t_1)u^*(t_2)]$, we reduce the problem to the calculation of the temporal auto-correlation function $X(\tau) = \langle u(t+\tau)u^*(t) \rangle$. Using Eq. (103) and the properties of charge fluctuations we get

$$X(\tau) = \langle v_{\perp}^2 \rangle \exp[-i\Omega_0\tau - \mathcal{K}^2(\Omega_{\text{ch}}\tau + e^{-\Omega_{\text{ch}}\tau} - 1)], \quad (105)$$

where $\mathcal{K} = \sigma_Z(\Omega_0/\Omega_{\text{ch}})$ is the Kubo number (which characterizes the charge modulation) and $\langle v_{\perp}^2 \rangle$ is the mean squared velocity (for a Maxwellian distribution, $\langle v_{\perp}^2 \rangle = 2T/m$). Taking into account that $D_{\perp} = \frac{1}{2}\text{Re} \int_0^{\infty} X(\tau)d\tau$, we finally derive

$$D_{\perp} = \frac{1}{2} \frac{\langle v_{\perp}^2 \rangle}{\Omega_{\text{ch}}} \int_0^{\infty} \cos\left(\frac{\Omega_0}{\Omega_{\text{ch}}}x\right) \exp[-\mathcal{K}^2(x - 1 + e^{-x})]dx. \quad (106)$$

This expression is applicable for arbitrary value of the Kubo number, but can be significantly simplified in the two limiting cases of fast ($\mathcal{K} \ll 1$) and slow ($\mathcal{K} \gg 1$) modulation.

Exercise. *Simplify Eq. (106) in the limits of fast and slow modulation.*

3 Kinetics of ensembles with nonconservative interactions

Since ensembles of particles with variable charges are generally non-Hamiltonian systems, the use of thermodynamic potentials to describe them is not really justified. An appropriate way to investigate the evolution of such systems is to use the kinetic approach. As long as properties of the charge variations are

known, one can consider the dynamics and kinetics of the grains independently from the plasma kinetics.

Let us start again with the case when charges depend on coordinates. First, we have to define the mutual interactions. The electrostatic potential created at \mathbf{r} by a charge located at \mathbf{r}_i is $\varphi_i(\mathbf{r}) = Q(\mathbf{r}_i)\varphi_{\text{unit}}(|\mathbf{r} - \mathbf{r}_i|)$, where $\varphi_{\text{unit}}(r)$ is the (isotropic) potential of a *unit charge*. The resulting electric field is $\mathbf{E}_i(\mathbf{r}) = -Q(\mathbf{r}_i)(\partial/\partial\mathbf{r})\varphi_{\text{unit}}(|\mathbf{r} - \mathbf{r}_i|)$. Hence, particles i and j interact via the force

$$\mathbf{F}_{ij} = -Q(\mathbf{r}_i)Q(\mathbf{r}_j)(\partial/\partial\mathbf{r}_i)\varphi_{\text{unit}}(|\mathbf{r}_i - \mathbf{r}_j|). \quad (107)$$

Note that the mutual interactions are reciprocal, $\mathbf{F}_{ij} = -\mathbf{F}_{ji}$, so that the total momentum of the system is conserved.

Principal features of non-Hamiltonian dynamics with interactions (107) can be understood by considering a 1D system of two charged grains which can move along the x -axis. The repulsing particles have to be confined externally. Generally, the confinement is electrostatic and, hence, charge-dependent. However, since electrostatic forces are potential in the 1D case, we can always write the confinement force on a particle as $F_{\text{conf}} = -dU_{\text{conf}}/dx$. We now introduce a 2D space $\mathbf{x} = (x_1, x_2)$, with $x_{1,2}$ being the particle coordinates, and define the external confinement potential as $U_{\text{ext}}(\mathbf{x}) \equiv U_{\text{conf}}(x_1) + U_{\text{conf}}(x_2)$. Then the equations of two particle motion can be written in the following vector form:

$$m_d(\ddot{\mathbf{x}} + \nu_{dn}\dot{\mathbf{x}}) = -\partial U_{\text{ext}}/\partial\mathbf{x} - Q_1Q_2(\partial\varphi_{\text{unit}}/\partial\mathbf{x}), \quad (108)$$

where $\varphi_{\text{unit}} = \varphi_{\text{unit}}(|x_2 - x_1|)$ and $Q_{1,2} \equiv Q(x_{1,2})$. In addition to the confinement and interaction forces, we introduced a friction force with the damping rate ν_{dn} . One can see from Eq. (108) that the 1D dynamics of two particles is mathematically identical to 2D dynamics of a single particle. The dynamics is *non-conservative*, because work W_{loop} done (due to mutual interactions) over a closed path (loop) ℓ in plane \mathbf{x} is not equal to zero. Using Stokes theorem, the work can be expressed via the integral over the surface S_ℓ bounded by the path:

$$W_{\text{loop}} = \pm \int_{S_\ell} (Q_1Q_2' + Q_1'Q_2)\varphi_{\text{unit}}' dx_1 dx_2,$$

where the prime denotes the derivative with respect to the argument.

The sign of W_{loop} is determined by the direction of motion along ℓ , i.e., the charge variations can serve either as a sink ($W_{\text{loop}} < 0$) or a source ($W_{\text{loop}} > 0$) of the energy. In the latter case the motion of interacting particles can be unstable. In dissipative systems one can expect that at the nonlinear stage motion converges asymptotically to a limit cycle, with the balance between the energy gain and frictional loss, $W_{\text{loop}} - 2\nu_{dn}\tau\langle\mathcal{E}_d\rangle_\tau = 0$, where τ is the oscillation period and $\langle\mathcal{E}_d\rangle_\tau$ is the mean kinetic energy averaged over τ . We see that the magnitude of the work done over path ℓ is determined by the area

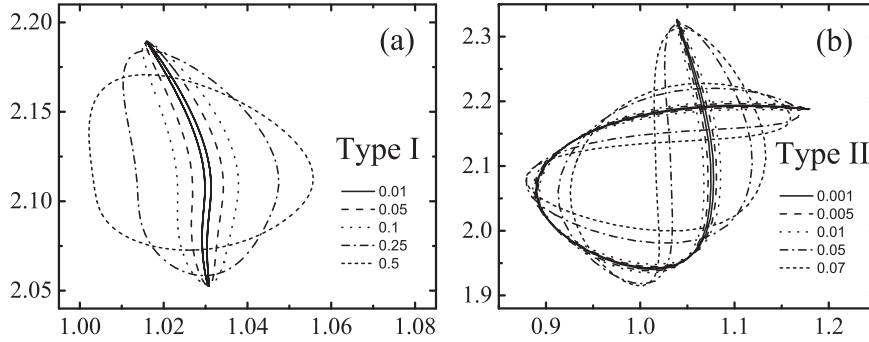


Fig. 15. “Mutual” phase portraits of self-excited particle oscillations triggered by spatially varying charges. Two particles perform a 1D motion, their coordinates (x_1, x_2) form periodic trajectories that are shown for several values of damping rate ν_{dn} , the highest values are chosen in the vicinity of the self-excitation cut-off. By varying initial momentums of the particles, one can obtain attractors of type I (a) or II (b). Coordinates are measured in units of the screening length λ and the damping rate ν_{dn} is normalized by the dust-lattice frequency scale $\Omega_{DL} = \sqrt{Q^2/m_d\lambda^3}$ (see Section VII.2).

S_ℓ . Hence, when $\nu_{dn} \rightarrow 0$ the contour ℓ of periodic motion (if such motion is possible at all) should degenerate into some line, so that S_ℓ tends to zero as well. This is illustrated in Fig. 15 for “2+2” particle system, where two outer particles are fixed and two inner particles movable. Particles interact via the Yukawa potential $\varphi_{\text{unit}}(x) = e^{-x/\lambda}/x$ with the screening length λ . Two different types of attractor are possible in this case, either type I (Fig. 15a) or type II (Fig. 15b), with no regular correspondence to the initial conditions (e.g., initial particle momenta). One can see that the oscillation contours become narrower and have a tendency to degenerate into a single line as the damping rate ν_{dn} decreases. On the other hand, there exists a critical friction beyond which self-sustaining oscillations are no longer possible.

Now let us briefly consider kinetics of particle ensembles with fluctuating charges (Ivlev *et al.*, 2005). As was shown in the previous section, charge fluctuations in the presence of electric field can result in a new type of the Fermi acceleration. For ensembles, the same mechanism of the stochastic acceleration can operate due to mutual interactions between the particles.

In the absence of external fields, the kinetics of charged grains is governed by the mutual collisions and by the collisions with neutrals, so that the kinetic equation is

$$df/dt = \text{St}_{dd}f + \text{St}_{dn}f. \quad (109)$$

The grain-neutral collision integral $\text{St}_{dn}f$ does not depend on particle charges and can be written in usual Fokker-Planck form. As regards the grain-grain collisions (here we investigate dilute gaseous ensembles and hence focus on the binary interactions only), one cannot use the collision integral in the classical Boltzmann form: Due to the exchange of energy with *free plasma charges*, the

subsystem of charged grains is not conservative – the momentum exchange during a collision is affected by the charging processes. Thus, we have to write the grain-grain collision integral in the most general form:

$$\text{St}_{dd}f(\mathbf{p}) = \int \left[w(\mathbf{p}', \mathbf{p}'_1; \mathbf{p}, \mathbf{p}_1) f(\mathbf{p}') f(\mathbf{p}'_1) - w(\mathbf{p}, \mathbf{p}_1; \mathbf{p}', \mathbf{p}'_1) f(\mathbf{p}) f(\mathbf{p}_1) \right] d\mathbf{p}_1 d\mathbf{p}' d\mathbf{p}'_1. \quad (110)$$

Here, $w(\mathbf{p}, \mathbf{p}_1; \mathbf{p}', \mathbf{p}'_1)$ is a probability function for a pair of colliding particles with momenta \mathbf{p} and \mathbf{p}_1 to acquire momenta \mathbf{p}' and \mathbf{p}'_1 , respectively, after the scattering. Equation (110) accounts for all possible transitions $(\mathbf{p}', \mathbf{p}'_1) \rightarrow (\mathbf{p}, \mathbf{p}_1)$ (sources) and $(\mathbf{p}, \mathbf{p}_1) \rightarrow (\mathbf{p}', \mathbf{p}'_1)$ (sinks), and then is averaged over \mathbf{p}_1 . The function w can be determined by solving the mechanical problem of the binary scattering with given interaction between the particles.

The mechanics of binary grain collisions can be conveniently considered in terms of the center-of-mass and relative coordinates. For a pair of particles with momenta \mathbf{p} and \mathbf{p}_1 , the center-of-mass and relative momenta are $\mathbf{p}_c = \frac{1}{2}(\mathbf{p} + \mathbf{p}_1)$ and $\mathbf{p}_r = \mathbf{p}_1 - \mathbf{p}$, respectively. In the absence of external forces, the center-of-mass momentum is conserved, and the relative momentum is changed during the collision,

$$\mathbf{p}'_c = \mathbf{p}_c, \quad \mathbf{p}'_r = \mathbf{p}_r + \mathbf{q}. \quad (111)$$

For constant charges, the absolute value of the relative momentum, $p_r \equiv |\mathbf{p}_r|$, is conserved (and only the direction changes, which corresponds to elastic scattering). For variable charges p_r varies as well. Hence, the exchange of the relative momentum can be divided into elastic and inelastic parts, $\mathbf{q} = \mathbf{q}_0 + \delta\mathbf{q}$: The elastic part keeps the magnitude of the relative momentum constant, $|\mathbf{p}_r + \mathbf{q}_0| = p_r$. The vector of inelastic momentum exchange, $\delta\mathbf{q}$, is parallel to \mathbf{p}'_r , and its magnitude is $\delta q = p'_r - p_r$.

The kinetics of particles with variable charges has a very important *hierarchy of time scales*: Each interparticle collision is accompanied by (i) elastic momentum exchange \mathbf{q}_0 , which provides the relaxation of the distribution function to the Maxwellian equilibrium – whilst keeping the mean kinetic energy of the particles \mathcal{E}_d constant, and (ii) inelastic momentum exchange $\delta\mathbf{q}$, which causes variation of \mathcal{E}_d . Due to the relative smallness of the charge variations, the resulting inelastic momentum exchange is small as well, $\delta q \ll q_0$. This implies that process (ii) is much slower than (i). Therefore, the velocity distribution remains close to the Maxwellian form, $f(\mathbf{p}) \simeq f_M(\mathbf{p})$, with the temperature $T_d = \frac{2}{3}\mathcal{E}_d$.

Thus the temperature is the only parameter that determines the evolution of the ensemble. This implies that the system of charged grains can be treated

with fluid equations: The momentum equation (with the friction force added) remains unaffected since the charge variations conserve the net momentum. In the temperature equation, along with the friction (sink) term one has to add a source term due to charge variations. In accordance with Eq. (109), the resulting combination of these terms is

$$\dot{T}_d = \int (p^2/3m_d) (\text{St}_{ddf} + \text{St}_{dnf}) d\mathbf{p}. \quad (112)$$

For the grain-neutral collisions the integral is simply equal to $-2\nu_{dn}(T - T_n)$. For the grain-grain collisions, one can expand the integrand into a series over δq . Retaining the linear and quadratic terms and integrating in parts, we obtain,

$$\int p^2 \text{St}_{df} d\mathbf{p} \simeq \frac{1}{2} \int (p_r \mathcal{A} + \mathcal{B}) f_M(\mathbf{p}_c) f_M(\mathbf{p}_r) d\mathbf{p}_c d\mathbf{p}_r, \quad (113)$$

where $\mathcal{A}(\mathbf{p}_c, \mathbf{p}_r) = \int \delta q \tilde{w} d\delta q$ and $\mathcal{B}(\mathbf{p}_c, \mathbf{p}_r) = \frac{1}{2} \int (\delta q)^2 \tilde{w} d\delta q$ are the Fokker-Planck coefficients, $\tilde{w}(\mathbf{p}_r, \mathbf{p}_c; \delta q) \equiv w(\mathbf{p}, \mathbf{p}_1; \mathbf{p}', \mathbf{p}'_1)$ and the momenta are related by Eq. (111). The smallness of coefficients \mathcal{A} and \mathcal{B} is ensured by the smallness of the charge variations (for constant particle charges, the inelastic momentum exchange is equal to zero and, hence $\mathcal{A} = \mathcal{B} \equiv 0$).

For particles interacting via a short-range screened electrostatic potential (with the screening length λ), the measure of the interaction strength is the “scattering parameter” $\beta_T^{dd} = Q^2/\lambda T_d$ (see Section IV.1). When β_T^{dd} is large enough the interaction is of the hard-spheres type. In the opposite case, when the ratio is small, the interaction is of the Coulomb type, similar to that between electrons and ions in usual plasmas. These two limits are referred to as the “low-temperature” and “high-temperature” regimes, respectively, with the transition temperature being $T_{tr} = Q^2/\lambda$. From Eqs (112) and (113) one can derive the following governing equation for the kinetic temperature:

$$\dot{T}_d \sim \alpha T_d^\gamma - 2\nu_{dn}(T_d - T_n). \quad (114)$$

The coefficient α and exponent γ in the source term depend on the temperature regime. Asymptotically, $\gamma = 2$ and $\gamma = 1$ for the low- and high-temperature regimes, respectively. Thus, the temperature can grow exponentially at $T_d \gg T_{tr}$, the acceleration coefficient in this regime is $\alpha \sim \sigma_Z^2 \omega_{pd}^2 / \Omega_{ch}$, where $\omega_{pd} = \sqrt{4\pi Q^2 n_d / m_d}$ is the dust plasma frequency. This process is ubiquitous and can be responsible for, e.g., anomalous acceleration of cosmic dust or dust in fusion devices.

Exercise. *Estimate (order of magnitude) the threshold damping rate ν_{dn} and the corresponding gas pressure threshold for the onset of stochastic acceleration in the high-temperature regime. Assume $a = 1 \mu m$, $n_d = 10^5 \text{ cm}^{-3}$, and $\Omega_{ch} = 10^5 \text{ s}^{-1}$.*

VII. Waves and instabilities

Charged dust grains embedded into plasmas not only change the electron composition and thus affect conventional wave modes (e.g., ion-acoustic waves), but also introduce new low-frequency modes associated with the microparticle motion, alter dissipation rates, give rise to instabilities, etc. Moreover, the particle charges vary in time and space, which results in important qualitative differences between complex plasmas and usual multicomponent plasmas.

A comprehensive kinetic approach to study waves in complex plasmas is accompanied by serious difficulties: One has to deal with the dust-dust and dust-ion collision integrals which, in contrast to usual plasmas, cannot be considered in a linear approximation for realistic experimental conditions. Also, the grain charge should be treated as a new independent variable in the kinetic equation, which makes the calculations much more complicated. On the other hand, in many cases the (relatively) simple fluid approach based on the analysis of the fluid equations allows us to catch essential physics of the processes and, hence, to understand major dynamical properties of complex plasmas. Therefore, the analysis of major wave modes and instabilities can be done with the fluid model. Of course, in some cases applicability of the obtained results have certain limitations, especially where the damping and/or the growth rates of the modes are concerned, and then the kinetic approach has to be employed.

1 Waves in ideal (gaseous) complex plasmas

Considering the dust species as an ideal gas, one can write the continuity and momentum equations for the dust density n_d and velocity \mathbf{v}_d in the following form:

$$\frac{\partial n_d}{\partial t} + \nabla \cdot (n_d \mathbf{v}_d) = 0, \quad (115)$$

$$\frac{\partial \mathbf{v}_d}{\partial t} + (\mathbf{v}_d \cdot \nabla) \mathbf{v}_d = -\frac{Q}{m_d} \nabla \varphi - \frac{\nabla(n_d T_d)}{m_d n_d} - \sum_{\beta} \nu_{d\beta} (\mathbf{v}_d - \mathbf{v}_{\beta}). \quad (116)$$

The last term in Eq. (116) describes the momentum transfer force (“drag”) on the dust particles caused by the collisions with the “light” species – electrons, ions, and neutrals ($\beta = e, i, n$). The corresponding momentum exchange rates derived in the binary collision approximation, $\nu_{d\beta}$, are given in Section IV.2.

The fluid equations for electrons and ions are ($\alpha = e, i$)

$$\frac{\partial n_\alpha}{\partial t} + \nabla(n_\alpha \mathbf{v}_\alpha) = q_{I\alpha} - q_{L\alpha} - J_\alpha n_d, \quad (117)$$

$$\frac{\partial \mathbf{v}_\alpha}{\partial t} + (\mathbf{v}_\alpha \cdot \nabla) \mathbf{v}_\alpha = -\frac{e_\alpha}{m_\alpha} \nabla \varphi - \frac{\nabla(n_\alpha T_\alpha)}{m_\alpha n_\alpha} - \sum_\beta \nu_{\alpha\beta}^{\text{orb}} (\mathbf{v}_\alpha - \mathbf{v}_\beta) - \left(\frac{q_{L\alpha}}{n_\alpha} + \nu_{\alpha d}^{\text{coll}} \right) \mathbf{v}_\alpha. \quad (118)$$

The continuity equations include source terms, $q_{I\alpha}$, and two types of sink – “discharge” loss $q_{L\alpha}$ and the “dust” loss $J_\alpha n_d$. The source of electrons and ions which sustains the discharge is usually the volume ionization in electron-neutral collisions, and then $q_{Ie} = q_{Ii} = \nu_I n_e$, where ν_I is the ionization frequency. The “discharge” loss term is usually due to the diffusion towards the discharge chamber walls and can be estimated as $q_{Le} = q_{Li} \sim (D_{ai}/L^2)n_i$, where D_{ai} is the ambipolar (ion) diffusion coefficient and L is the spatial scale of the “global” plasma inhomogeneity (i.e., the distance between the rf electrodes or the radius of the dc discharge tube). The “dust” loss terms, which are due to electron and ion absorption on the grain surface, are determined by the corresponding fluxes on a grain, J_α , described in Chapter I.

The representation of the momentum transfer force in the form $\nu_{\alpha\beta}(\mathbf{v}_\alpha - \mathbf{v}_\beta)$ is valid as long as the mean free path of the species is shorter than the spatial scale of the perturbations (e.g., the inverse wave vector k^{-1}). The reciprocal momentum transfer rates are related to each other via $m_\alpha n_\alpha \nu_{\alpha\beta} = m_\beta n_\beta \nu_{\beta\alpha}$. An important difference between the drag force due to collisions with neutrals (“neutral drag”) and the force caused by the collisions with the charged species (“ion drag”) is that the latter includes both the direct collisions with the grain surface (“collection” part) and elastic scattering by the grain electrostatic potential (“orbital” part), i.e., $\nu_{d\beta} = \nu_{d\beta}^{\text{coll}} + \nu_{d\beta}^{\text{orb}}$ (see Section V.5).

Variability of the grain charges implies that the fluid equations for the density and momentum should be coupled to the charge transport equation which has the following form:

$$\frac{\partial Z}{\partial t} + \mathbf{v}_d \cdot \nabla Z = J_i - J_e, \quad (119)$$

where $Z = Q/e$ is the charge number. The system of equations is closed by the Poisson equation,

$$\nabla^2 \varphi = -4\pi e(n_i - n_e + Zn_d). \quad (120)$$

One can also take into account the temperature variation of the species caused by the wave perturbations. There are two limiting cases – isothermal and adiabatic variations. The partial pressure of each species, $n_\alpha T_\alpha$, scales as $\propto n_\alpha^{\gamma_\alpha}$, where γ_α is the effective polytropic index in the relevant case.

1.1 Major wave modes

In ideal unmagnetized plasmas only longitudinal wave modes can be sustained. The dispersion relations of these modes can be written as a sum of the partial susceptibilities (plasma responses),

$$\varepsilon(\omega, \mathbf{k}) = 1 + \chi_e + \chi_i + \chi_d = 0, \quad (121)$$

where the electron and ion responses are expressed via density and potential perturbations as $\chi_{e,i} = \pm 4\pi e k^{-2} \delta n_{e,i} / \delta \varphi$. The dust response depends also on the charge variations, so that $\chi_d = -4\pi k^{-2} (Z \delta n_d + n_d \delta Z) / \delta \varphi$. By linearizing Eqs (115)-(120) one can obtain the partial responses in general case.

In order to retrieve the wave modes sustained in complex plasmas, let us first consider the case of the multicomponent plasmas – when the variations of the grain charges are neglected. At this point we also neglect collisions and assume the equilibrium plasma ionization and loss: This approach allows us to obtain satisfactory results for the real part of the dispersion relations $\omega(k)$, unless the actual damping (growth) rate of the waves is comparable with ω . The partial plasma responses in this case are

$$\chi_\alpha = -\frac{\omega_{p\alpha}^2}{\omega^2 - \gamma_\alpha k^2 v_{T\alpha}^2}, \quad (122)$$

where $\omega_{p\alpha}$ is the plasma frequency of the corresponding species. (When the flow is present with the drift velocities \mathbf{u}_α , one should simply substitute $\omega \rightarrow \omega - \mathbf{k} \cdot \mathbf{u}_\alpha$.) For the plasma waves (plasmons with $\omega \gg kv_{T_e}$) the microparticles remain at rest and, therefore, the functional form of the dispersion relation, $\omega^2 = \omega_{pe}^2 + 3k^2 v_{T_e}^2$, is not affected by the presence of the dust grains. However, the electron plasma frequency ω_{pe} is changed because the charged grains affect the quasineutrality condition for unperturbed densities, $n_i = n_e + |Z|n_d$, and hence the electron density. A similar effect is also observed for the ion-acoustic (IA) waves, $kv_{T_i} \ll \omega \ll kv_{T_e}$, where the electrons provide equilibrium neutralizing background and dust remains at rest. For electrons we have $\chi_e = (k\lambda_{De})^{-2}$ and then Eqs (121) and (122) yield

$$\frac{\omega^2}{k^2} = \gamma_i v_{T_i}^2 + \frac{\omega_{pi}^2 \lambda_{De}^2}{1 + \lambda_{De}^2 k^2} \quad (123)$$

Usually the first term is relatively small and can be neglected compared to the second term, which actually represents the IA mode. This IA term depends on the ion-to-electron density ratio, which can be conveniently characterized by the ‘‘Havnes parameter’’ P ,

$$n_i/n_e - 1 = |Z|n_d/n_e \equiv P. \quad (124)$$

Generally, when $P \ll 1$ the effect of dust on the conventional (plasma and ion-acoustic) modes can be neglected. Otherwise, for $P \gtrsim 1$, the role of dust can be significant and then, in order to highlight this effect, the IA waves are referred to as the *dust ion-acoustic* (DIA) mode (Shukla and Silin, 1992). In the long-wavelength limit $k\lambda_{De} \ll 1$ the phase velocity of the DIA mode can be conveniently expressed via the ion thermal velocity,

$$C_{\text{DIA}} = \omega_{pi}\lambda_{De} \equiv \sqrt{(1+P)\tau} v_{Ti}, \quad (125)$$

where $\tau = T_e/T_i$ is the electron-to-ion temperature ratio, which is much larger than unity for typical rf and dc discharges, so that C_{DIA} exceeds significantly the ion thermal velocity (note that C_{DIA} does not depend on T_i).

The presence of dust gives rise to another acoustic mode associated with the motion of charged grains, whereas both the electrons and ions provide equilibrium neutralizing background. For $kv_{Td} \ll \omega \ll kv_{Ti}$ we have $\chi_{e,i} = (k\lambda_{De,i})^{-2}$, and then Eqs (121) and (122) yield

$$\frac{\omega^2}{k^2} = \gamma_d v_{Td}^2 + \frac{\omega_{pd}^2 \lambda_D^2}{1 + \lambda_D^2 k^2}, \quad (126)$$

where $\lambda_D^{-2} = \lambda_{De}^{-2} + \lambda_{Di}^{-2}$ is the linearized Debye length. The phase velocity of this *dust acoustic* (DA) mode does not depend on the dust temperature and in the long-wavelength limit $k\lambda_D \ll 1$ can be written as (Rao *et al.*, 1990)

$$C_{\text{DA}} = \omega_{pd}\lambda_D \equiv \sqrt{\frac{P\tau}{1+(1+P)\tau}} \sqrt{|Z|\frac{T_i}{T_d}} v_{Td}. \quad (127)$$

There is a clear similarity between the ion and dust acoustic modes: Equations (125) and (127) show that for both modes the ratio of the phase velocity to the thermal velocity is determined by the temperature ratio of the light-to-heavy species – T_e/T_i for DIA waves and T_i/T_d for DA waves. Peculiarity of the DA waves is that the charge-to-mass ratio of the dust grains is typically $10^8 - 10^{10}$ times smaller than that of the ions and, therefore, the dust waves have relatively low frequencies, $\sim 10 - 100$ Hz. Since the typical values of $|Z|$ are of the order of thousands, the phase velocity of DA waves can be much larger than v_{Td} , even if T_d exceeds T_i .

Exercise. Estimate the phase velocity of dust acoustic waves for $Z = 10^3$ and $a = 3 \mu\text{m}$, assuming $P \gtrsim 1$.

1.2 Damping and instabilities of the DIA and DA modes

The wave modes can only exist when the damping is weak, so that the actual imaginary part of the dispersion relation, $|\omega_i|$, is much smaller than the real part ω_r – only then one can speak about the wave propagation. The waves can also be unstable, because of various mechanisms operating in complex plasmas. As long as $|\omega_i|$ is much smaller than ω_r , the latter is approximately determined by the real part of the permittivity (121), i.e., $\text{Re } \varepsilon(\omega_r, \mathbf{k}) \simeq 0$, and the former is given by

$$\omega_i \simeq - \frac{\text{Im } \varepsilon(\omega, \mathbf{k})}{\partial \text{Re } \varepsilon(\omega, \mathbf{k}) / \partial \omega} \Big|_{\omega=\omega_r}.$$

This is very convenient formula for the practical use.

First we discuss the kinetic effects – namely, the role of the Landau damping. For each wave mode, the Landau damping can be due to wave resonance with “heavy” species (i.e., ions for DIA waves and dust for DA waves) and with “light” species (electrons for DIA waves and ions for DA waves). The damping caused by heavy species scales as $|\omega_i/\omega_r| \propto \exp(-\frac{1}{2}C^2/v_T^2)$, where C and v_T are the corresponding phase velocity and the thermal velocity of heavy species, respectively. From Eqs (125) and (127) we see that even in isothermal complex plasmas the C/v_T ratios can be quite large: C_{DIA}/v_{T_i} is large when $P \gg 1$, and C_{DA}/v_{T_d} is large because $|Z| \gg 1$. This makes substantial difference compared to usual plasmas, where C_{IA}/v_{T_i} can be large and, thus, the IA waves can propagate only when $\tau \gg 1$.

In the absence of the plasma flows the Landau damping on light species is relatively weak as well, because of the small charge-to-mass ratios: For DIA waves the (relative) damping rate is $|\omega_i/\omega_r| \lesssim \sqrt{(1+P)m_e/m_i}$, whereas for DA waves $|\omega_i/\omega_r| \lesssim \sqrt{P(1+P)^{-1}|Z|m_i/m_d}$. The Landau damping is, of course, modified when a stream of light species exists in a plasma (see below).

Let us mention other mechanisms responsible for the damping and instabilities of the DIA and DA waves.

DIA mode. Along with the Landau damping the major dissipation mechanisms are the collisions with neutrals and variations of the grain charges. In addition, there is a counterplay between ionization and loss – this can cause either damping or instability, depending on the value of P . As regards the DIA instabilities, the major mechanism operating in experiments is associated with the electron drift relative to ions – the so-called “current-driven instability” which is well-known for the IA waves in usual plasmas. Essentially, this instability is the reversed electron Landau damping – the energy exchange due to the

resonance electron-wave interaction changes the sign when the drift velocity u_e exceeds the phase velocity of the DIA waves C_{DIA} .

DA wave mode. The major damping mechanism operating in experiments with complex plasmas is certainly neutral gas friction, and the resulting damping rate is $2\omega_i \simeq -\nu_{dn}$. However, along with the damping there are a number of instability mechanisms which turn out to be quite important in experiments. Below we mention the most important types of the DA instability:

(i) Ion streaming instability: It can be triggered when ion currents are present in a plasma (e.g., due to electric fields in rf sheaths and dc striations). The mechanism of the (DA) ion streaming instability is completely identical to that of the (DIA) current-driven instability. The ion streaming instability is often observed in complex plasma experiments performed in different discharges. Figure 16 shows an example of such instability observed in a rf capacitively coupled discharge.

The presence of the ion flux modifies properties of the DA mode. This can be appropriately taken into account by using the kinetic expression for the ion susceptibility. Also, the kinetic approach allows us to include properly the effect of the ion-neutral collisions. When $|\omega - \mathbf{k} \cdot \mathbf{u}_i + i\nu_{in}| \ll kv_{T_i}$ we obtain

$$\chi_i(\omega, \mathbf{k}) \simeq \frac{1}{(k\lambda_{Di})^2} \left[1 + i\sqrt{\frac{\pi}{2}} \frac{\omega - \mathbf{k} \cdot \mathbf{u}_i}{kv_{T_i}} \right], \quad (128)$$

where \mathbf{u}_i is the drift velocity of ions. The real part in Eq. (128) coincides with the results of the fluid approach in this limit [see Eq. (122)], the imaginary part is due to the Landau damping. In the opposite limit $|\omega - \mathbf{k} \cdot \mathbf{u}_i + i\nu_{in}| \gg kv_{T_i}$ the resulting susceptibility can be written in the following form:

$$\chi_i(\omega, \mathbf{k}) \simeq -\frac{\omega_{pi}^2}{(\omega - \mathbf{k} \cdot \mathbf{u}_i)(\omega - \mathbf{k} \cdot \mathbf{u}_i + i\nu_{in}) - k^2v_{T_i}^2}. \quad (129)$$

This limit denotes either strongly collisional case or the case of “cold hydrodynamics” (when $u_i \gg v_{T_i}$, so that the thermal motion can be neglected). In both cases the fluid approach is applicable and, hence, Eq. (129) can be directly obtained from Eqs (117) and (118), assuming equilibrium ionization/recombination and neglecting other collisions.

(ii) Ionization instability (D’Angelo, 1998): Unlike the DIA waves, ionization cannot directly cause the instability of the DA waves – because the ionization creates new ions, but not dust grains. Nevertheless, ionization can in fact trigger the dust instability, because the ions can effectively transfer their momentum to the grains via the ion drag force. The whole instability mechanism operates as follows: When the dust density fluctuates in some region – say, decreases – ionization increases (because the electron density grows keeping

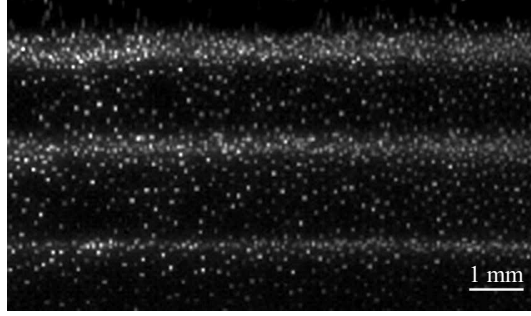


Fig. 16. *Spontaneous excitation of dust waves observed in laboratory experiments (courtesy of M. Schwabe). The experiments were carried out in a argon rf discharge at a pressure of 23 Pa with particles of 1.28 μm diameter.*

quasineutrality), which creates additional ion outflow from the region. This flux exerts an additional ion drag force pushing the grains away and, thus, the dust density decreases further. Obviously, this instability is of the aperiodic type (i.e., $\omega_r = 0$) and, thus, is independent of ν_{dn} . It is responsible for the onset of the void formation in complex plasmas.

(iii) Charge variation instability (Fortov *et al.*, 2000): It is due to the grain charge variations induced by the DA wave. In contrast to the DIA waves, now the charges are very close to the momentary equilibrium (because $|\omega| \ll \Omega_{\text{ch}}$) and, therefore, their variations alone are unlikely to be a reason for an instability or damping. However, in the presence of an external electric field \mathbf{E} (e.g., ambipolar fields or the fields in rf sheaths and dc striations) the wave-correlated charge variations result in non-zero (average) work done by the electric force.

2 Waves in plasma crystals

The theoretical model of waves in crystals – the so-called “dust-lattice” (DL) waves – is based on the analysis of the equation of motion for individual particles. For a particle having the coordinate \mathbf{r} the equation of motion is

$$m_d \ddot{\mathbf{r}} + m_d \nu_{dn} \dot{\mathbf{r}} = -\nabla U_{dd} + \mathbf{F}_{\text{ext}}. \quad (130)$$

Here $U_{dd} = \sum_i U(\mathbf{r} - \mathbf{r}_i)$ is the total energy of the electrostatic dust-dust coupling, where $U(\mathbf{r})$ is the pair interaction potential (the summation is over all particles with $\mathbf{r}_i \neq \mathbf{r}$). The force $\mathbf{F}_{\text{ext}}(\mathbf{r}, t)$ includes all “external” forces (except for the neutral drag force which is explicitly included to the left-hand side), e.g., confinement, excitation (lasers, electric pulses, beams, etc.), thermal noise (Langevin force), etc. Such diversification of the forces is convenient because the eigenmodes of the system do not depend on \mathbf{F}_{ext} .

In general, linear dispersion relations $\omega(\mathbf{k})$ are determined by eigenvalues of a dynamical matrix \mathbf{D} . The latter is derived by considering small perturbations of Eq. (130) of the form $\propto \exp(-i\omega t + i\mathbf{k} \cdot \mathbf{r})$. Elements of \mathbf{D} are determined by properties of interparticle interactions and are functions of \mathbf{k} . Below we show that if the pair interactions are reciprocal then \mathbf{D} is Hermitian; in this case, the eigenvalues are always real (i.e., the modes are stable) and the eigenvectors are orthogonal. The situation changes if the interactions are nonreciprocal – the eigenvalues can become complex.

To illustrate waves in plasma crystals, let us first assume reciprocal pair interactions of the Yukawa form, $U(r) = Q^2 r^{-1} e^{-r/\lambda}$, and consider the simplest model of the so-called “particle string”. The string model shows very good agreement with the first experiments performed with one-dimensional plasma crystals suspended horizontally in a rf plasma sheath. Moreover, when particle separation Δ exceeds the screening length λ , so that only the interaction with the *nearest neighbors* is important, the string model turns out to be appropriate to describe DL waves also in 2D plasma crystals (see below). The dispersion relation for the longitudinal (horizontal) mode obtained in the nearest neighbor approximation is

$$\omega(\omega + i\nu_{dn}) = 4\Omega_{\text{DL}}^2 e^{-\kappa} (\kappa^{-1} + 2\kappa^{-2} + 2\kappa^{-3}) \sin^2 \frac{1}{2} k\Delta, \quad (131)$$

where $\Omega_{\text{DL}}^2 = Q^2/m_d\lambda^3$ is the DL frequency scale and $\kappa = \Delta/\lambda$ is the lattice parameter. When damping is neglected, the longitudinal wave has an acoustic dispersion, $\omega \rightarrow 0$ for $k \rightarrow 0$. The experimentally observed wave frequencies usually vary from a few Hz for strings up to a few dozens of Hz for monolayers. Simple formula (131) is very convenient to evaluate spectra of the longitudinal DL waves.

Exercise. *Derive Eq. (131) assuming Yukawa pair interaction.*

In addition to the longitudinal waves, the particles can also sustain transverse (vertical) DL wave mode. The vertical mode is due to the balance between gravity and strongly inhomogeneous vertical electric force on a particle (e.g., in rf sheaths), as discussed in Chapter VI. This implies the vertical parabolic (lowest-order) confinement characterized by the frequency of a single particle oscillations, Ω_{conf} [which was defined as Ω_v in Eq. (94); here, subscript “conf” is used to avoid confusion with the vertical wave mode used below]. The resulting dispersion relation for the vertical DL mode (in nearest neighbor approximation) is

$$\omega(\omega + i\nu_{dn}) = \Omega_{\text{conf}}^2 - 4\Omega_{\text{DL}}^2 e^{-\kappa} (\kappa^{-2} + \kappa^{-3}) \sin^2 \frac{1}{2} k\Delta. \quad (132)$$

This is an optical branch, $\omega \rightarrow \Omega_{\text{conf}}$ for $k \rightarrow 0$, which has a negative dispersion, so that the group and phase velocities have opposite signs.

In 2D plasma crystals, two in-plane (horizontal) wave modes can be sustained. Both modes have an acoustic dispersion, one of them is longitudinal [as in the string model, similar to Eq. (131)] and the other is transverse. Another transverse wave mode associated with the vertical out-of-plane oscillations also has an optical dispersion [similar to Eq. (132)].

Theory predicts that, for plasma crystals suspended in a rf plasma sheath, DL wave modes strongly depend on parameters of the plasma wakes (see Section II.5). However, the far more important effect is that plasma wakes mediate interparticle interactions, making them *nonreciprocal*, which results in *linear coupling* between different DL modes. Below we identify the conditions when the wake-mediated coupling becomes critical for waves in 2D crystals.

2.1 Nonreciprocal wake-mediated interactions

Importance of plasma wakes has been long recognized. First experiments with complex plasmas were performed in highly inhomogeneous regions of rf plasma sheaths or dc striations. The magnitude of the vertical electric field in these regions can be so large that ions are accelerated to suprathermal velocities. The attractive forces exerted by wakes can cause the particle alignment – the formation of vertical chains along the flow, as illustrated in Fig. 17b.

The wakes play the role of a “third body” in the pair interaction and make it nonreciprocal (Melzer *et al.*, 1999), as explained in Fig. 17a. This results in a very efficient mechanism of converting the energy of the flowing ions into the kinetic energy of grains. One can easily demonstrate this by considering a pair of charged grains in the center-of-mass and relative coordinates, $\mathbf{r}_c = \frac{1}{2}(\mathbf{r}_1 + \mathbf{r}_2)$ and $\mathbf{r}_r = \mathbf{r}_2 - \mathbf{r}_1$, respectively. The center-of-mass momentum of such system is *not conserved* – it is governed by the force depending on the relative coordinate, $\mathbf{F}_c(\mathbf{r}_r) \propto (\partial/\partial\mathbf{r}_r)[\varphi(-\mathbf{r}_r) - \varphi(\mathbf{r}_r)]$, where $\varphi(\mathbf{r}_r) [\neq \varphi(-\mathbf{r}_r)]$ is the net (“particle+wake”) potential produced by each grain. When the system performs finite motion where $\mathbf{r}_r(t)$ and $\mathbf{r}_c(t)$ are correlated (for instance, due to resonances), one can construct such a loop for the center-of-mass coordinate that $\oint \mathbf{F}_c d\mathbf{r}_c \neq 0$, i.e., the total kinetic energy can grow due to wake-mediated interactions. In particular, this results in the mode-coupling instability discussed below.

2.2 Wave modes for nonreciprocal interactions

Let us generally assume non-reciprocity of the interparticle interactions and discuss common properties of waves in 2D plasma crystals. The dynamical

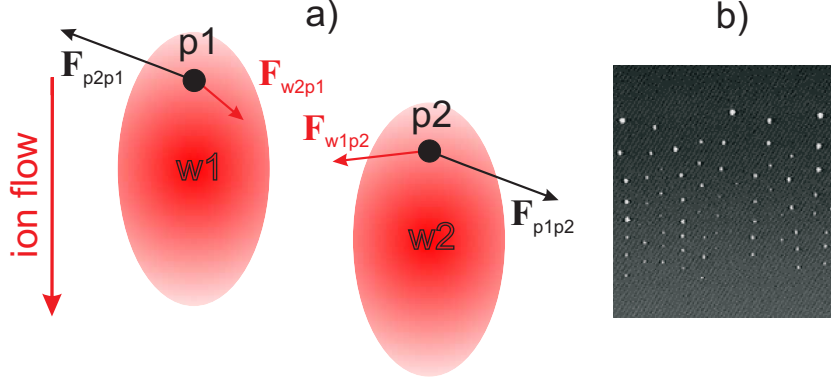


Fig. 17. *Nonreciprocal wake-mediated interactions.* a) The total force exerted on particle “p1” by particle “p2” is the sum of direct particle-particle interaction, \mathbf{F}_{p2p1} , and indirect force from wake “w2”, \mathbf{F}_{w2p1} (and vice versa for the force on particle “p2”). While the direct forces are reciprocal, $\mathbf{F}_{p2p1} = -\mathbf{F}_{p1p2}$, the wake forces are not, $\mathbf{F}_{w2p1} \neq -\mathbf{F}_{w1p2}$. b) Typical example of vertically aligned chains due to wake-mediated interactions. Shown is the side view with particles of $6.9 \mu\text{m}$ diameter levitating in a rf sheath (courtesy of H. Thomas).

matrix has the following form in this case:

$$\mathbf{D} = \begin{pmatrix} \alpha_h - \beta & 2\gamma & i\sigma_y \\ 2\gamma & \alpha_h + \beta & i\sigma_x \\ i\sigma_y & i\sigma_x & \Omega_{\text{conf}}^2 - 2\alpha_v \end{pmatrix}. \quad (133)$$

The elements $\alpha_h(\mathbf{k})$, $\beta(\mathbf{k})$, and $\gamma(\mathbf{k})$ determine the dispersion of two in-plane (horizontal) modes, $\alpha_v(\mathbf{k})$ characterizes the out-of-plane (vertical) mode, and the elements $\sigma_{x,y}(\mathbf{k})$ emerge due to non-reciprocity, making \mathbf{D} non-Hermitian. All these elements are proportional to Ω_{DL}^2 and depend on the screening parameter κ . The matrix is calculated for the reference frame shown in Fig. 18(a) assuming that vertically the particles are confined in a parabolic potential well characterized by the resonance frequency Ω_{conf} . The resulting dispersion relations $\omega(\mathbf{k})$ are determined from

$$\det[\mathbf{D} - \omega(\omega + i\nu_{dn})\mathbf{I}] = 0, \quad (134)$$

where \mathbf{I} is the unit matrix. Thus, $\omega(\omega + i\nu_{dn}) \equiv \Omega^2$ are the eigenvalues of \mathbf{D} , i.e., the DL *wave modes*. The effect of friction on the *dispersion relations* $\omega(\mathbf{k})$ is straightforward: For weakly damped waves (when $|\Omega| \gg \nu_{dn}$, which is typical for experiments), one readily obtains $\omega(\mathbf{k}) \simeq \Omega(\mathbf{k}) - \frac{1}{2}i\nu_{dn}$. From the practical point of view this implies that one can analyze undamped dispersion relations and afterwards simply add $-\frac{1}{2}i\nu_{dn}$ to the resulting imaginary part.

We note that for the analysis of wave modes in a crystal it is sufficient to consider the wave vectors from within the first Brillouin zone which is shown in Fig. 18b. This zone is nothing but the Wigner-Seitz cell of the reciprocal

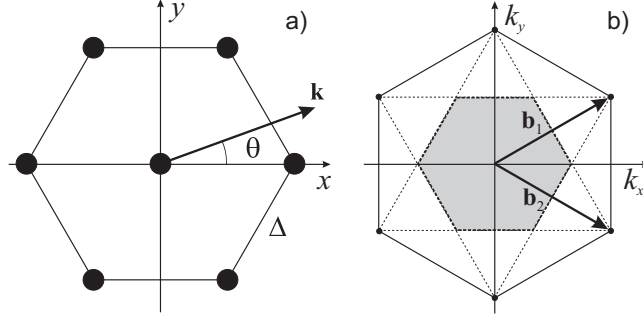


Fig. 18. (a) Elementary hexagonal lattice cell with the frame of reference, the lattice constant is Δ . (b) The reciprocal lattice in \mathbf{k} -space, the basis vectors of the lattice are $\mathbf{b}_{1,2} = 2\pi\Delta^{-1}(1, \pm\frac{1}{\sqrt{3}})$. Due to the lattice symmetry, it is sufficient to consider the wave vectors \mathbf{k} at $0^\circ \leq \theta \leq 30^\circ$ and from within the first Brillouin zone (gray region enclosed by dashed lines), so that $|\mathbf{k}|\Delta \leq \frac{4}{3}\pi$ for $\theta = 0^\circ$ and $|\mathbf{k}|\Delta \leq \frac{2}{\sqrt{3}}\pi$ for $\theta = 30^\circ$.

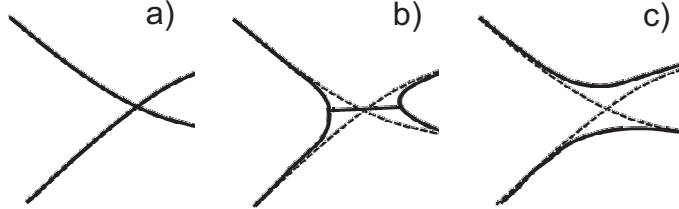


Fig. 19. Modification of coupled modes in the vicinity of their crossing. The sketch depicts the modes in the $(\Omega, |\mathbf{k}|)$ plane (a) in the absence of coupling (reciprocal interactions) and for the (b) negative or (c) positive sign of the coupling (nonreciprocal interactions). The negative coupling results in the formation of a hybrid mode and can trigger the mode coupling instability; the positive coupling causes the mode reconnection, while the modes remain stable and form a “forbidden band”.

lattice formed by the basis vectors \mathbf{b}_1 and \mathbf{b}_2 . Hence, the wave vectors \mathbf{k} and $\mathbf{k}' = \mathbf{k} + \mathbf{G}$ which are different by a linear combination of the basis vectors ($\mathbf{G} = m\mathbf{b}_1 + n\mathbf{b}_2$) are equivalent for wave modes, i.e., $\Omega(\mathbf{k} + \mathbf{G}) \equiv \Omega(\mathbf{k})$.

For reciprocal interactions $\sigma_{x,y} = 0$ and then Eqs (133) and (134) yield

$$(\Omega^2 - \Omega_{h\parallel}^2)(\Omega^2 - \Omega_{h\perp}^2)(\Omega^2 - \Omega_v^2) = 0. \quad (135)$$

There are three independent and real DL modes: Two *acoustic* in-plane modes $\Omega^2(\mathbf{k}) = \alpha_h \pm \sqrt{\beta^2 + 4\gamma^2} \equiv \Omega_{h\parallel,\perp}^2(\mathbf{k})$ (where \parallel and \perp indicate the longitudinal and transverse polarizations and correspond to the plus and minus signs, respectively) and an *optical* out-of-plane mode $\Omega^2(\mathbf{k}) = \Omega_{\text{conf}}^2 - 2\alpha_v \equiv \Omega_v^2(\mathbf{k})$. When solved for $\omega(\mathbf{k})$, each mode yields a couple of conjugate branches.

When interactions are nonreciprocal the modes are modified – they are described by Eq. (135) with nonzero r.h.s. which is proportional to $\sigma_x^2 + \sigma_y^2$ and can be either positive or negative (Ivlev *et al.*, 2001). The DL modes become strongly coupled with each other if they cross, as illustrated in Fig. 19.

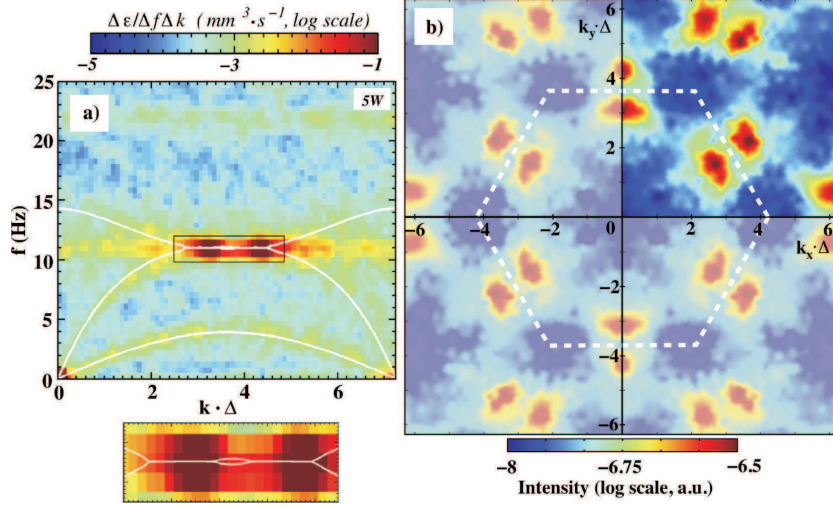


Fig. 20. *Fluctuation spectra for 2D plasma crystal at the onset of the mode-coupling instability triggered by the wake-mediated interactions (courtesy of L. Couedel). The spectra were measured in the experiment performed with particles of $9.15 \mu\text{m}$ diameter. The logarithmic color coding is used for the “fluctuation intensity” $\Delta\epsilon/\Delta k\Delta f$ (energy density, for unit mass, per unit wave number and frequency): Yellow ridges represent stable wave modes, the unstable hybrid mode are the dark-red “hot spots”. (a) Dispersion relations at $\theta = 30^\circ$, solid lines are theoretical curves for three DL wave modes: out-of-plane transverse, in-plane longitudinal, and in-plane transverse (from top to bottom). The wave number k is normalized by the inverse interparticle distance Δ^{-1} , the shown range of k corresponds to the first two Brillouin zones (branches are symmetric with respect to the border between the two zones). Below the fluctuation spectra the magnified hybrid mode in the unstable regime (marked by a rectangular box) is shown. (b) Fluctuation spectra in the \mathbf{k} plane integrated over frequency. Dashed hexagon indicates the border of the first Brillouin zone, red spots represent the unstable hybrid mode.*

The analysis shows that the negative coupling results in the emergence of an unstable *hybrid mode* operating in a certain proximity of the crossing point. This happens upon the crossing of longitudinal in-plane and transverse out-of-plane branches, $\Omega_{h\parallel}(\mathbf{k})$ and $\Omega_v(\mathbf{k})$. The coupling is strongest for $\theta = 30^\circ$ (see Fig. 18), when the modes are governed by the following equation:

$$(\Omega^2 - \Omega_{h\parallel}^2)(\Omega^2 - \Omega_v^2) + \sigma_y^2 = 0.$$

Crossing of the two branches ensures the resonance between them and triggers the *mode-coupling instability*, which is the main non-generic (i.e., plasma-specific) mechanism of melting of 2D plasma crystals. The mode-coupling instability is illustrated in Fig. 20: The branches cross in the vicinity of the first Brillouin zone boundary, resulting in the anomalous energy release (dark-red “hot spots”).

The influence of wake-mediated interactions on the particle dynamics in 2D plasma crystals can be completely eliminated by avoiding the mode intersec-

tion. Practically, this is achieved by increasing the strength of the vertical confinement.

3 Nonlinear waves

Complex plasmas, as any other plasmas are nonlinear media where the waves of finite amplitude cannot be generally considered independently. Nonlinear phenomena in complex plasma are very diverse, due to a large number of different wave modes which can be sustained. The wave amplitude can reach a nonlinear level because of different processes: This is not necessarily an external forcing, or the wave instabilities – it can also be a regular collective process of nonlinear wave steepening. In the absence of dissipation (or, when the dissipation is small enough), nonlinear steepening can be balanced by wave dispersion which, in turn, can result in the formation of *solitons*. When the dissipation is large, it can overcome the role of dispersion and then the balance of nonlinearity and dissipation can generate *shock waves*. In many cases the lowest-order nonlinear terms are quadratic, and then the weakly nonlinear soliton dynamics is governed by the Korteweg-de Vries (KdV) equation. For solitons of arbitrary amplitude, the method of the Sagdeev pseudopotential is very convenient: In particular, this method allows us to determine the upper value of the Mach number beyond which the dispersion is no longer sufficient to balance the nonlinearity and, thus, the collisionless shock is formed due to “collective” dissipation.

3.1 Ion solitons and shocks

The theory predicts that in complex plasmas (as well as in electronegative plasmas) both compressive and rarefactive dust ion-acoustic solitons are possible. It was shown that properties of the DIA solitons (profile and the range of Mach numbers where the solitons can exist) are strongly affected by the form of the electron and ion distribution function, in particular – by the presence of “cold” and “hot” populations and trapped electrons. As regards the DIA shocks, depending on the parameter regime different dissipation mechanisms can play the major role: Along with the ion viscosity, these are grain charge variations and Landau damping. The general trend is that in the absence of dust the shock front exhibits pronounced oscillatory structure typical for collisionless ion-acoustic shocks. As the dust density increases the peaks become smoothed and eventually disappear, leaving the monotonic front profile, as shown in Fig. 21.

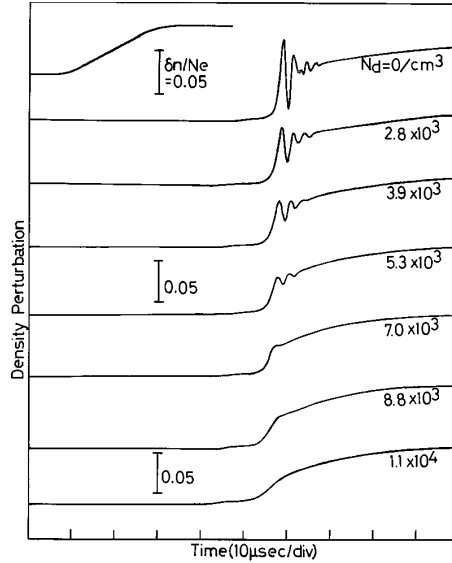


Fig. 21. DIA shock observed in a double plasma device (courtesy of Y. Nakamura). Experiments were performed with argon gas at pressure about $(2 - 4) \times 10^{-2}$ Pa, for different densities n_d of the dust particles of about $8.9 \mu\text{m}$ diameter. The DIA waves were excited with a positive ramp voltage applied to the source anode, and the signals were detected by the movable Langmuir probe. The electron density perturbations were recovered from the perturbations of the electron saturation current on the probe.

3.2 Dust solitons and shocks

Figure 22 shows the evolution of the soliton propagating in a crystalline monolayer. Theoretical study of the soliton dynamics is based on the analysis of Eq. (130). Defining \mathbf{x} as the propagation vector and retaining the lowest-order nonlinearity and dispersion terms, the resulting equation for the nonlinear wave dynamics is

$$\frac{\partial^2 u}{\partial t^2} + \nu_{dn} \frac{\partial u}{\partial t} = C^2 \frac{\partial^2}{\partial x^2} \left(u + \ell^2 \frac{\partial^2 u}{\partial x^2} + \frac{1}{2} \Lambda u^2 \right). \quad (136)$$

Here $u = \partial \delta \mathbf{r} / \partial \mathbf{x} \simeq -\delta n_d / n_d$ is the particle density modulation (expressed via the longitudinal derivative of the in-plane displacement $\delta \mathbf{r}$) and C is the long-wavelength DL phase velocity which is always independent of the direction of propagation. The two further parameters are the dispersion coefficient ℓ^2 which generally can have *either* sign (it has the dimension of squared length) and the nonlinear coefficient Λ ; for crystals, these usually have a weak dependence on the orientation of \mathbf{x} with respect to the crystalline axis. Without the frictional dissipation, Eq. (136) is readily reduced to the KdV equation by employing the stretched coordinates $(x - Ct, t)$. The soliton can only exist when ℓ^2 and Λ have opposite signs, so that the following relations can be fulfilled: $-\frac{1}{3} \Lambda A = 4\ell^2 / L^2 = M^2 - 1$, where A and L are the soliton amplitude and width, respectively, and $M = V/C$ is the Mach number for the soliton

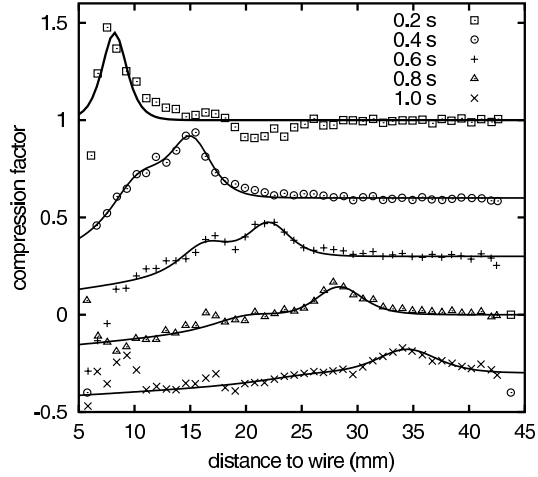


Fig. 22. *Dust soliton observed in experiments with a monolayer hexagonal lattice (courtesy of D. Samsonov). Experiments were performed in rf discharge in argon gas at a pressure about 1 – 2 Pa, with plastic particles of about 8.9 μm diameter. Compression factor $1 + \delta n_d/n_d$ versus distance to the wire is plotted at different times. The solid lines show the theoretical fits to the experimental data. The fits and experimental points at later times are offset down.*

velocity. The Mach number is a convenient control parameter which defines the soliton profile, $-u = A \cosh^{-2}(\xi/L)$, with $\xi = x - Vt$.

In two-dimensional hexagonal lattices, ℓ^2 is always positive and has a very weak dependence on the direction of propagation, Λ is always negative and can depend on the direction substantially. Such a combination of signs implies that only compressive ($A > 0$) supersonic ($M > 1$) solitons can propagate in crystalline monolayers, as it is observed in experiments. If the neutral gas pressure is low enough the friction does not destroy the soliton. The perturbation simply slows down, approaching the asymptote $V = C$, and the form of the soliton changes in accordance with the analytical solution (i.e., the amplitude decreases and the width increases, keeping the “soliton relation” $AL^2 = \text{const}$, see Fig. 22). Thus, one can speak about a “weakly dissipative soliton” when the dissipation time scale, $\sim \nu_{dn}^{-1}$, exceeds the time scale of the wave itself, $\sim \Omega_{DL}^{-1}$.

As regards the dust shock waves, “pure” shocks were only observed so far in two-dimensional crystals (term “pure” implies here that the momentum exchange in dust-dust collisions prevails over the momentum loss due to neutral gas friction). These shocks caused melting of the crystal behind the front, as shown in Fig. 23. As the shock propagated and weakened it was seen that the melting ceased. Further propagation of the pulse was in the form of a soliton, as in Fig. 22.

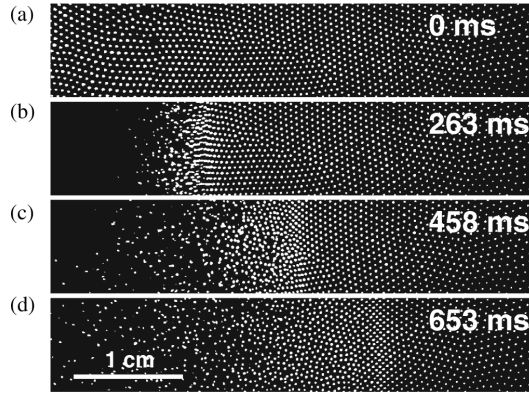


Fig. 23. *Dust shock wave propagating in a monolayer hexagonal lattice (courtesy of D. Samsonov). Experimental conditions and the wave excitation technique are described in Fig. 22. Initially undisturbed particles (a) were swept from left to right (b) and (c) forming a shock with a sharp front. The lattice melted behind the front. At later times (d) the shock weakened due to the neutral drag and a soliton was formed.*

3.3 Mach cones

Dispersion relations of dust modes in complex plasmas suggest that, irrespective of the plasma state the phase velocity attains the maximal value in the long-wavelength limit. For acoustic modes this velocity – the “sound speed” C – is finite and therefore, similar to conventional media, the supersonic perturbations are always localized behind the object which produces these perturbations. The perturbation front has a conical form in a three-dimensional case and therefore it is called a “Mach cone”. In a two-dimensional case the same name is adopted, although the front is a planar V-shaped perturbation. The opening angle μ of the front at large distances from the object (where the nonlinearity should not play important role) is determined by the well-known relation $\sin \mu = C/V \equiv M^{-1}$.

The Mach cones in two-dimensional plasma crystals can be generated by single particles moving slightly beneath or above the monolayer, or can be excited by the radiation pressure of a focused laser beam. The wake reveals a multiple cone structure behind the front, as shown in Fig. 24. Generally, the wake structure is determined by the dispersion and nonlinear properties of particular wave modes excited behind the front. The formation of the second cone behind the first one, with the opening angle smaller for the second cone can be prescribed to the shear (transverse) wave front, because the (longitudinal) sound speed C is larger than the shear phase velocity. It was proposed to use the Mach cones as a tool to determine the local parameters of complex plasmas, e.g., particle charge and the screening length, making use of the measured sound speed.

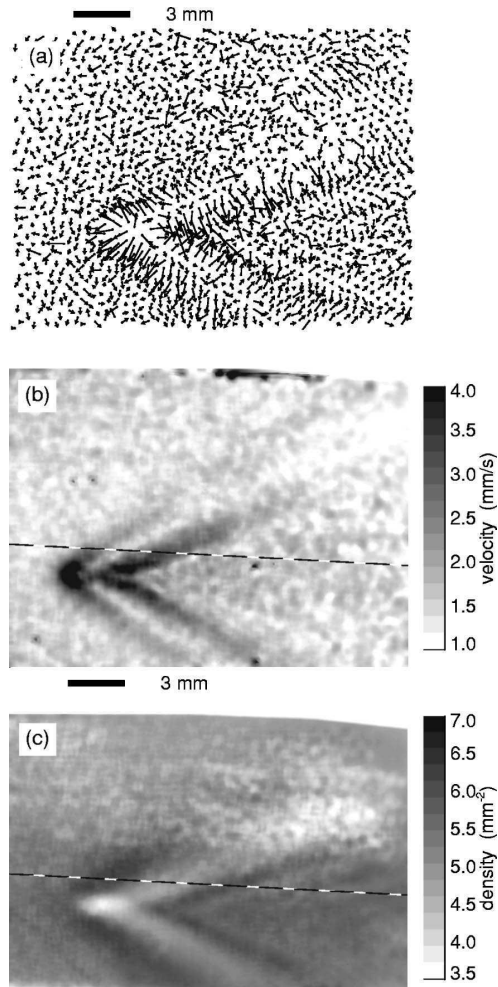


Fig. 24. Mach cone observed in a monolayer hexagonal lattice (courtesy of D. Samsonov). Experiments were performed in a GEC rf chamber in krypton gas at pressure about 1.2 Pa, with plastic particles of 8.9 μm diameter. The cone was excited by a supersonic particle which moved spontaneously beneath the monolayer. (a) Particle velocity vector map derived from particle positions in two consecutive video fields, (b) gray-scale speed map, and (c) gray-scale number density map. The first cone consists of particles moving forward, and it coincides with the high density region. The second cone has particles moving backward, and it coincides with the low density region.

Symbols (cgs)

Major Notations

a	particle radius
B, \mathbf{B}	magnetic field
c	speed of light
C_{DA}	dust acoustic velocity
C_{DIA}	dust ion acoustic velocity
$C_{\text{IA}} = \sqrt{T_e/m_i}$	ion sound velocity
d, \mathbf{d}	dipole moment
D	diffusion coefficient
D_j	diffusion constant of j -th component ($j = e, i$)
e	elementary charge
E, \mathbf{E}	electric field
$f(\mathbf{v}), f$	velocity distribution function
$f_j(\mathbf{v})$	velocity distribution of the j -th component ($j = e, i, n$)
F, \mathbf{F}	force
g	gravitational acceleration
I	radiation intensity
J_j	flux of the j -th component ($j = e, i$)
J_{eq}	equilibrium electron/ion flux
k, \mathbf{k}	wave number
k_{D}	inverse (linearized) Debye radius
$k_{\text{D}j} \equiv \lambda_{\text{D}j}^{-1}$	inverse Debye radius of the j -th component ($j = e, i$)
ℓ_i	ion mean free path
m	mass
m_j	mass of the j -th component ($j = e, i, n, d$)
n_j	volume number density of the j -th component ($j = e, i, n, d$)
$n_{\text{r}} = \sqrt{\varepsilon_{\text{r}}}$	relative refractive index
n_0	unperturbed plasma density
p	pressure
p, \mathbf{p}	momentum
Q	particle electric charge
Q_{eq}	equilibrium particle charge
r	distance
r_0	distance of the closest approach
R_{C}	Coulomb radius
R_0	characteristic interaction radius

St_{ij}	collision integral for i - j collisions ($i, j = n, d$)
T_j	temperature of the j -th component ($j = e, i, n, d$)
u, \mathbf{u}	relative drift velocity
u_j, \mathbf{u}_j	drift velocity of the j -th component ($j = e, i$)
$U(r)$	pair potential/energy
v, \mathbf{v}	velocity
$v_{T_j} = \sqrt{T_j/m_j}$	thermal velocity of the j -th component ($j = e, i, n, d$)
$W(Z)$	charge distribution function
$Z = Q/e$	charge number
Z_{eq}	equilibrium charge number
$Z_1(t)$	fluctuating part of the charge
β	recombination coefficient
γ_j	effective polytropic index of the j -th component
γ_0	steepness of the interaction potential
$\Delta = n^{-1/3}$	mean interparticle distance
η	viscosity
κ_n	thermal conductivity of neutral gas
λ	(effective) screening length, radiative wavelength
λ_D	(linearized) Debye radius
$\lambda_{Dj} = \sqrt{T_j/4\pi e^2 n_j}$	Debye radius of the j -th component ($j = e, i$)
λ_{eff}	effective screening length
Λ	Coulomb logarithm
Λ_{ij}	Coulomb logarithm for i - j collisions ($i, j = e, i, d$)
μ	reduced mass
ν	relevant damping rate
ν_{ij}	damping rate for i - j collisions ($i, j = e, i, n, d$)
ν_I	ionization frequency
ν_j	damping rate of the j -th component
ν_L	characteristic frequency of ambipolar losses
ρ	impact parameter, particle mass density
ρ_c	maximum impact parameter for collection
ρ_*	transitional impact parameter
$\sigma(v), \sigma$	relevant (velocity dependent) cross section
σ_Z^2	relative charge dispersion
σ_Σ	total effective cross section (for several processes)
$\varphi(r)$	electrostatic potential
φ_s	electrostatic potential at the particle surface
χ	scattering angle
χ_j	plasma response of the j -th component ($j = e, i, d$)
ω	wave frequency
$\omega_{pj} = \sqrt{4\pi e^2 n_j/m_j}$	plasma frequency of the j -th component ($j = e, i$)
$\omega_{pd} = \sqrt{4\pi Q^2 n_d/m_d}$	dust plasma frequency

$\omega_{r,i}$	real, imaginary parts of wave frequency
Ω_{ch}	charging frequency
Ω_{conf}	confinement frequency
Ω_{h}	characteristic frequency of horizontal confinement
Ω_{v}	characteristic frequency of vertical confinement
$\Omega_{\text{DL}} = \sqrt{Q^2/m_d\lambda^3}$	frequency scale of dust lattice oscillations

Major Similarity (Dimensionless) Numbers

M	Mach number (for several processes)
$M_T = u_i/v_{T_n}$	thermal Mach number of ions
$P = Z n_d/n_e$	Havnes parameter
$z = e \varphi_s /T_e$	reduced particle surface potential
$\beta(v), \beta$	scattering parameter
β_T^{ij}	thermal scattering parameter for i - j collisions ($i, j = e, i, d$)
$\kappa = \Delta/\lambda$	screening parameter
$\mu = m_e/m_i$	electron-to-ion mass ratio
$\tau = T_e/T_i$	electron-to-ion temperature ratio